This is to certify that the

thesis entitled

A Material Characterization of a Silicon Carbide Whisker-reinforced Aluminum Metal-matrix Composite, with an Emphasis on Cyclic-bending

presented by

Sean Michael Fleming

has been accepted towards fulfillment
of the requirements for

Master's degree in Mechanics

Gary Lee Clark
Major professor

Date 18 November 1993

A MATERIAL CHARACTERIZATION OF A SILICON CARBIDE WHISKER-REINFORCED ALUMINUM METAL-MATRIX COMPOSITE, WITH AN EMPHASIS ON CYCLIC-BENDING

By

Sean Michael Fleming

A THESIS

Submitted to
Michigan State University
in partial fulfillment of the requirements
for the degree of

MASTER OF SCIENCE

Department of Materials Science and Mechanics

1993

ABSTRACT

A MATERIAL CHARACTERIZATION OF A SILICON CARBIDE WHISKER-REINFORCED ALUMINUM METAL-MATRIX COMPOSITE, WITH AN EMPHASIS ON CYCLIC-BENDING

By

Sean Michael Fleming

A material characterization of a silicon carbide whisker-reinforced aluminum metal-matrix (MMC) is analyzed and presented with an emphasis on cyclic-bending. Initially the tensile, flexural and shear, monotonic material properties were measured, where all testing was performed along the *axial* direction and along the *transverse* direction. The thrust of the research was cyclic 3-point bending of the MMC along the axial (preferred) direction and transverse to the axial direction. The dynamic flexural modulus was measured as a function of (cyclic-bending) cycles to observe any general trends, e.g. microcracking or strain-hardening, throughout the fatigue life of the cyclic-bending specimens.

The cyclic-bending study consisted of using a specially designed 3-point-bend-fixture which had a deflection-mechanism mounted mid-span. An extensometer was attached to the deflection-mechanism to measure maximum deflection. The fixture was attached to an Instron load frame and the cyclic-bending test was controlled and driven by a closed-loop, servo-

hydraulic Instron materials testing machine interfaced with a digital computer. The nature of the cyclic-bending was compression-compression, the waveform was sinusoidal and the controlled-variable was deflection.

Three fatigue relations were used to model the cyclic-bending experiments, stress-life, elastic strain-life and elastic deflection-life. A power-law was used for the three models mentioned with very satisfactory results, the best being for the elastic deflection-life models. The fundamental discoveries were that the cyclic-bending specimens in the axial direction could withstand considerably greater strain for the same fatigue life even though the axial specimens were ~ 42% stiffer than the transverse specimens. The transverse specimen's fatigue lives were more predictable, than the axial specimens, from one specimen to the next. It was discovered that for the cyclic-bending study the elastic modulus was not a *constant*. This phenomenon has been observed for several britttle materials.

ACKNOWLEDGEMENTS

The author wishes to express his sincerest appreciation to his advisor and mentor, Dr. Gary L. Cloud, for his invaluable advise, guidance and latitude throughout the course of this research.

The author also wishes to thank his committee members, Drs. James Lucas and Dashin Liu.

Finally, the author would like to thank Lan Meng for her greatly appreciated assitance during the cyclic-bend set-up and testing, and Henry Wede for modifying a computer program to capture the cyclic-bend load-displacement data.

TABLE OF CONTENTS

Page

LIST OF TABLES v

LIST OF FIGURES viii

CHAPTER 1 INTRODUCTION 1

1.1 A STRUCTURAL COMPOSITE 1

1.2 PROBLEM OUTLINE 1

1.3 OBJECTIVES AND SCOPE 3

1.4 APPROACH TO PROBLEM 4

CHAPTER 2 STATIC CHARACTERIZATION OF THE MMC 7

2.1 INTRODUCTION 7

2.2 SEM EVALUATION OF THE PRINCIPAL PLANES OF THE MMC EXTRUDATE 8

2.3 MONOTONIC TENSILE TEST 11

2.3.1 Experimental Procedure 11

2.3.2 Results 13

2.4 POISSON'S RATIO ν, AND YOUNG'S MODULUS E 16

2.4.1 Experimental Procedure 16

2.4.2 Sample Calculations 19

2.4.3 Results 23

2.5 FLEXURAL MODULUS AND BENDING STRENGTH 30

2.5.1 Experimental Procedure 30

2.5.2 Sample Calculations 32

2.5.3 Results..... 34
2.5.4 Discussion..... 34
2.6 SHEAR MODULUS G, AND SHEAR STRENGTH τ_{max}..... 41
2.6.1 Introduction..... 41
2.6.2 Test Fixture..... 41
2.6.3 Test Specimen..... 45
2.6.4 Experimental Procedure..... 47
2.6.5 Sample Calculations..... 48
2.6.6 Results..... 49
2.6.7 Discussion..... 52
CHAPTER 3 3-POINT CYCLIC-BENDING..... 54
3.1 INTRODUCTION..... 54
3.2 EXPERIMENTAL PROCEDURE..... 57
3.3 SAMPLE CALCULATIONS..... 59
3.4 THEORY..... 61
3.5 RESULTS AND DISCUSSION..... 64
3.5.1 Applied Load Vs. Displacement (Deflection)..... 64
3.5.2 Stress Amplitude $\Delta\sigma/2$, Vs. Cycles to Failure N_f.....66
3.5.3 Strain Amplitude $\Delta\varepsilon/2$, Vs. Cycles to Failure N_f.....71
3.5.4 Deflection Amplitude $\Delta\delta/2$, Vs. Cycles to Failure N_f.. 80
CHAPTER 4 DYNAMIC FLEXURAL MODULUS AS A FUNCTION OF CYCLES TO NEAR FAILURE..... 86
4.1 RESULTS FOR TRANSVERSE SPECIMENS..... 87
4.1.1 Specimens with maximum deflection of 0.10mm..... 87

4.1.2 Specimens with maximum deflection of 0.15mm..... 87
4.1.3 Specimens with maximum deflection of 0.20mm..... 91
4.1.4 Specimens with maximum deflection of 0.25mm..... 94
4.1.5 Specimens with maximum deflection of 0.28mm..... 99
4.1.6 Specimens with maximum deflection of 0.30mm..... 99
4.2 RESULTS FOR AXIAL SPECIMENS..... 104
4.2.1 Specimens with maximum deflection of 0.10mm..... 104
4.2.2 Specimens with maximum deflection of 0.15mm..... 108
4.2.3 Specimens with maximum deflection of 0.20mm..... 108
4.2.4 Specimens with maximum deflection of 0.25mm..... 112
4.2.5 Specimens with maximum deflection of 0.28mm..... 118
4.2.6 Specimens with maximum deflection of 0.30mm..... 118
4.3 DISCUSSION OF E-N RESULTS..... 121
CHAPTER 5 CONCLUSIONS AND RECOMMENDATIONS..... 123
REFERENCES..... 132
APPENDIX A..... 137

LIST OF FIGURES

Figure Page

1.1 Typical Metal-Matrix (MMC) Extrudate form and respective directions....6

2.1 The top micrograph (A) illustrates the whisker/matrix relation along the Y-Z plane, this corresponds to the transverse direction. The bottom micrograph (B) illustrates the whisker/matrix relation along the X-Z plane, this corresponds to the axial direction.... 9

2.2 The top micrograph (A) illustrates the whisker/matrix relation along the X-Z plane of the extrudate, this corresponds to the axial direction. The bottom micrograph (B) illustrates the Y-Z plane and corresponds to a top view of the axial direction, (the Z-axis is normal to the micrograph)....10

2.3 Flat Tension Specimen Design for Standard Test Method (ASTM D 3552-77) for Tensile Properties of Fiber-Reinforced Metal-Matrix Composites....12

2.4 Typical Stress-Strain plots of the static tension tests for the transverse (top) specimen and axial (bottom) specimen directions respectively....14

2.5 Schematic of "strain bars" dimensions and strain gage (RSG) configuration....18

2.6 Schematic showing labeling configuration and loading technique. Note the ease with which bending could occur....18

2.7 MicroMeasurements Load-Frame (top) used to load the "Strain-Bars" and the actual load configuration (bottom). Notice 4 sets of lead wires, i.e. 2 RSGs per side....20

2.8 Typical Load-Strain plots for the transverse (top) and axial (bottom) "Strain-Bars" with Poisson's ratio....22

2.9 Elastic Stress-Strain graphs for the transverse (top) and axial (bottom) "strain bars" with Young's Modulus....24

2.10 Fixture used for the static, 3-point bend test.....31

2.11 Load-Deflection plots of static 3-point bend test for the transverse (top) and axial (bottom) directions, with Flexural Modulus.....36

2.12 Force, Shear and Moment Diagrams for the Iosipescu Shear Test Method.....43

2.13 Schematic of the loading fixture for an Iosipescu Shear Test.....45

2.14 Photograph of actual test fixture used for executing the Iosipescu Shear Test at MSU.....45

2.15 Iosipescu Shear Test Specimen Dimensions.....46

2.16 Stress-Strain plots of the Iosipescu Shear Test, for both the transverse (top) and axial (bottom) directions.....50

2.17 Linear-Elastic Stress-Strain diagrams from the Iosipescu Shear Test, with Shear Modulus, G. Both the transverse (top) and axial (bottom) directions are illustrated.....51

2.18 Post-mortem photograph (~ 7X) of the Iosipescu Shear Test specimens for both the transverse (top) and axial (bottom) directions.....53

3.1 Cyclic-bending fixture (top) and experimental set-up (bottom) used for the fatigue study.....56

3.2 Loading technique used for the cyclic-bending study.....58

3.3 Typical load-displacement (deflection) plot reduced from the hexadecimal data, see Eq.[3.1].....65

3.4 Stress-Life (S-N) plots of the cyclic-bending specimens for the Transverse (top) and Axial (bottom) directions. Note the respective "endurance limits" and power-law models.....68

3.5 Strain-Life (ε-N_f) plots of the cyclic-bending specimens for the Transverse (top) and Axial (bottom) directions. Note the models with and with out mean-stress effects.....72

3.6 Deflection-Life (δ-N_f) plots of the cyclic-bending specimens for the Transverse (top) and Axial (bottom) directions. Note: deflection was the controlled variable.....82

4.1 Dynamic flexural modulus as a function of cycles to near failure.

Maximum deflection was 3.973 x 10^{-3}in. (0.10mm).....88

4.2 Dynamic flexural modulus as a function of cycles to near failure.
Maximum deflection was 5.906 x 10^{-3}in. (0.15mm).....91

4.3 Dynamic flexural modulus as a function of cycles to near failure.
Maximum deflection was 7.874 x 10^{-3}in. (0.20mm).....93

4.4 Dynamic flexural modulus as a function of cycles to near failure.
Maximum deflection was 9.843 x 10^{-3}in. (0.25mm).....96

4.5 Dynamic flexural modulus as a function of cycles to near failure.
Maximum deflection was 11.024 x 10^{-3}in.(0.28mm).....100

4.6 Dynamic flexural modulus as a function of cycles to near failure.
Maximum deflection was 11.811 x 10^{-3}in. (0.30mm).....102

4.7 Dynamic flexural modulus as a function of cycles to near failure.
Maximum deflection was 3.973 x 10^{-3}in. (0.10mm).....105

4.8 Dynamic flexural modulus as a function of cycles to near failure.
Maximum deflection was 5.906 x 10^{-3}in. (0.15mm).....107

4.9 Dynamic flexural modulus as a function of cycles to near failure.
Maximum deflection was 7.874 x 10^{-3}in. (0.20mm).....110

4.10 Dynamic flexural modulus as a function of cycles to near failure.
Maximum deflection was 9.843 x 10^{-3}in. (0.25mm).....113

4.11 Dynamic flexural modulus as a function of cycles to near failure.
Maximum deflection was 11.024 x 10^{-3}in. (0.28mm).....116

4.12 Dynamic flexural modulus as a function of cycles to near failure.
Maximum deflection was 11.811 x 10^{-3}in. (0.30mm).....119

LIST OF TABLES

Table		Page
2.1	Fracture strength and maximum strain at fracture for a static, uniaxial tensile test for the (3) specimens tested for the transverse and axial directions respectively	**15**
2.2	Average strain (lateral and axial) values and respective uniaxial stress for the *transverse* strain-bar. The lateral and axial strain values were averaged from the raw data in Table 2.3	**26**
2.3	Load-Strain (axial and lateral) data for the *transverse* strain-bar to determine Young's (elastic) modulus, E and Poisson's ratio,v	**27**
2.4	Average strain (lateral and axial) values and respective uniaxial stress for the *axial* strain-bar. The lateral and axial strain values were averaged from the raw data in Table 2.5	**28**
2.5	Load-Strain (axial and lateral) data for the *axial* strain-bar to determine Young's (elastic) modulus, E and Poisson's ratio,v	**29**
2.6	Static Flexural Bending Test results	**35**
2.7	Typical 3-point static-loading (load-unload-reload) data for the transverse specimen 15AB	**37**
2.8	Typical 3-point static-loading (load-unload-reload) data for the axial specimen 16TB	**39**
3.1	Stress-Life (S-N) data from the cyclic-bending study for the transverse specimens. The model stress was reduced from actual stress data	**69**
3.2	Stress-Life (S-N) data from the cyclic-bending study for the axial specimens. The model stress was reduced from actual stress data	**70**
3.3	Elastic modulus and stress data for strain-life analysis of transverse specimens	**73**

transverse specimens....73

3.4 Strain-Life (ε-N_f) data from cyclic-bending study for transverse specimens. The model strain data was reduced from the Strain-Life models, with and without mean stress effects....74

3.5 Elastic modulus and stress data for strain-life analysis of axial specimens....75

3.6 Strain-Life (ε-N_f) data from cyclic-bending study for axial specimens. The model strain data was reduced from the Strain-Life models, with and without mean stress effects....76

3.7 Deflection-Life (δ-N_f) data for transverse specimen orientation. The $\Delta\delta$ / 2 model data was reduced from a power-law, (δ-N_f), Eq.(3.16)....83

3.8 Deflection-Life (δ-N_f) data for axial specimen orientation. The $\Delta\delta$ / 2 model data was reduced from a power-law, (δ-N_f), Eq.(3.16)....84

4.1 Elastic modulus data as a function of cyclic interval for the transverse specimen (1AB) with a maximum deflection of 3.973 x 10^{-3}in. (0.10mm)....89

4.2 Elastic modulus data as a function of cyclic interval for the transverse specimen with a maximum deflection of 5.906 x 10^{-3}in. (0.15mm)....92

4.3 Elastic modulus data as a function of cyclic interval for the transverse specimen's 4AB, 10AB & 13AB with a maximum deflection of 7.874 x10^{-3}in (0.20mm)....95

4.4 Elastic modulus data as a function of cyclic interval for the transverse specimen 6AB, 7AB &12AB with a maximum deflection of 9.843 x10^{-3}in. (0.25mm)....97

4.5 Elastic modulus data as a function of cyclic interval for the transverse specimen 11AB, with a maximum deflection of 11.024 x 10^{-3}in. (0.28mm)....101

4.6 Elastic modulus data as a function of cyclic interval for the transverse specimen 8AB & 9AB, with a maximum deflection of 11.811 x10^{-3}in. (0.30mm)....104

4.7 Elastic modulus data as a function of cyclic interval for the axial specimen 1TB, with a maximum deflection of 3.973 x

10^{-3}in. (0.10mm)....106

4.8 Elastic modulus data as a function of cyclic interval for the axial specimen 2TB, with a maximum deflection of 5.906 x 10^{-3}in. (0.15mm)....107

4.9 Elastic modulus data as a function of cyclic interval for the axial specimen's 2ATB with a maximum deflection of 7.874 x10^{-3}in. (0.20mm)....111

4.10 Elastic modulus data as a function of cyclic interval for the axial specimen 3TB, 5TB, 12TB &17TB, with a maximum deflection of 9.843 x10^{-3}in. (0.25mm)....114

4.11 Elastic modulus data as a function of cyclic interval for the axial specimen 10TB, with a maximum deflection of 11.024 x 10^{-3}in. (0.28mm)....117

4.12 Elastic modulus data as a function of cyclic interval for the axial specimen 7TB & 8TB, with a maximum deflection of 11.811 x10^{-3}in. (0.30mm)....120

CHAPTER 1

INTRODUCTION

1.1 A STRUCTURAL COMPOSITE

A structural composite can be defined as a load-bearing material in which physically distinct phases, (usually particulates or fibers), are introduced into the matrix to achieve improved properties for the combined material (1). A primary driving force for composite development has been to provide materials with a specific strength and stiffness greater than conventional, single-phase materials.

1.2 PROBLEM OUTLINE

Metal matrix composites (MMC) have become greatly diversified over the past few years. MMC's provide the opportunity to combine ductility and relative ease of manipulation of metals with the higher strength/stiffness and low density of ceramic reinforcement. In aluminum MMC's, SiC particle reinforcement predominates (1). The composites market has grown at such a rate that the materials research community has not had a chance to create, or agree on, standardized testing methods for (MMC) composites. The manufacturing companies have had to rely instead upon already existing

techniques to test, analyze and evaluate MMC's. These test procedures were initially created and intended for use on monolithic, near-isotropic material. This type of testing and evaluation can lead to invalid results. Therefore, without appropriate and widely accepted test methods, one cannot generate the level of data base required (1) for industrial use.

Nearly all of the MMC has been evaluated only in the preferred, or extruded direction. The discontinuously reinforced aluminum composites have been most frequently exploited (2-5), since they have the advantage that they can be generated by a wide range of well established primary processing techniques (6-9) (e.g. casting, powder processing, spray forming),with the material subsequently being converted into product form,where necessary, by conventional secondary processing,(such as forging, rolling, extrusion, machining, etc.). Antithetically, production of continuously reinforced composites is extremely labor intense and almost exclusively limited to defense applications and the aerospace industry.

Given increasing popularity of MMC's, it is pertinent that extensive testing be done initially in the machine (axial) direction and transverse to the axial direction. This testing will establish a material properties database for the two critical (principal) directions. An MMC material property database will give the designer/technician a best-worst scenario of the MMC. Ultimately MMC's will be evaluated along several angles between the two principal directions. This type of MMC evaluation and subsequent database is essential to understand the potential of an MMC per direction. This type of investigation is

essential if the industrial community is to recognize MMC's as the wave of the future, and more than just a substitute for a single-phase, near-isotropic metal. A detailed database will give the MMC community a fundamental understanding of the material characteristics and allow the designer a greater range of application, resulting in more for the end-users money.

1.3 OBJECTIVES AND SCOPE

The main objectives in this study are:

(a) To test and evaluate the static mechanical properties of the MMC using experimental techniques. The monotonic tensile, bending and shear properties were to be measured. These properties were measured along both the axial (machine) direction and transverse to the axial direction. The rationale for testing along the above mentioned directions is to determine if the material is isotropic, and if not, type of anisotropy.

(b) To qualitatively gain insight into the reliability of the MMC subjected to mechanical fatigue per deflection-level. Also, to obtain a comparison of the fatigue life in the axial (preferred) direction relative to the transverse direction. Therefore, several deflection-controlled, cyclic-bending tests were performed on the MMC specimens at various deflection levels for the axial and transverse directions.

1.4 APPROACH TO THE PROBLEM

The mechanical properties and stress-strain response in MMC's with discontinuous reinforcements are difficult to characterize relative to a single-phase, isotropic metal (e.g. aluminum or structural steel). The parameters affecting the composite material properties and reliability can be divided into three groups:

1. Process parameters
   a. primary process technique (e.g. powder, casting, spray forming)
   b. secondary process technique (e.g. extrusion, rolling, forging)
   c. post-processing technique (e.g. heat treating, artificial aging)

2. Material parameters
   a. reinforcement form (whisker, fiber or particulate)
   b. reinforcement volume fraction
   c. reinforcement surface treatment
   d. reinforcement type (e.g. SiC, alumina, etc.)
   e. matrix type (e.g. aluminum, titanium, etc.)

3. Machining parameters - This parameter describes basically the location or orientation from which the test specimen is cut or machined,(with respect to the extrudate), and ultimately evaluated. This orientation is described by the nomenclature used in the Standard Test Method for Plain-Strain Fracture Toughness, (ASTM E 399) (4).

The best, or most consistent, technique for machining specimens from rolled MMC or extruded MMC stock is along one of the three orthogonal axes. These are defined in the ASTM E 399 standard as; L (longitudinal or extruded direction), T (long transverse direction or width) and S (short transverse direction or thickness). The specimens for this study were machined along the axial or longitudinal axes and transverse to the longitudinal axes. Figure 1.1 clearly shows these two principal directions relative to the typical MMC extrudate.

A major problem in MMC load-bearing applications is that the material properties are a function of several parameters, unlike monolithic metals. Although MMC's look similar to single-phase metals at the surface, they respond completely different. Some MMC producers are claiming that their MMC's are "as isotropic as aluminum",(e.g. Advanced Composite Materials Corp. Vice-President), or evaluting the MMC along only the "preferred-axis". This study will characterize a SiC/Al MMC in a way that the end-user can maximize it's physical potential relative to the two critical axes. Evaluating the MMC as it rightly deserves will give rise to more accurate and suitable applications for the MMC. Ultimately the demand for such material will rise, reducing the final cost of the MMC to the end-user. Since ignorance has no place in specialized materials such as MMC's, it is essential to initially qualify and ultimately quantify the MMC's material properties. It is this type of rigorous evaluation that will maximize a specific MMC's potential, while minimizing the dangerous underengineering which can result from invalid properties.

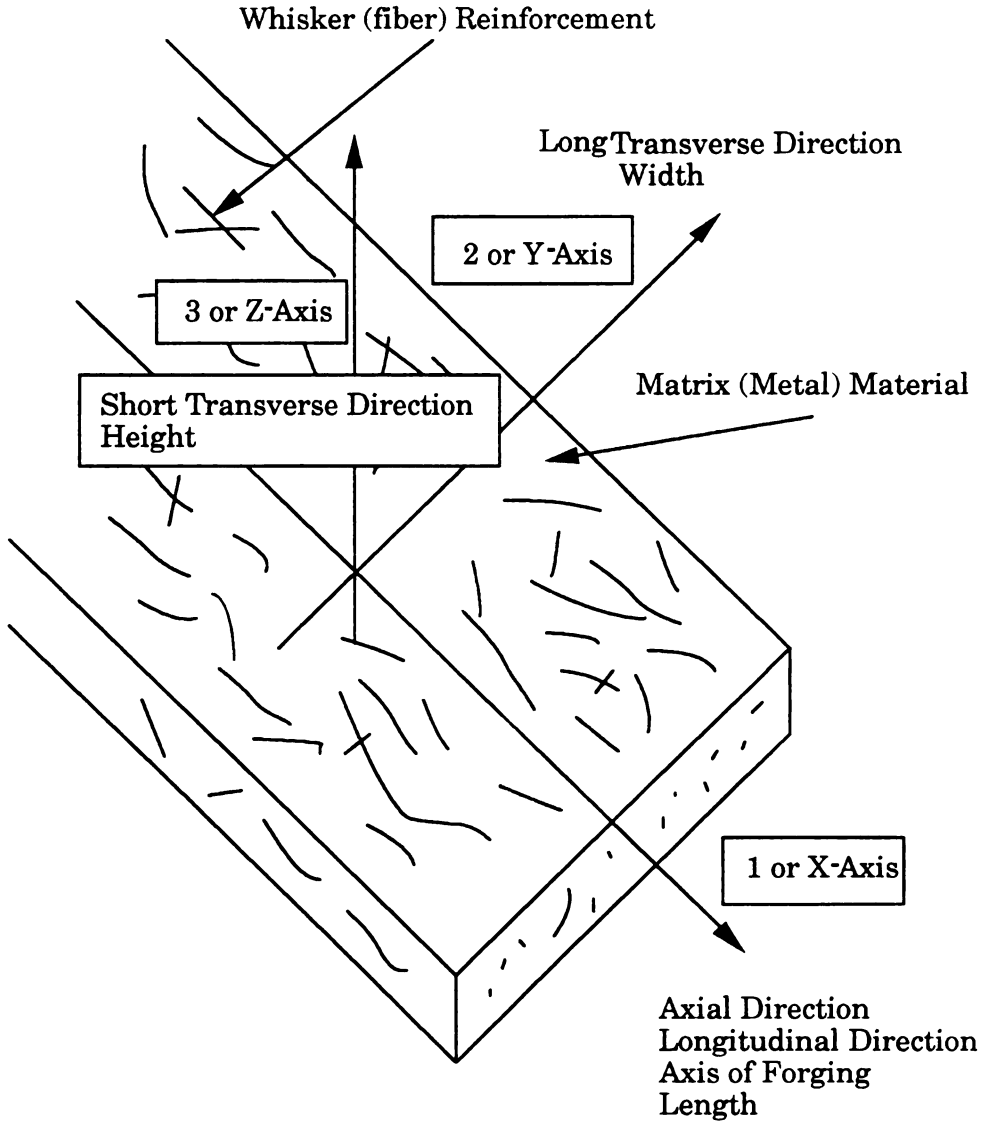

Figure 1.1 Typical Metal-Matrix (MMC) Extrudate form and the reference axes.

CHAPTER 2

STATIC CHARACTERIZATION OF THE MMC

The material used in this investigation was a silicon carbide whisker-reinforced (SiC_w) aluminum metal-matrix composite, supplied by Advanced Composite Materials Corp. (ACM), in extrudate form. The MMC extrudate was approximately 3'x 6"x 3/4". The ANSI standard for this material is 2009-SiC-15W-T8. The reinforcements were 15% by volume. The average whisker diameter was 1/2 μmeter and an average whisker aspect ratio s (length/diameter) of 8-12.

2.1 INTRODUCTION

This chapter entails experimental test procedure, experimental set-up, results and discussion of the Al/SiC MMC, for both transverse and axial orientations.

The static characterization tests, i.e. Chapter 2, were not mandatory since the "material properties" for the MMC were obtained from the manufacturer, Advanced Composite Materials Corp. (ACM). There was one problem, the material properties communicated by ACM were nearly-isotropic. The representative from ACM stated that, "although no material is truly isotropic, it [the MMC] is as isotropic as aluminum." It was this type of thinking that prompted the testing of the static material properties.

2.2 SEM EVALUATION OF THE PRINCIPAL PLANES OF THE MMC EXTRUDATE

Before testing was initiated, the 3 principal planes of the MMC extrudate were examined with a scanning electron microscope (SEM). The two principal planes to be investigated, the X-Z plane and the Y-Z plane are illustrated in Figure 2.1. These two planes correspond to the axial direction and (long) transverse direction, respectively. (See Figure 1.1 for specific axes coordinates). Qualitatively speaking, in Figure 2.1, the SiC whiskers resemble a row of cylinders. If Figure 2.1B represents a side view of the cylinders, then Figure 2.1A represents a front or back view of the same cylinders, which appear as circles or dots.

Figure 2.2A shows another micrograph normal to the X-Z plane, which is along the axial direction Figure 2.2B provides a micrograph normal to the X-Y plane, an airplane view of the axial direction. Figures 2.1 and 2.2 follow the same "cylinder" idea, where the primary direction of the whiskers is also the flow direction of the extrudate. Although this "idea" may sound obvious, this SEM investigation was necessary so any discrepancies between the properties ACM provided and the material properties measured at Michigan State could be rationalized. The micrographs strongly suggest an anisotropic composite, or at best an orthotropic composite. The microstructure of this MMC does not remotely resemble the microstructure of a single-phase, isotropic aluminum.

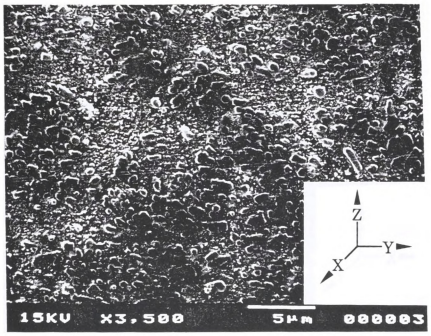

A

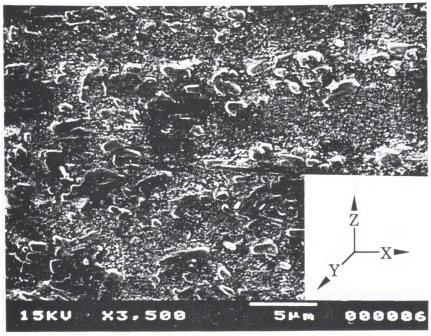

B

Figure 2.1 The top micrograph (A) illustrates the whisker/matrix relation along the Y-Z plane, this corresponds to the transverse direction. The bottom micrograph (B) illustrates the whisker/matrix relation along the X-Z plane, this corresponds to the axial direction.

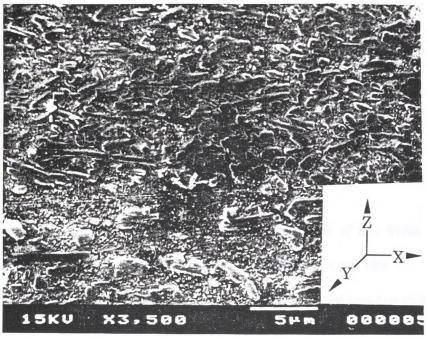

A

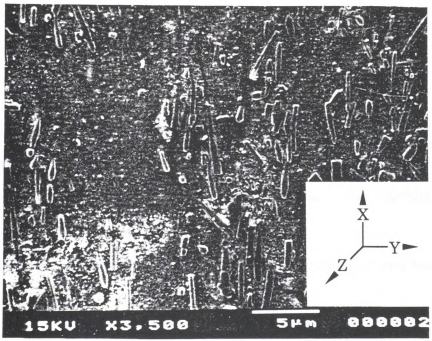

B

Figure 2.2 The top micrograph (A) illustrates the whisker/matrix relation along the X-Z plane of the extrudate, this corresponds to the axial direction. The bottom micrograph (B) illustrates the X-Y plane and corresponds to a top view of the axial direction, (the Z-axis is normal to micrograph).

The directions of the MMC to be evaluated are parallel to the X-Z plane and the Y-Z plane, or the axial and (long) transverse direction respectively.

2.3 MONOTONIC TENSILE TEST

2.3.1 Experimental procedure

The test procedure used to measure the tensile properties of the MMC was ASTM designation D 3552 - 77 (11). This test method covers the determination of the tensile properties of metal-matrix composites reinforced by continuous and discontinuous high-modulus fibers. The method applies only to specimens tested in the direction of the reinforcement and normal to the direction of reinforcement.

The test specimens were machined on an electrical discharge machine (EDM) and tested in an as-received condition. The reason for using the EDM was to minimize the chance for abrading of the whiskers near the surface and creating superficial stress raisers. The test specimens were cut in the machine, or axial direction and transverse to this direction.
A sketch of the specimen dimensions can be seen, for the axial and transverse orientations, in Figure 2.3.

The testing machine used was a closed-loop, servo-hydraulic Material Testing Systems (MTS) machine. The testing machine was interfaced with a digital computer that collected the elastic-plastic stress-strain test data.

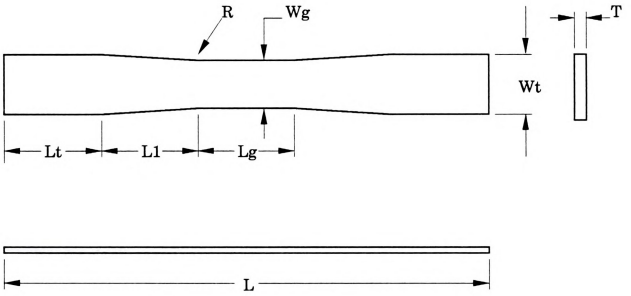

Dimensions are in inches unless otherwise specified.

Orientation	L	Lt	L1	Lg	Wg	R	T	Wt
Axial	5	1.00	1.00	1.00	0.375	1.0	0.125	0.625
Transverse	3	0.75	0.25	1.00	0.250	0.5	0.125	0.500

Figure 2.3 Flat Tension Specimen Design for Standard Test Method (ASTM D 3552-77) for Tensile Properties of Fiber-Reinforced Metal-Matrix Composites.

Initially resistance strain gages (RSG) were mounted on the tensile bars to measure (axial) strain. The RSG's tended to pop off the test specimens before the tensile test was completed, therefore it was decided to use an extensometer to measure strain.

2.3.2 Results

Table 2.1 gives the fracture strength and the maximum strain for the three specimens tested along the transverse and axial directions. The average ultimate tensile strength (UTS) along the transverse direction was **54,242 psi** and approximately **71,987 psi** for the axial direction.

Figure 2.4 clearly illustrates that the failures were brittle and the yield strengths and UTS were nearly equal. The typical tensile specimen for the transverse direction had a σ_{yield}**= 46,656 psi.** The typical tensile specimen for the axial direction had a σ_{yield}**= 67,500 psi.** In short, the stress-strain curve was primarily elastic with minimal yielding (less than 1% neckdown) at failure.

The UTS that ACM reported was **88,000 psi** for the transverse direction and **95,000 psi**, for the axial direction. Therefore the UTS's reported by ACM for the transverse direction and the axial direction were **32%** and **62%** greater than the values measured. This test was a clear indication of the importance of testing the MMC independently, before trusting the test results of an outside source.

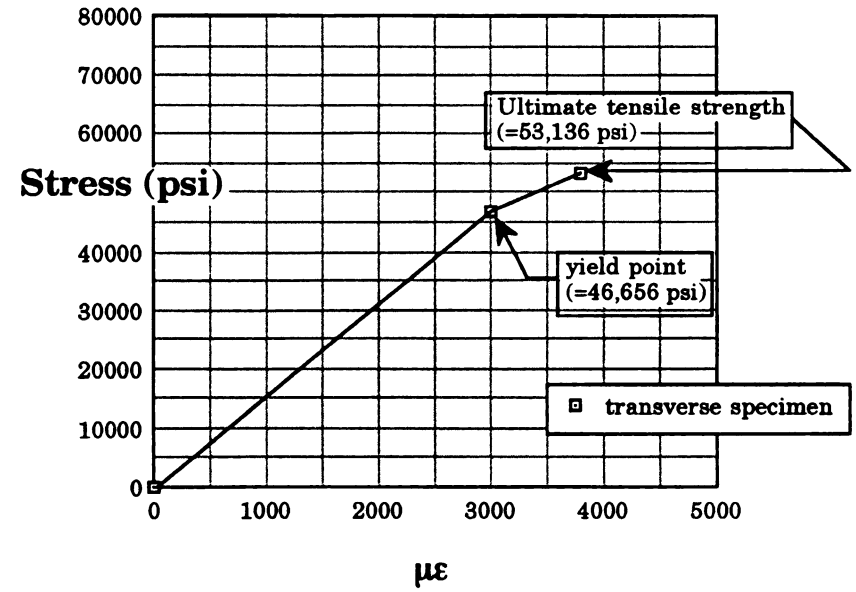

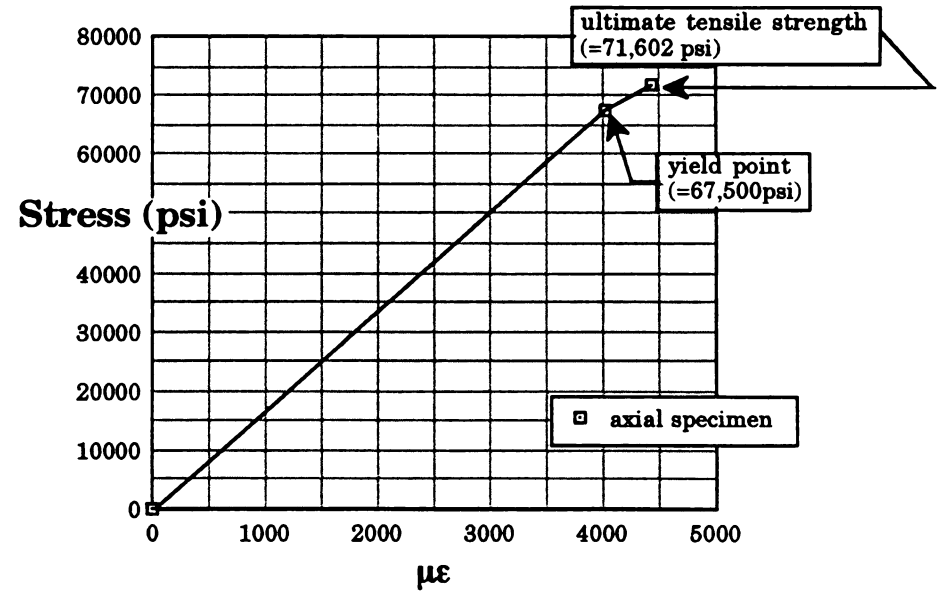

Figure 2.4 Typical Stress-Strain plots of the static tension tests for the Transverse (top) specimen and Axial (bottom) specimen directions respectively.

Table 2.1 Fracture strength and maximum strain at fracture for a static, uniaxial tensile test for the (3) specimens tested for the transverse and axial direction respectively.

nominal cross-sectional area = 3.125 x 10^{-2} $in.^2$

Specimen Number	Ultimate Tensile Strength, UTS (psi)	Maximum Strain at Fracture, ε_{max} ($\mu\varepsilon$)
T1	54,640	3940
T2	54,949	4105
T3	53,136	3800
	UTS_{avg}=54,242	

nominal cross-sectional area = 4.688 x 10^{-2} $in.^2$

Specimen Number	Ultimate Tensile Strength, UTS (psi)	Maximum Strain at Fracture, ε_{max} ($\mu\varepsilon$)
A1	71,602	4437
A2	72,571	5204
A3	71,787	4506
	UTS_{avg}=71,987	

The most obvious observation was that the tensile specimens transverse to the axial direction failed in shear. The tensile specimens machined along the longitudinal axis failed in tension, although the fracture surface was not plane-normal to the load axis, as would be expected with single-phase aluminum. The failure surface was jagged and random. This type of failure can be accounted for due to the SiC whisker reinforcements arresting and resisting crack growth after the aluminum matrix had failed.

Another general observation, for both orientations, was that the failures were brittle and catastrophic. This behavior is not desired and gives very little indication of calamitous failure,(e.g. no plastic yielding). Elastic failure is normally undesired for load-bearing applications. This is especially so when the safety factors approach 1.0, (e.g. fighter jet turbines or airframes). This condition initially sounds malignant, although failure can usually be predicted accurately if the mechanical properties, static and dynamic, are accurately known. Process techniques are of cardinal importance for an MMC or any composite, since it is these steps that ultimately determine the mechanical, electrical and chemical properties of a composite.

2.4 POISSON'S RATIO, ν AND YOUNG'S MODULUS, E

2.4.1 Experimental procedure

Since material conservation was a significant factor, it was hoped that some MMC material that had been machined could be used to determine Poisson's ratio and Young's modulus. Thus, leaving the virgin extrudate for the primary

research.

Rectangular bars had been machined (EDM) previous to my arrival and then never used. Several bars had been machined along both the axial direction and the transverse direction. The bar's dimensions were approximately 4"x 1"x 0.25". It was decided that with slight modifications these bars could be used to experimentally determine Poisson's ratio and Young's modulus for the two principal directions.

Resistance strain gages (RSG's) were mounted on the bars along the long axis and transverse to this axis. The RSG's were obtained from MicroMeasurements, gage type EA-13-060LZ-120. These gages were mounted as close to the center (w.r.t the length and width axis) as physically possible. The significance of mounting the gages so near the centroid (excluding depth) was to eliminate edge effects, such as Saint Venant's effect (12), especially near the vicinity of where the load frame fastens to the specimen. This mounting location can be schematically seen in Figure 2.5. This mounting was done along the top and bottom, relatively speaking, to account for, and cancel effects due to bending. Had the specimens been very thin (e.g. 1/16") then a single set of gages would have been sufficient. This procedure was performed for both axial and transverse specimen directions.

The load frame used was a mechanical MicroMeasurements load frame with a 2000 pound load cell. Figure 2.7 shows the load-frame and actual specimen load configuration.

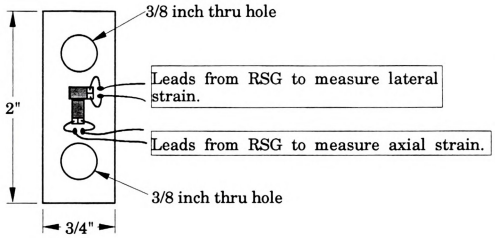

Figure 2.5 Schematic of strain-bar's dimensions and strain gage (RSG) configuration.

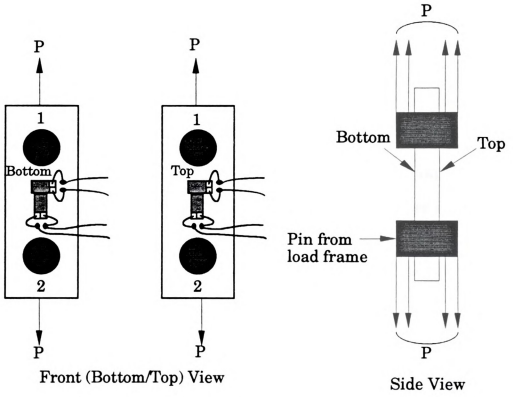

Figure 2.6 Schematic showing labeling configuration and loading technique. Note the ease with which bending can occur.

The load cell was connected to a strain indicator calibrated to read out in pounds. An additional strain indicator, with a switch-and-balance box, was used to connect the four strain gages per bar. Before any strain data was recorded, the strain gages were cycled (loaded) approximately five times. This was to account for any gage conditioning that often occurs during the first few loadings applied to new RSG's and contributes to extraneous values (pseudo-strain) and zero-load drift.

There was one strain bar per orientation, (i.e. 1 axial and 1 transverse). Each bar was loaded from 0 lbs. to 1400 lbs. in increments of 200 lbs. The strain indicator was also checked and zeroed after each loading interval to re-balance the bridge. The strain-bars were loaded twice for each of the four positioning orientations. There were four positioning orientations, (1T,1B,2T & 2B), were w.r.t. the top front of the load frame shown in Figure 2.6.

The reason for several collections of data was to arrive at a valid, average value for Poisson's ratio and Young's modulus, since these material constants are used to model and describe most materials. Accurate values were also of cardinal importance since an MMC was being characterized; the level and type of anisotropy, (e.g. orthotropy) needed to be known.

2.4.2 Sample Calculations

Poisson's ratio is a unitless elastic constant relating the lateral strain to the axial strain by the following expression;

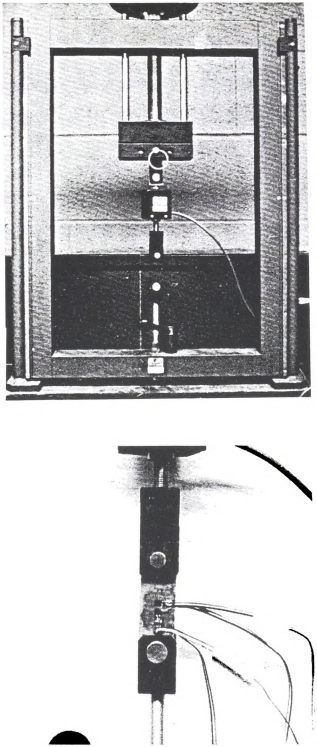

Figure 2.7 MicroMeasurements Load-Frame (top) used to load the "Strain-Bars" and the actual load configuration (bottom). Notice 4 sets of lead wires, i.e. 2 RSGs per side.

ν = -lateral strain/ axial strain [2.1]

This strain, lateral and axial, for a typical test are plotted as a function of load for both the transverse and axial specimens in Figures 2.8 a and b respectively. The Poisson's ratio,ν is also included for illustration.

Young's (elastic) modulus is simply the gradient of a linear elastic stress - strain curve from the fundamental relation;

$$\mathbf{E} = \sigma/\varepsilon \qquad [2.2]$$

where,

E = Young's modulus, psi

σ = tensile stress, psi

ε = tensile (axial) strain, $\mu\varepsilon$

load must be converted to stress from the fundamental relation;

$$\sigma = \mathbf{P/A} \qquad [2.3]$$

where,

σ = uniaxial stress, psi

P = applied load, lbs

A = cross-sectional area, $in.^2$

Axial strain was experimentally determined from the strain gages (RSG's) that were mounted on the strain-bars. Figure 2.9 gives the elastic stress - strain behavior and Young's modulus for both the transverse and axial bars.

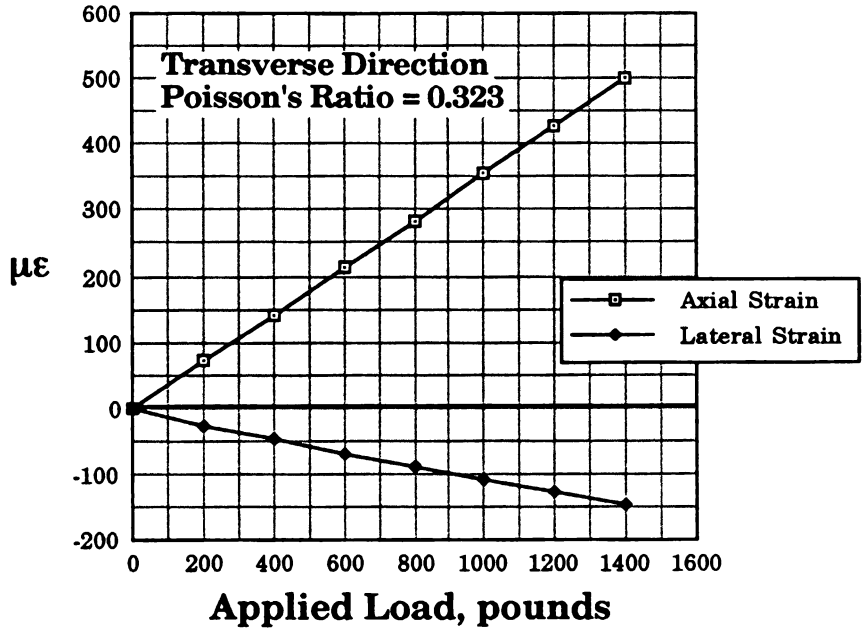

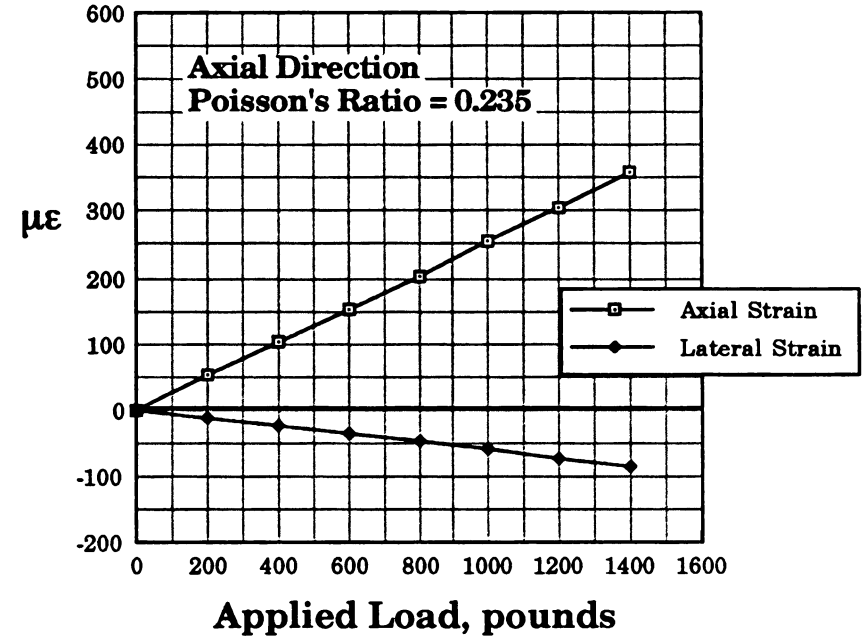

Figure 2.8 Typical load-strain plots for the transverse (top) and axial (bottom) specimens with Poisson's ratio.

2.4.3 Results

Tables 2.3 and 2.5 list the raw load-strain data, parallel and normal to the loading axis, for the transverse strain bar and axial strain bar, respectively. The strain was recorded for both gages per bar side, for each of the four specimen orientations previously mentioned in the procedure,(see Figure 2.5 for RSG schematic and Figure 2.6 for the (4) loading orientations). This loading was performed twice per loading orientation and both strain values are included in the tables.

Tables 2.2 and 2.4 give the applied load, applied uniaxial stress, σ and averaged axial strain, ε_a and averaged lateral strain, ε_l. The axial and lateral median strains are also included, below the respective axial and lateral strains, in brackets. If the median strain (lateral and axial) is relatively close to the corresponding averaged strain (lateral and axial) then this would lend considerable credibility to the averaged strains. Tables 2.2 and 2.4 show this trend to be true. Poisson's ratio,ν is given for each load plus an overall average ν for both specimen directions. Figures 2.8 a & b show the axial and lateral strain plotted as a function of applied load, for the transverse and axial strain bar respectively. The axial and lateral gages were assumed to be mounted coincident to the principal directions and the loading uniaxial. The axial and lateral strain were the maximum and minimum principal strains respectively, (i.e. $\varepsilon_a = \varepsilon_1$ & $\varepsilon_l = \varepsilon_2$).

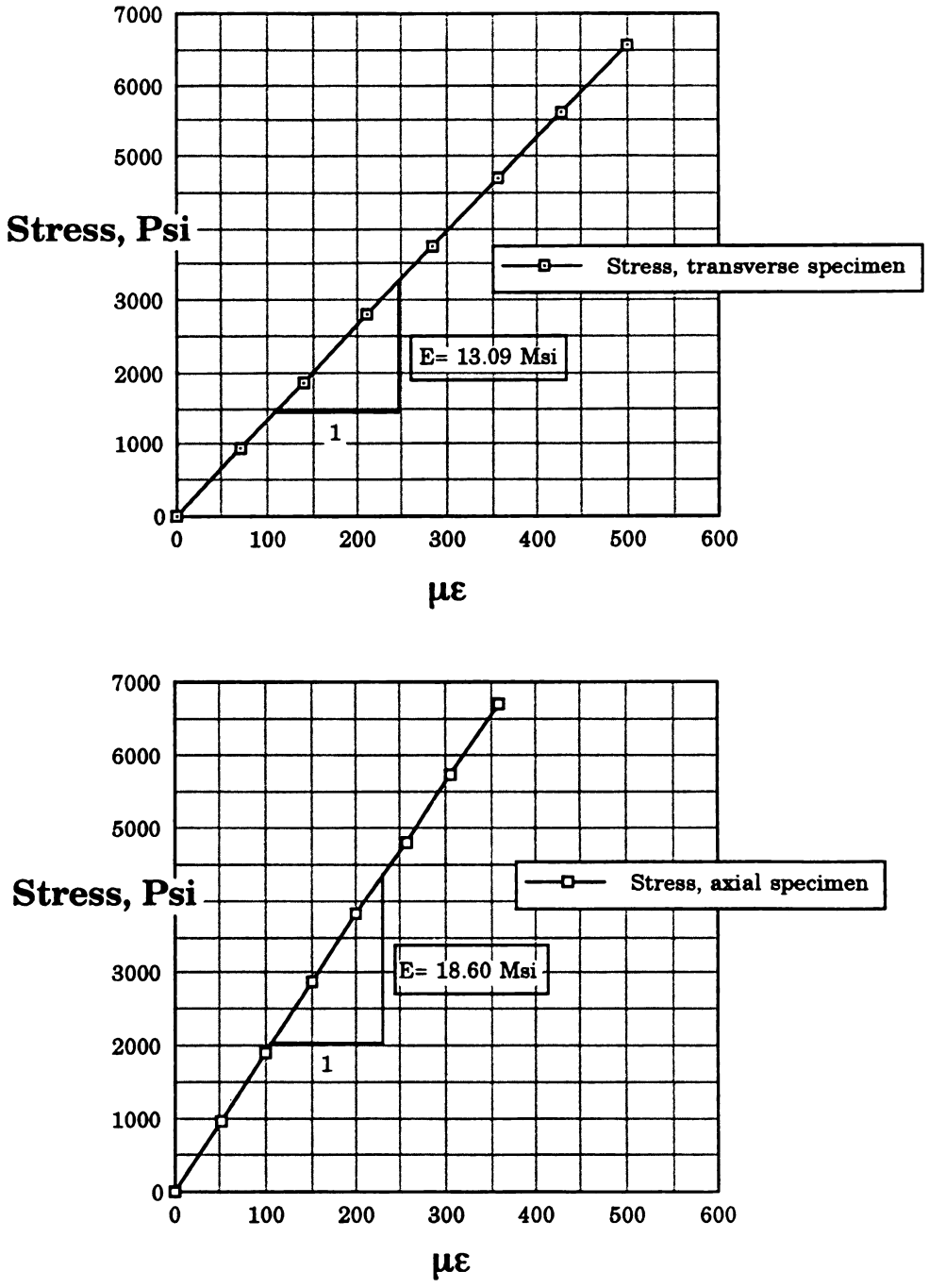

Figure 2.9 Elastic stress-strain graphs for the transverse (top) and axial (bottom) specimens with Young's modulus.

Poisson's ratio was simply, by Eq. [2.1], the negative of the lateral strain divided by the axial strain. Figures 2.9 a and 2.9 b illustrate the stress-strain behavior of the strain bars. A linear regression was performed on the stress-strain data of the transverse and axial strain-bars. From this regression an elastic modulus was determined for the transverse and axial directions. The linear regression yielded a correlation coefficient of 1.00 for both the axial and transverse directions.

The experimental results were as follows:

for the axial specimen, E_1 = 18.60 Msi and ν_{12} = 0.235.

for the transverse specimen, E_2 = 13.09 Msi and ν_{21} =0.323.

Table 2.2 Average strain (lateral and axial) values and respective uniaxial stress for the *transverse* strain-bar. The lateral and axial strain values were averaged from the raw data in Table 2.3.

cross-sectional area = 2.132×10^{-1} in^2

Applied Load (Lbs.)	Uniaxial Stress, σ (Psi)	Average Axial Strain [median] $\mu\varepsilon$	Average Lateral Strain [median] $\mu\varepsilon$	Poisson's Ratio, ν
0	~ 0	~ 0	~ 0	~ 0
200	938.1	69.9 [70.0]	-26.8 [-27.0]	0.383
400	1876.2	140.6 [140.5]	-47.8 [-48.5]	.340
600	2814.3	212.1 [211.0]	-68.8 [-69.5]	.324
800	3752.3	284.0 [284.0]	-89.4 [-86.0]	.315
1000	4690.4	355.9 [357.0]	-109.1 [-105.5]	.307
1200	5628.5	427.6 [428.5]	-128.1 [-123.5]	.300
1400	6566.6	499.4 [499.0]	-147.1 [-143.0]	.295
				avg. ν = 0.323

Table 2.3 Load-Strain (axial & lateral) data for the *transverse* strain-bar to determine Young's (elastic) modulus, E and Poisson's ratio, ν.

Orientation *1T*

Applied Load (Lbs.)	Gage #5 Axial Strain, με	Gage #6 Lateral Strain, με	Gage #7 Axial Strain, με	Gage #8 Lateral Strain, με
0	~ 0	~ 0	~ 0	~ 0
200	12 / 10	-3 / -12	125 / 135	-44 / -46
400	42 / 33	-12 / -18	236 / 253	-79 / -81
600	84 / 74	-36 / -29	340 / 357	-109 / -112
800	140 / 125	-53 / -43	428 / 448	-134 / -140
1000	195 / 184	-68 / -59	512 / 537	-158 / -167
1200	245 / 241	-74 / -73	620 / 617	-186 / -186
1400	298 / 302	-86 / -88	708 / 698	-211 / -207

Orientation *2T*

0	~ 0	~ 0	~ 0	~ 0
200	50 / 52	-24 / -24	92 / 89	-31 / -29
400	132 / 125	-51 / -47	148 / 158	-46 / -50
600	217 / 199	-76 / -71	204 / 227	-61 / -69
800	311 / 292	-106 / -100	257 / 276	-76 / -83
1000	381 / 373	-126 / -125	328 / 334	-96 / -98
1200	467 / 460	-153 / -151	379 / 394	-110 / -115
1400	535 / 538	-172 / -174	457 / 459	-132 / -134

Orientation *1B*

0	~ 0	~ 0	~ 0	~ 0
200	56 / 36	-30 / -17	78 / 108	-28 / -35
400	111 / 76	-45 / -27	170 / 203	-55 / -63
600	165 / 130	-61 / -42	256 / 293	-79 / -88
800	216 / 182	-75 / -55	344 / 387	-105 / -116
1000	271 / 238	-87 / -69	433 / 477	-131 / -141
1200	335 / 290	-104 / -83	521 / 559	-155 / -165
1400	401 / 358	-118 / -100	593 / 642	-172 / -188

Orientation *2B*

0	~ 0	~ 0	~ 0	~ 0
200	58 / 59	-28 / -26	78 / 81	-26 / -25
400	146 / 135	-56 / -50	134 / 147	-40 / -44
600	224 / 205	-79 / -70	197 / 222	-55 / -64
800	300 / 276	-100 / -89	270 / 292	-74 / -82
1000	377 / 348	-121 / -109	340 / 366	-91 / -102
1200	438 / 418	-137 / -127	419 / 439	-112 / -120
1400	507 / 497	-154 / -149	497 / 506	-132 / -137

Table 2.4 Average strain (lateral and axial) values and respective uniaxial stress for the *axial* strain-bar. The lateral and axial strain values were averaged from the raw data in Table 2.5.

cross-sectional area = 2.091 x 10^{-1} in^2

Applied Load (Lbs.)	Uniaxial Stress, σ (Psi)	Average Axial Strain [median] με	Average Lateral Strain [median] με	Poisson's Ratio, ν
0	~ 0	~ 0	~ 0	-
200	956.5	50.6 [49.0]	-12.1 [-13.0]	0.239
400	1913.0	101.0 [93.0]	-23.6 [-23.0]	.234
600	2869.4	151.3 [150.0]	-35.4 [-33.5]	.234
800	3825.9	202.3 [204]	-47.4 [-45.5]	.234
1000	4782.4	255.8 [261.0]	-58.3 [-58.0]	.228
1200	5738.9	306.2 [308.0]	-72.2 [-75.5]	.236
1400	6695.4	358.8 [356.5]	-85.2 [-84.0]	.237
				avg. ν = 0.235

Table 2.5 Load-Strain (axial & lateral) data for the *axial* strain-bar to determine Young's (elastic) modulus, E and Poisson's ratio, ν.

Orientation *1T*

Applied Load (Lbs.)	Gage #5 Axial Strain, με	Gage #6 Lateral Strain, με	Gage #7 Axial Strain, με	Gage #8 Lateral Strain, με
0	~ 0	~ 0	~ 0	~ 0
200	31 / 30	-4 / -5	71 / 74	-18 / -18
400	86 / 79	-13 / -17	133 / 125	-30 / -29
600	139 / 137	-26 / -30	182 / 168	-42 / -37
800	193 / 193	-36 / -44	233 / 215	-52 / -47
1000	244 / 246	-48 / -55	295 / 276	-66 / -61
1200	284 / 289	-58 / -64	352 / 340	-79 / -75
1400	324 / 331	-67 / -75	425 / 407	-96 / -91

Orientation *2T*

0	~ 0	~ 0	~ 0	~ 0
200	46 / 40	-16 / -14	52 / 53	-11 / -12
400	104 / 93	-31 / -25	90 / 93	-18 / -21
600	175 / 161	-48 / -43	117 / 124	-24 / -26
800	230 / 232	-61 / -61	153 / 148	-31 / -31
1000	293 / 295	-76 / -76	188 / 190	-38 / -38
1200	343 / 346	-91 / -90	233 / 236	-49 / -50
1400	396 / 397	-104 / -105	285 / 277	-61 / -60

Orientation *1B*

0	~ 0	~ 0	~ 0	~ 0
200	10 / 9	4 / 4	89 / 92	-25 / -25
400	46 / 42	-7 / -6	151 / 157	-40 / -41
600	98 / 91	-20 / -16	199 / 206	-51 / -52
800	158 / 146	-36 / -32	244 / 254	-62 / -63
1000	217 / 206	-48 / -48	289 / 294	-71 / -71
1200	278 / 272	-64 / -68	325 / 328	-79 / -78
1400	348 / 347	-85 / -86	350 / 356	-83 / -83

Orientation *2B*

0	~ 0	~ 0	~ 0	~ 0
200	18 / 20	-1 / -7	87 / 87	-23 / -22
400	58 / 55	-12 / -16	151 / 153	-36 / -36
600	103 / 99	-25 / -28	214 / 208	-50 / -48
800	158 / 150	-40 / -42	268 / 262	-61 / -60
1000	222 / 218	-53 / -46	315 / 305	-70 / -68
1200	291 / 284	-84 / -76	356 / 342	-76 / -74
1400	358 / 357	-103 / -98	398 / 384	-83 / -82

2.5 FLEXURAL MODULUS AND BENDING STRENGTH

2.5.1 Experimental Procedure

A static 3-point test was performed on the SiC/Al MMC for both the axial and transverse directions. The nominal specimen dimensions were 1/4"x1/4" with a 2"span. A Servo-Hydraulic Instron (model 1320) materials testing machine was used to conduct the test. The 3-point fixture had an extensometer mounted to a mechanism mid-span, (Figure 2.10), which measured maximum deflection. The strain channel was used to control the machine, since deflection was the controlled-variable.

The extensometer had a maximum strain range of 10%, therefore the maximum deflection was 1 mm. The gage length was 1 cm (10mm). Each specimen was deflected in increments of 0.02mm (5% on LED meter) and the corresponding load was recorded. This loading was performed until the specimen failed. From this load-deflection data, both the elastic and plastic behavior are known. This test was performed for six specimens, three per axial direction and three per transverse direction.

Initially, using uniaxial data, it was calculated that approximately 0.5mm deflection, or 50% extensometer range, would create adequate stress to fracture for both the axial and transverse specimens. While conducting the tests, it was discovered that even 1mm deflection, or 100% , was not sufficient to induce specimen fracture for either the axial or transverse direction.

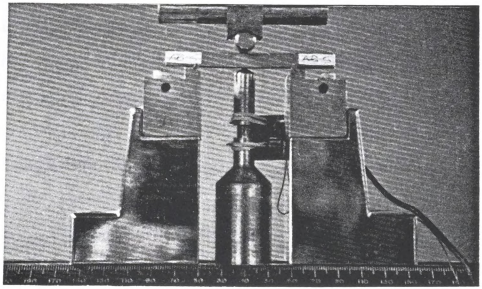

Figure 2.10 Fixture used for the static, 3-point bend test

Since 1mm deflection was the maximum range of the extensometer and the specimen didn't fail, it was decided to do the following for each static 3-point test: (1) load the specimen to 1mm or 100%, (2) unload the specimen to zero load and record the deflection reading on the LED meter, this would be the plastic (permanent) deflection and (3) after recording the plastic deflection, zero this channel and again perform test as stated previously until specimen fracture. From the second set of deflection-load data points the plastic deflection (step 2) had to be added to the deflection recorded from the LED. This procedure allowed the specimen to be deflected beyond 1mm, (maximum extensometer travel), and yet yielded valid elastic-plastic data.

2.5.2 Sample Calculations

For this test, the loads and deflections were recorded right off the LED meter on the Instron. The load was in pounds (English) and the deflection was in millimeters (SI). The deflection was converted to inches (English) to keep the data consistent. The English system was chosen arbitrarily.

From the elastic load-deflection data, the Flexural Modulus was computed from the following relation,

$$E = -PL^3/48\delta_e I \qquad [2.4]$$

Where,

P = applied load, lbs

L = span of specimen, in.

δ_e = elastic deflection, in.

I = moment of inertia, in.^{4}

E = flexural modulus, psi

After a few simple manipulations the previous expression reduced to the following equation,

$$\mathbf{E = 512\ P/\delta_e} \qquad [2.4']$$

This equation is now in a form where only the measured variables load, P and deflection, δ_e are needed to determine flexural modulus, E.

From the load-deflection data representative flexural bending strength could be determined from the flexural formula,

$$\sigma = \mathbf{MY/I} \qquad [2.5]$$

Where,

M = bending moment, in-lbs.

Y = distance from neutral axis to outer fiber, in.

I = moment of inertia, in.^{4}

σ = maximum bending stress (outer fiber), psi

After some data reduction, Eq.[2.5] reduced to the following expression for our specimen geometry;

$$\sigma = \mathbf{192(P)} \qquad [2.5']$$

From this expression, the only quantity that was experimentally required was the flexural load P, and the flexural stress could then be calculated.

2.5.3 Results

Note: The flexural strengths obtained for this test are *anomalous*. The test specimens failed after an appreciable amount of plastic deflection, thus violating the Flexural Formula, Eq.[2.5], which assumes linearly-elastic deflection. This will be addressed in the discussion.

Table 2.6 shows the anomalous flexural strength of the 3 specimens tested per orientation. The average anomalous flexural strength for the transverse and axial orientation was **89,012 psi** and **116,300 psi** respectively. Tables 2.7 and 2.8 list the discrete load-displacement data for two typical 3-point-static-bend specimens, along the corresponding transverse and axial directions. Figure 2.11 demonstrates the typical flexural load-deflection behavior of the SiC/Al MMC. The loading scheme was a load-unload-reload to fracture procedure, therefore the test consisted of essentially 2 cycles. Eventhough the load cycles were static, by the second cycle the material had already began to strain-harden (i.e. the flexural modulus E increased). This stiffening, or hardening, is clearly illustrated in Figure 2.11.

2.5.4 Discussion

The flexural strengths obtained for the axial and transverse were anomalous, due to the violation of the flexure formula. Since the deformation was largely plastic, the calculations for bending strength, Eq.[2.5], were much larger than the actual fracture stress. The reason for this is that the flexure formula

assumes linearly-elastic deformation, thus when the strength was determined the equation assumed the deformation was elastic. It is common knowledge that once a material begins to plasticly yield it takes much less stress to continue to deform the respective material. The monotonic stress-strain curve of the MMC was quasi-elastic for the tensile test, See Figure 2.4, thus it was assumed that this behavior would also follow for the static bend test. This was definitely not the case as can be seen in Figure 2.11. Since the plastic bending analysis is beyond the scope of this study, the flexural strengths in this section will simply be referred to as "anomalous".

The static flexural test yielded very interesting results. Besides measuring the flexural moduli,E and anomalous flexural strength, the test also showed the elastic-plastic behavior of 2 static cycles to fracture, per specimen direction. Normally, with a monolithic aluminum, the elastic load-deflection gradient of the second cycle would be nearly identical to that of the first cycle, therefore performing such a test would be redundant. Although, for the SiC/Al MMC this was not the case. The MMC exhibited very distinct behavior; the first cycle, (for both transverse and axial specimens), resembled that of a single-phase aluminum, where the *matrix* seemed to be resisting the load. The second cycle looked very similar to that of an elastic-perfectly plastic material, especially for the transverse specimen. Both the transverse and axial specimens flexural modulus increased approximately 4% on the second cycle, which is respectable.

The anomalous flexural strength for the transverse specimen was 50% greater than the respective transverse UTS and the anomalous flexural strength for

Table 2.6 Static Flexural Bending Test results.

Specimen Number	Specimen Orientation	Anomolous Flexural Strength psi
15AB	Transverse	84,864
18AB	Transverse	88,138
19AB	Transverse	90,034
	Average	**89,012**
16TB	Axial	117,504
20TB	Axial	116,171
21TB	Axial	115,224
	Average	**116,300**

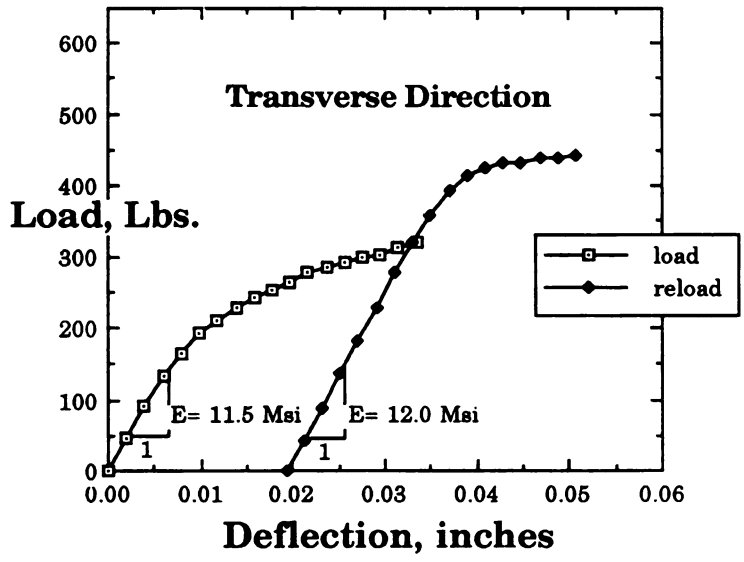

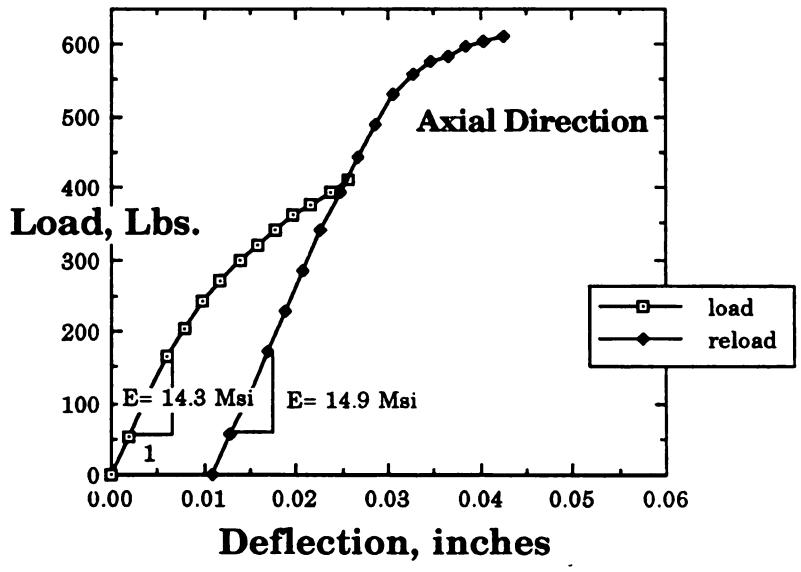

Figure 2.11 Load-Deflection plots of the static 3-point bend test for the transverse (top) and the axial (bottom) directions, with the flexural modulus.

Table 2.7 Typical 3-point static-loading (load-unload-reload) data for the transverse specimen 15AB.

Bending Load (Lbs.)	Deflection (in x 10^{-3})	Bending Load (Lbs.)	Deflection (in x 10^{-3})
0	0		
44	1.968	320	33.464
91	3.937	reload-2nd cycle 0	19.256
132	5.905	41	21.224
166	7.874	88	23.193
192	9.842	136	25.161
211	11.811	183	27.130
227	13.779	230	29.098
241	15.748	276	31.067
253	17.716	318	33.035
264	19.685	358	35.004
276	21.653	393	36.972
283	23.622	416	38.984
290	25.590	425	40.909
298	27.559	432	42.878
302	29.527	433	44.846
313	31.496	438	46.815

Table 2.7 (cont'd)

Bending Load (Lbs.)	Deflection (in x 10^{-3})
439	48.783
442	50.752

Table 2.8 Typical 3-point static-loading (load-unload-reload) data for the axial specimen 16TB.

Bending Load (Lbs.)	Deflection (in x 10^{-3})	Bending Load (Lbs.)	Deflection (in x 10^{-3})
0	0	56	12.926
54	1.968	113	14.895
110	3.937	172	16.863
164	5.905	229	18.832
205	7.874	284	20.800
241	9.842	340	22.769
271	11.811	393	24.737
298	13.779	443	26.706
320	15.748	488	28.674
342	17.716	529	30.643
361	19.685	559	32.611
377	21.653	575	34.580
395	23.622	585	36.548
411	25.590	596	38.517
0	10.958	603	40.485
		612	42.454

axial specimen was 64% greater than its respective axial UTS. This can most likely be attributed to the linear-elastic violation of the flexural formula.

2.6 SHEAR MODULUS, G AND SHEAR STRENGTH, τ_{max}

2.6.1 Introduction

Currently there is an interest in devising an accurate, simple and inexpensive test technique for measuring the shear properties of anisotropic materials, especially those materials which are fiber-reinforced. Although there are many shear test methods, none of the test specimen geometries meet the criteria of being small, easy to fabricate and capable of measuring both shear strength and shear modulus.

A test that does meet the above three criteria is a test first suggested by Nicolae Iosipescu of Rumania in the early 1960's. Although Iosipescu was primarily interested in testing isotropic metals, this test has been used quite extensively and successfully by Walrath and Adams (14,16) at the University of Wyoming on several anisotropic composite materials.

2.6.2 Test Fixture

The Iosipescu shear test achieves a pure state of shear loading within the test section of the specimen by application of two counteracting moments produced by two force couples. The force, shear and moment diagrams for this test are

based on elementary mechanics of beams; they are illustrated in Figure 2.12. The total applied load is measured at the testing machine load cell. The distance "a" is measured between forces of the outermost force couple and "b" is the distance between the innermost force couple. A state of constant shear loading is induced at the center section of the test specimen, as demonstrated in Figure 2.12b. This shear force is equal, in magnitude, to the applied load P. The induced moment at the center of the specimen is zero because the two induced moments cancel each other out at this point; this is shown in Figure 2.12c. Therefore, the loading is pure shear at the specimen midlength. Also, the shear stress distribution is shifted from parabolic to uniform, due to the 90^0 notches in the test specimens; these notches are illustrated in Figure 2.12a.

Loading is achieved by restraining the ends of the specimen from rotating by the loading fixture and at the same time undergoing shear loading as the right half of the fixture moves relative to the left half. Figure 2.12b illustrates the state of shear loading described above. A schematic of the test fixture used is demonstrated in Figure 2.13.

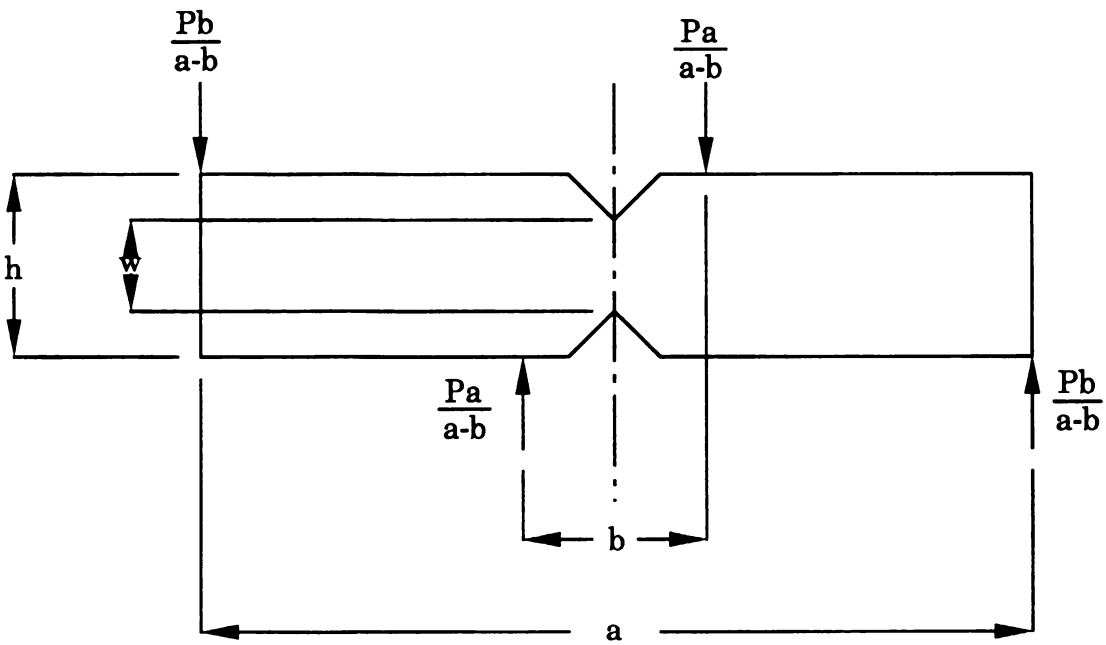

a. Force Diagram

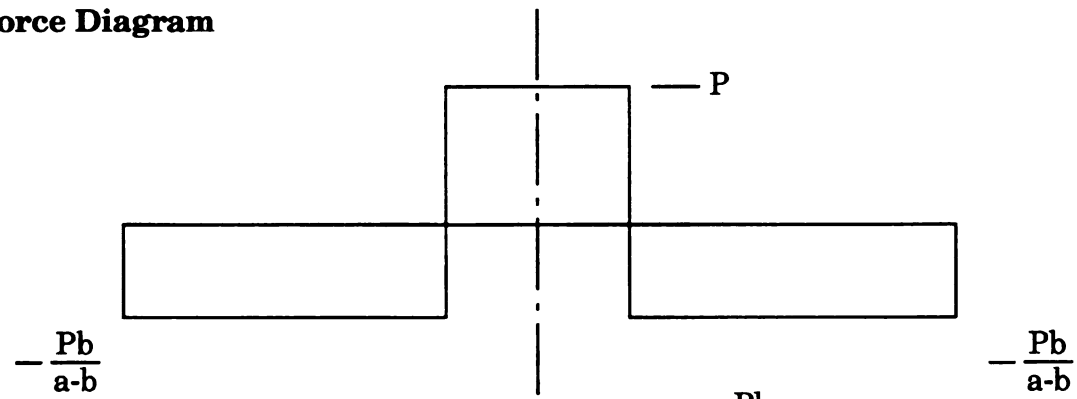

b. Shear Diagram

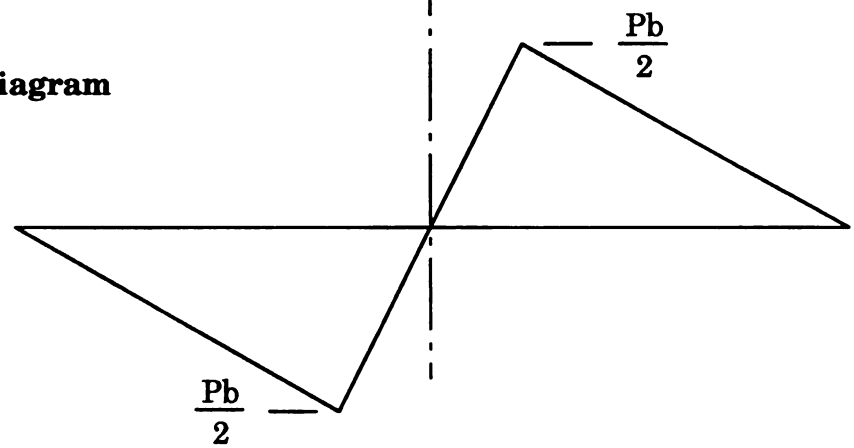

c. Moment Diagram

Figure 2.12 Force, Shear and Moment Diagrams for the Iosipescu Shear Test Method.

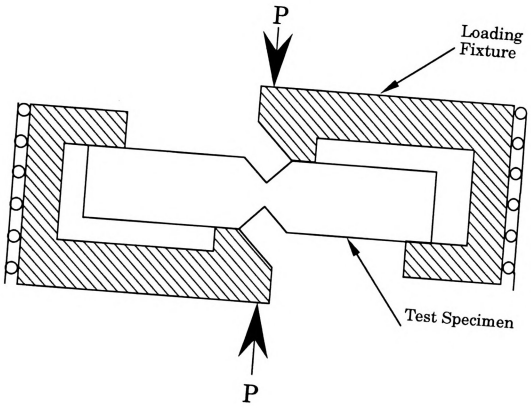

Figure 2.13 Schematic of the loading fixture for an Iosipescu Shear Test.

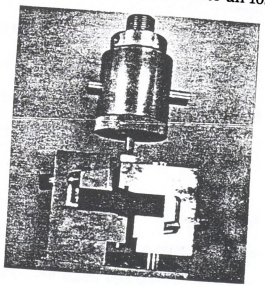

Figure 2.14 Photograph of actual test fixture used for executing the Iosipescu Shear Test.

2.6.3 Test Specimen

The test specimens used in the fixture shown in Figure 2.14 are 2 in. (51mm) long, 0.5 in (12.7mm) wide and of arbitrary "as received" material thickness, as shown in Figure 2.15. Although no specimen thickness is given, it should be on the order of 0.1in (2.5mm) or greater to avoid compressive buckling-induced failures, for this specific study the specimen thickness was approximately 0.25 inch. A 90^0 notch is cut into each edge of the specimen at the midlength to a depth of 0.1 in (2.5mm). Iosipescu determined that by cutting 90^0 notches on each edge of the test specimen, the shear stress distribution, within an isotropic test specimen, could be altered from the parabolic shear stress present in beams of constant cross-section to that of a nominally uniform shear stress distribution in the region between the notches. No tensile or compressive stress risers are caused by these notches, at least not for isotropic materials. Iosipescu believed that stress concentrations didn't occur because the normal stresses are parallel to the sides of the notches at that point in the test specimen (16). Therefore the shear stress obtained using the Iosipescu method is simply the applied load P, divided by the cross-sectional area A between the notch tips.

For this study two specimens, one per orientation, were machined on an electronic discharge machine (EDM) at the machine shop in the Physic's & Astronomy building at MSU. An EDM was used to reduce the chance of any surface defects. Using an EDM, the specimen was "burned" out of the extrudate instead of a machine tool physically cutting the specimen from the

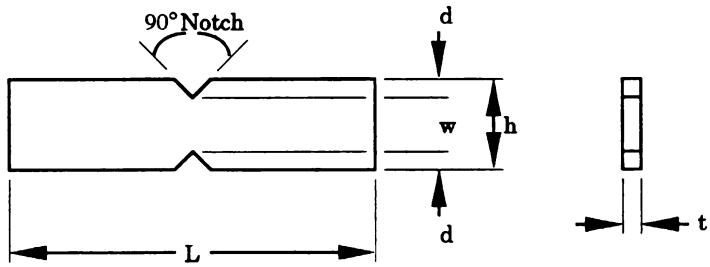

t = "as machined"

w = 7.62 mm (0.3 in)

d = 2.54 mm (0.1 in)

L = 50.8 mm (2.0 in)

h = 2d + w = 12.7 mm (0.5 in)

Figure 2.15 Iosipescu Shear Test specimen dimensions

extrudate which would greatly reduce the useful life of the tool, due to the abrasiveness of the SiC whiskers.

The technique for measuring the shear strain in the Iosipescu shear test was with strain gages (RSG's). The strain gage was a biaxial strain gage, Micromeasurements gage type EA-13-062TV-350. This gage was oriented at + 45^0 to the longitudinal axis of the test specimen and bonded at the specimen midlength.

2.6.4 Experimental Procedure

The specimens were inserted into the loading fixture (Figure 2.14) and centered using an alignment bar located beneath the lower specimen notch. Steel shims were placed in the horizontal slots between the specimen and fixture and were pressed against the specimen by tightening the horizontal screws. The Iosipescu shear test was conducted on a servo-hydraulic MTS testing machine (Model 880), using a 20-Kip load cell and a cross-head speed of 0.02 in/min (0.5mm/min). The strain gages and load cell were connected to a Micromeasurements (model 2150) data acquisition system that was interfaced with a 386 Compuadd digital computer. The strain gage rosettes monitored the compression and tension independently, as opposed to connecting them in a half-bridge as is commonly done. The reason for monitoring the gages, (tension and compression), independently was to make sure that the strain readings were equal (in magnitude) and that this was maintained throughout the test. The data that was recorded for each test was tensile and compressive strain,

load and time, and this data was stored as an ASCII file.

The testing was performed at the Composite Material and Structures Corporation (CMSC) at MSU, where Pedro Jesus Herrera Franco, a research associate, assisted in the tests. The tests were conducted at room temperature, 72^{0}F and 50% relative humidity.

2.6.5 Sample Calculations

Shear stress τ was simply the applied load P, which is the shear force, divided by the area A, parallel to the loading plane between the notch tips.

$$\tau_{ij} = P/A \qquad \text{where } i,j = 1,2,3 \qquad [2.8]$$

The shear strain γ was calculated by adding the magnitude of the tensile strain ε_t and the compressive strain ε_c obtained from the strain gages and finally dividing by 2.

$$\gamma_{ij} = (\varepsilon_t - \varepsilon_c)/2 \qquad [2.9]$$

The shear modulus G was determined by dividing the elastic shear stress τ_e by the respective elastic shear strain γ_e.

$$G_{ij} = \tau_e/\gamma_e \qquad [2.10]$$

Another relationship that was analyzed was the expression for a homogeneous, isotropic material (13) which equates shear modulus G_{iso} ,from the two independent material constants, Young's modulus E and Poisson's ratio ν.

$$G_{iso} = E_i / 2(1 + \nu) \qquad [2.11]$$

2.6.6 Results

The results for this experiment were also very interesting. The **shear strength** for both the transverse and axial specimen were relatively close; **24,401 psi** and **28,278 psi** respectively. Figure 2.16 illustrates the measured shear stress-shear strain behavior for both specimen orientations. The linearly-elastic portion of the Iosipescu shear test is shown in Figure 2.17, from this curve a linear regression was performed to determine the experimental shear modulus $G_{exp.}$ The experimental (Iosipescu) shear modulus was compared with the theoretical (isotropic) shear modulus $G_{iso.}$ The G_{iso} was calculated using Equation [2.11] listed above, which is usually limited to homogeneous, isotropic material. Both G_{exp} and G_{iso} were determined for both specimen directions and are listed below, along with the material constants from the tensile test;

Axial specimen: $G_{exp} = 8.04$ Msi $E_1 = 18.60$ Msi, $\nu_{12} = 0.235$

$G_{iso} = 7.60$ Msi

Transverse specimen: $G_{exp} = 5.43$ Msi

$G_{iso} = 4.96$ Msi $E_2 = 13.09$ Msi, $\nu_{21} = 0.323$

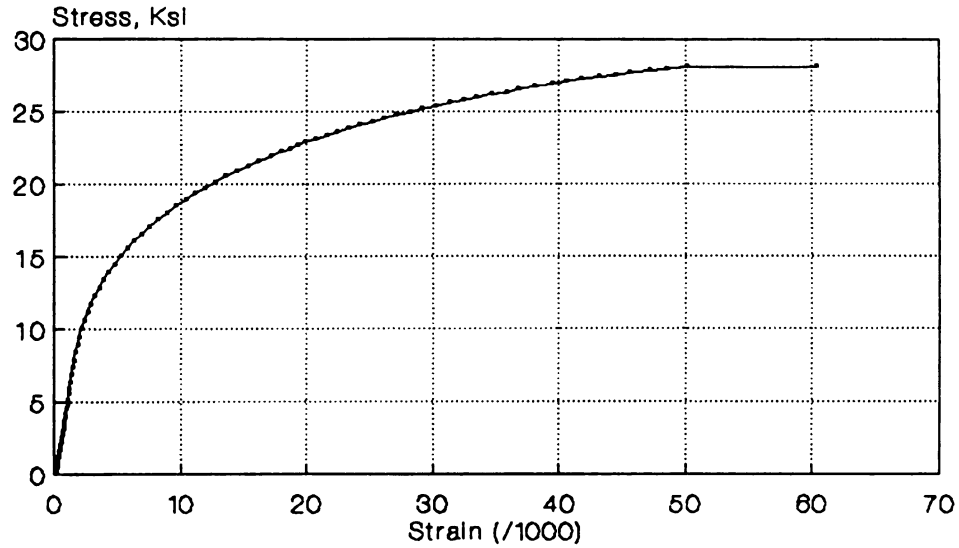

transverse direction

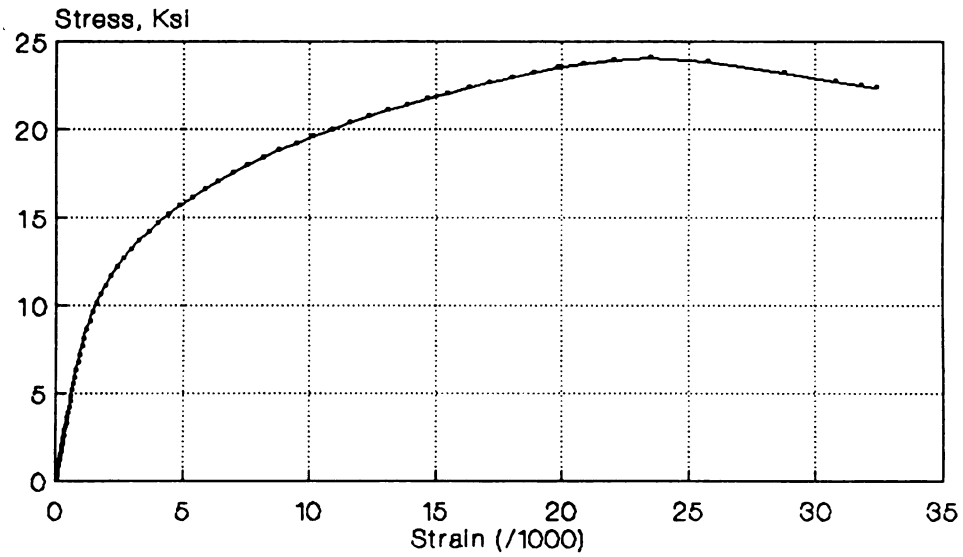

Figure 2.16 Stress-strain plots of the Iosipescu Shear Test for both the transverse (top) and axial (bottom) specimens.

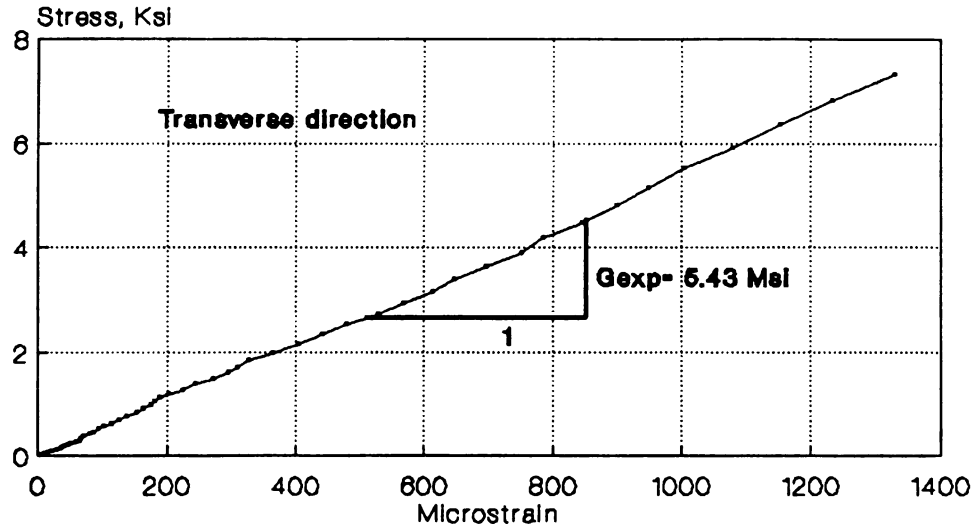

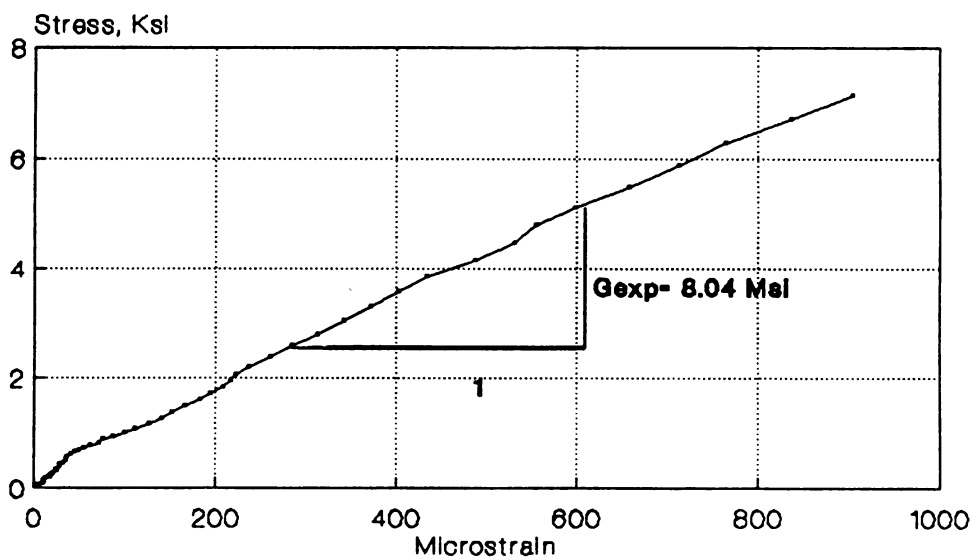

Figure 2.17 Linear-elastic stress-strain diagrams from the Iosipescu Shear Test, with shear modulus, G. Both the transverse (top) and axial (bottom) directions are illustrated.

2.6.7 Discussion

The Iosipescu Shear Test was definitely the most intriguing of the four static tests performed. The most captivating aspect, at least visually, was the fracture pattern of the test specimens, especially when comparing the transverse specimen to the axial specimen. The transverse specimen failed in a very predictable fashion; the crack initiated at the top notch tip and propagated in a direction nearly plumb to the bottom notch tip where the specimen failed. On the other hand, the axial specimen failed in a very jagged and torturous manner. One crack initiated at the top notch tip, a second crack initiated on the bottom side of the specimen, although this crack started slightly below the bottom notch tip. Both of these cracks propagated in an almost circular trend, traveling in opposite directions until the specimen reached complete fracture, this failure is illustrated in Figure 2.18. From the photograph, it is also apparent that both cracks propagated around the strain gage leaving it nearly untouched. To try to explain the axial specimen crack growth mechanisms would be extremely bold and vain at this stage. It is clear that the radical failure of the axial specimen is due to the SiC whiskers remarkab! ability to arrest crack growth.

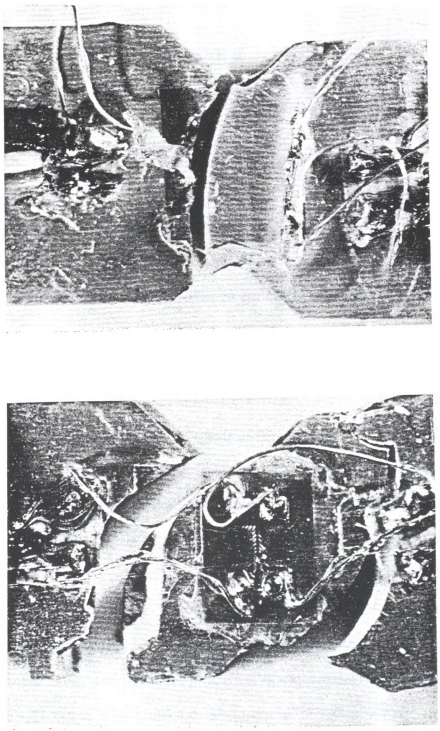

Figure 2.18 Post-mortem photograph (~ 7X) of the Iosipescu Shear Test specimens for both the transverse (top) and axial (bottom) directions.

CHAPTER 3

3-POINT CYCLIC-BENDING

3.1 INTRODUCTION

MMC's are rapidly becoming the material of choice for load-bearing applications, and the area of fatigue, or reliability needs a critical and thorough investigation. The reason this area is of such concern is that MMC's are becoming more and more feasible to manufacture, resulting in increasing application for the designer and end-user. The problem is that no valid database or testing standards have been established. This lack of literature or control on testing techniques (e.g. ASTM standards) has produced a significant concern among the materials community with respect to MMC's. It was this lack of research and literature of a potentially great material (MMC) that enticed the characterizing of an MMC, with an emphasis on reliability. The reason for the emphasis on reliability was two-fold: First, many of the MMC applications are load-bearing and involve high stresses, where a premature failure would prove catastrophic, possibly fatal. Secondly, many fatigue experts knowledge is limited to single-phase metals and most MMC's are less than a decade old. Since MMCs are a combination of chemistry and processing,a materials scientist is best suited for the job of MMC processing. Due to the youthful nature of MMCs, many materials scientists are also involved with the evaluation of such MMCs.

The material property evaluation is where the experimental mechanist is best qualified.

The MMC fatigue studies currently performed are usually evaluated only along the "preferred" or extruded-axis. This approach is fine if loads or stresses are always applied along this "preferred" direction. This preferred-axis testing is choice for a continuous-fiber composite. For a discontinuous-fiber MMC, several angles relative to the preferred-axis must be evaluated for a comprehensive material characterization.

Given the lack of MMC fatigue data or literature, it was decided to design a reliability test that was qualitative, valid and conservative with respect to material. A 3-point cyclic-bending test was chosen. The controlled-variable was deflection, which was measured with an extensometer mounted mid-span to a deflection-mechanism,(Figure 3.1a). The specimens were approximately 1/4"x 1/4" (6.35mm x 6.35mm) with a 2" (50mm) span. A computer program was written that interfaced with the testing machine and captured loads and displacements at specified intervals. The objective of this study was to analyze the cyclic-bending data of transverse and axial specimens, ultimately proposing a fatigue model for both specimen directions.

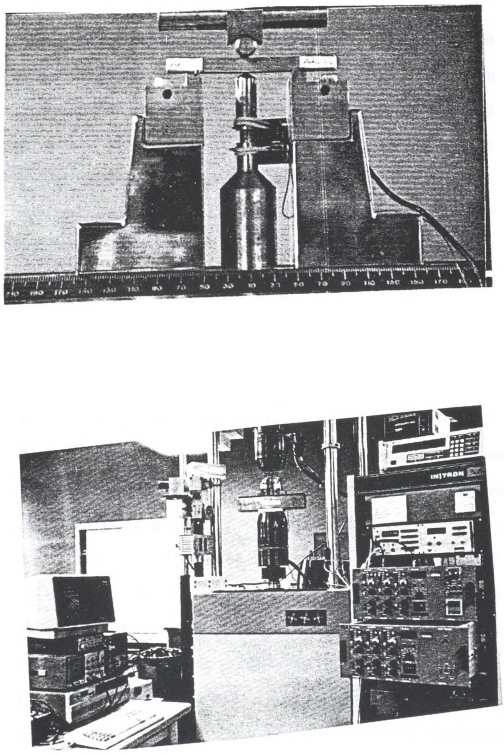

Figure 3.1 Cyclic-bending fixture (top) and experimental set-up (bottom) used for the fatigue study.

3.2 EXPERIMENTAL PROCEDURE

The fatigue specimens were machined as described above with an electrical discharge machine (EDM). This machining technique was to minimize surface effects (e.g. superficial whisker abrasions) and to eliminate machine tooling wear-out. All tests were performed at room temperature and 50% relative humidity. The specimens were tested in a specially designed 3-point test fixture as described above. The 3-point test fixture was connected to a servo-hydraulic Instron (model 1320) materials testing machine. This testing setup is illustrated in Figure 3.1b. The fatigue specimens were cycled until fracture, or 20 million cycles. The 3-point cyclic-bending test was compression-compression and the waveform was sinusoidal (see Figure 3.2). The mean level (DC offset) was dialed in on the Instron's strain (deflection) channel, The amplitude and cyclic frequency were input to a programmable Wavetek, (model 175), function generator. (Note: The function generator on the Instron was ill-functional, therefore an external function generator had to be utilized). The maximum deflection ranged from 3.937e- 03 inches (0.10 mm) to 11.181e - 03 inches (0.30 mm) with a 1.969e - 03 inch (0.05 mm) increment. The R (deflection) ratio = 0.1, therefore maximizing the cyclic range while maintaining a compressive load throughout the entire cycle. This procedure greatly reduced the chance of impacting the specimen. Between 1 and 4 specimens were tested depending on the deflection level, due to the length of test time per specimen. The cyclic frequency ranged from 1 hertz to 20 hertz depending on the deflection level. Since many fatigue experts agree that fatigue tests consisting of frequencies less than 30 or 40 hertz are usually invariant of the

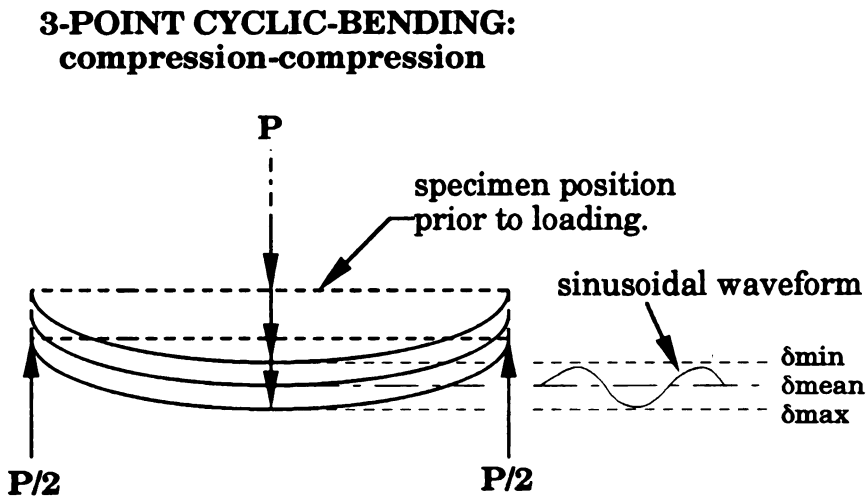

Figure 3.2 Loading technique used for the cyclic-bending study.

fatigue life, frequency was not a considered parameter in this study.

3.3 Sample Calculations

As stated above, the load-deflection data was captured and stored at designated intervals throughout each fatigue test. Approximately 100 points were sampled at each interval and these points were stored as hexadecimal numbers. From this form they had to first be converted to voltage and then to respective loads and displacements. The conversion from hexadecimal numbers to voltage is easily developed. First note that the voltage range was from -10volts to +10volts (i.e. 20v range) this range was equal to 0 to 4096 bits, therefore there is a linear relation between voltage and hexadecimal numbers. The following relation converts hexadecimal numbers to voltage,

$$\mathbf{Y_{volts} = 4.8828e\text{-}3(X_{hex}) - 10} \qquad [3.1]$$

Next, the voltage must be converted to a useable form, the respective loads and displacements. The following are the appropriate conversion factors,

for displacement @ 10% (strain) range, load @ 5% load range,

1volt = 0.01mm **1volt = 100 Lbs.**

= 3.937e- 4 in.

@ 20% (strain) range,

1volt = 0.02mm

= 7.874e- 4 in.

@ 50% (strain) range,

1volt = 0.05mm

= 19.685e- 4 in

To obtain the English conversion for displacement, the metric conversion was simply divided by 25.4 to translate millimeters (mm) to inches (in.).

Since all the data was stored as an ASCII file it could easily be downloaded to a spreadsheet program where all data reduction could efficiently be performed. From the load-displacement information, 2 fundamental material properties could be determined, Young's modulus, E and Flexural stress, σ. The equations to determine Young's modulus and the Flexural stress were given in section 2.5.2; sample calculations for static flexural loading;

$$\mathbf{E = 512(P/\delta_e)} \qquad [2.4']$$

and $$\mathbf{\sigma = 192(P)} \qquad [2.5']$$

where Young's modulus was determined from a linear regression of the load-displacement data and the expression for stress was left in a very generic form, because in fatigue a variety of stresses can be determined, (e.g. maximum stress, stress amplitude, mean stress, etc.) and this stress will be specified when necessary.

The following expressions are commonly used when discussing fatigue;

$$\Delta\sigma = \sigma_{max} - \sigma_{min} = \textbf{stress range} \qquad [3.2]$$

$$\sigma_a = (\sigma_{max} - \sigma_{min})/\,2 = \textbf{stress amplitude} \qquad [3.3]$$

$$\sigma_m = (\sigma_{max} + \sigma_{min})/\,2 = \textbf{mean stress} \qquad [3.4]$$

$$\mathbf{R = \delta_{min}/\delta_{max} = deflection\ ratio} \qquad [3.5]$$

3.4 THEORY

Deflection was the controlled-variable, so the Stress-Life, Strain-Life and Deflection-Life relations were used to create fatigue models. Some basic fatigue background will be presented to assist in understanding the fatigue terminology and relationships. First, the total strain range is the sum of elastic ε_e and plastic ε_p strain ranges,

$$\Delta\varepsilon = \Delta\varepsilon_e + \Delta\varepsilon_p \qquad [3.6]$$

or in terms of amplitudes,

$$\Delta\varepsilon / 2 = \Delta\varepsilon_e / 2 + \Delta\varepsilon_p / 2 \qquad [3.7]$$

using Hooke's law, the elastic term may be replaced by $\Delta\sigma/E$.

$$\Delta\varepsilon / 2 = \Delta\sigma / 2E + \Delta\varepsilon_p / 2 \qquad [3.8]$$

Basquin (17) observed that stress-life (S-N) data could be plotted linearly on log-log scale. Using stress amplitude, the graph could be linearized by the following expression,

$$\Delta\sigma / 2 = \sigma_f' (2N_f)^b \qquad [3.9]$$

where $\Delta\sigma / 2$ = stress amplitude

$2N_f$ = reversals to failure (1 rev = 1/2 cycle)

σ_f' = fatigue strength coefficient

b = fatigue strength exponent (Basquin's exponent)

σ_f' and b are fatigue properties of the material. The elastic term can also be written as

$$\Delta\varepsilon_e / 2 = \Delta\sigma / 2E \qquad [3.10]$$

Using Eq. [3.9] one can restate the RHS of Eq. [3.10] in terms of life to failure:

$$\Delta\varepsilon_e / 2 = \sigma_f (2N_f)^b / E \qquad [3.11]$$

Coffin (18) and Manson (19), discovered independently, in the 1950's, that plastic strain-life (ε-N) data could also be linearized on log- log coordinates. This plastic strain can be related by the following power-law relation,

$$\Delta\varepsilon_p / 2 = \varepsilon_f (2N_f)^c \qquad [3.12]$$

where $\Delta\varepsilon_p / 2$ = plastic strain amplitude

$2N_f$ = reversals to failure

ε_f = fatigue ductility coefficient

c = fatigue ductility exponent

Using Eq. [3.7] the total strain can be rewritten using Eqs. [3.11] and [3.12].

$$\Delta\varepsilon / 2 = \sigma_f (2N_f)^b / E + \varepsilon_f (2N_f)^c \qquad [3.13]$$

Equation [3.13] is the basis of the strain-life method and is termed the strain-life relation. For this cyclic-bending study, strain was assumed to be elastic-only, i.e. $\Delta\varepsilon_p / 2 = 0$. This assumption was confirmed as valid from the linear behavior exhibited by the load-displacement data, collected from the Instron test machine. Therefore, the strain-life relation used for this study was:

$$\Delta\varepsilon / 2 = \Delta\varepsilon_e / 2 = \sigma_f (2N_f)^b / E \qquad [3.13^e]$$

Since this cyclic-bending test had a mean-stress it was decided to create an elastic strain-life model that accounted for mean stress effects. This model would be compared with that of the strain-life model from Eq. [3.13^e].

Bannantine, Comer and Handrock (20) have shown that mean stresses have a significant effect on fatigue life, especially at longer lives. Modifications have been made to the strain-life equation [3.13] to account for the mean stress effects. Morrow (21) suggested that the mean stress effects could be taken into account by simply modifying the elastic part of the strain-life relation [3.13] with the mean stress, σ_o.

$$\Delta\varepsilon_e / 2 = \Delta\sigma / 2E = (\sigma_f - \sigma_o)(2N_f)^b / E \qquad [3.14]$$

The complete expression for strain-life, accounting for mean stress is simply Eq. [3.14] plus the plastic portion of [3.13] or,

$$\Delta\varepsilon / 2 = (\sigma_f - \sigma_o)(2N_f)^b / E + \varepsilon_f (2N_f)^c \qquad [3.15]$$

Since we are assuming $\Delta\varepsilon_p / 2 = 0$, Eq. [3.14] will be used for this study.

Manson and Halford (22) also modified the strain-life relation, Eq. [3.13], to account for mean stress effects. The modification Manson and Halford made to the *elastic* portion of Eq.[3.13] was the same as Morrow's modification [3.13], thus it will not be restated. Manson and Halford had a different plastic term modification than Morrow, although it is not included, since the plastic strain is assumed zero for this study.

The study was cyclic-bending, not uniaxial fatigue, and since the controlled-variable was actually deflection, not strain, it was decided to create a deflection-life fatigue model for cyclic-bending. This power relation is of the same form as Eq.[3.11]; the main difference is that the dependent variable is *elastic-deflection*, not elastic-strain. The expression is of the form,

$$\Delta\delta / 2 = D(N_f)^f \qquad [3.16]$$

Where $\Delta\delta / 2$ = elastic-deflection amplitude

D = flexural fatigue constant

$\mathbf{N_f}$ = cycles to failure

f = flexural fatigue exponent

3.5 RESULTS AND DISCUSSION

The results from the cyclic-bending study were exciting, especially after performing data reductions from the load-displacement (deflection) data. The following relations were analyzed:

(1) Applied Load versus Displacement (deflection)

(2) Stress Amplitude, $\Delta\sigma/2$ versus Cycles to Failure, N_f

(3) Strain Amplitude, $\Delta\varepsilon/2$ versus Cycles to Failure, N_f

(4) Deflection Amplitude, $\Delta\delta/2$ versus Cycles to Failure, N_f

3.5.1 Applied Load vs. Displacement (Deflection)

The load-deflection data analysis was three-fold; (1) For several load-displacement intervals (section 3.2) throughout each test the ASCII data were dumped to a spreadsheet program; Lotus 1-2-3, and plotted as shown in Figure 3.3. This plot was evidence to determine if the cyclic-bending test was elastic, as the initial assumption states. The test was elastic if the load-deflection curve was linear, and if it intersected the X-axis near the origin at zero-load.

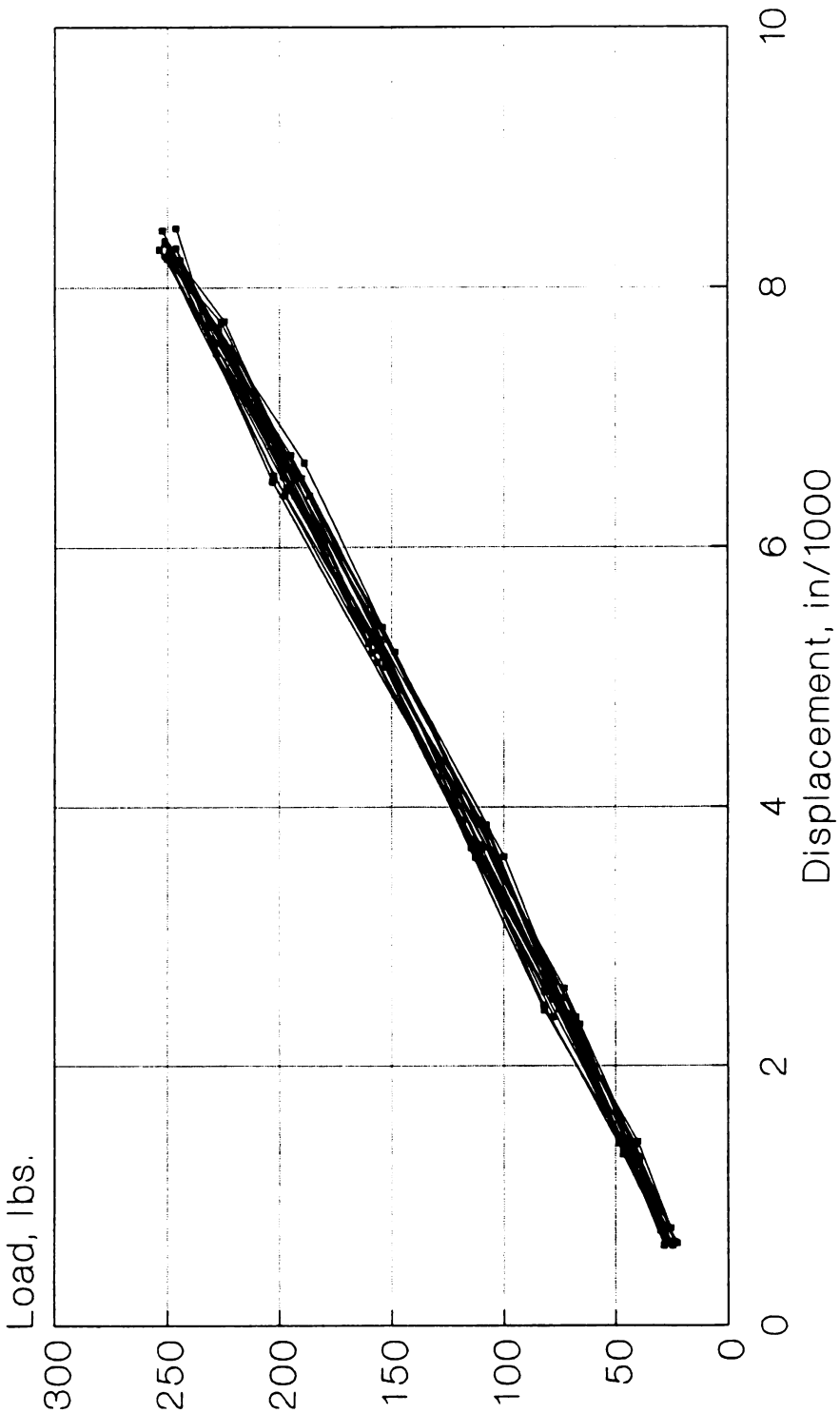

Figure 3.3 Typical load-displacement (deflection) plots reduced from the hexidecimal data, see Eq. (3.1).

If the curve crossed the +X-axis,(deflection axis), at zero-load, this would imply that there was plastic or permanent deformation, (deflection), and the assumption that the cyclic-bending was linearly-elastic would have been violated. The second reason for the load-deflection data analysis was to perform a linear regression and determine the elastic modulus, E as a function of cycles. The E-N study will be illustrated and discussed in Chapter 4. Finally (3) the load-deflection data were reduced, in conjunction with the number of cycles to failure, to determine the Stress-Life ($S\text{-}N_f$), Strain-Life ($\varepsilon\text{-}N_f$) and the Deflection-Life ($\delta\text{-}N_f$) data, curves and ultimately fatigue models. These results will be discussed in sections 3.5.2-4 respectively.

3.5.2 Stress Amplitude, $\Delta\sigma/2$ Vs. Cycles to Failure, N_f

The Stress-Life, S-N, method was the first approach used in an attempt to understand and quantify metal fatigue (20). The S-N approach is used widely for applications where the stresses are within the elastic limit and where the number of cycles is high, $N_f > 10^4$ cycles. Since the cyclic-bending is assumed elastic, the S-N relation parallels the cyclic-bending criteria quite well. The S-N cyclic-bending data is plotted on log-log coordinates, as is illustrated for the transverse and axial specimen's in Figures 3.4a & b respectively. The S-N cyclic-bending data for the transverse and axial specimens are listed in Tables 3.1 and 3.2 respectively. Using the stress amplitude, $\Delta\sigma/2$ the plots were linearized by a power-law of the form of Eq. [3.9]

$$\Delta\sigma / 2 = \sigma_f' (2N_f)^b \qquad [3.9]$$

This power-fit model was applied to the corresponding transverse and axial specimens.

The fatigue models are as follows,

S-N model for the (12) Transverse cyclic-bending specimens,

$$\Delta\sigma_t / 2 = 72{,}303(N_f)^{-.110}$$

with a correlation coefficient of 0.88.

S-N model for the (10) Axial cyclic-bending specimen,

$$\Delta\sigma_a / 2 = 116{,}762(N_f)^{-.116}$$

with a correlation coefficient of 0.85.

The coefficients of the S-N models are the Fatigue Strength Coefficient(s) and technically represent the magnitude of applied flexural stress,(in psi), that the specimen could resist for $N_f = 1$. The exponent(s) are called the Fatigue Strength Exponent (Basquin's exponent) and are simply the slope of the linearized curves. The S-N models are usable only within the experimental cyclic life range, as is illustrated in Figures 3.4a & b. The "Endurance Limits" are included in these plots. The endurance limit for the transverse and axial S-N plots is, $\Delta\sigma/2 \sim 15{,}000$ Psi and ~ 23,000 Psi respectively. Qualitatively speaking, the axial specimen's endurance limit is approximately 50% greater than the transverse specimen's endurance limit. Historically, the endurance limit represented a stress amplitude below which the material would have an "infinite", cyclic or fatigue life. An infinite life was considered to be 1 million cycles. The endurance limit was usually found by simply drawing a best-fit linear line through the S-N data points until the line reached $N_f = 10^6$ cycles,

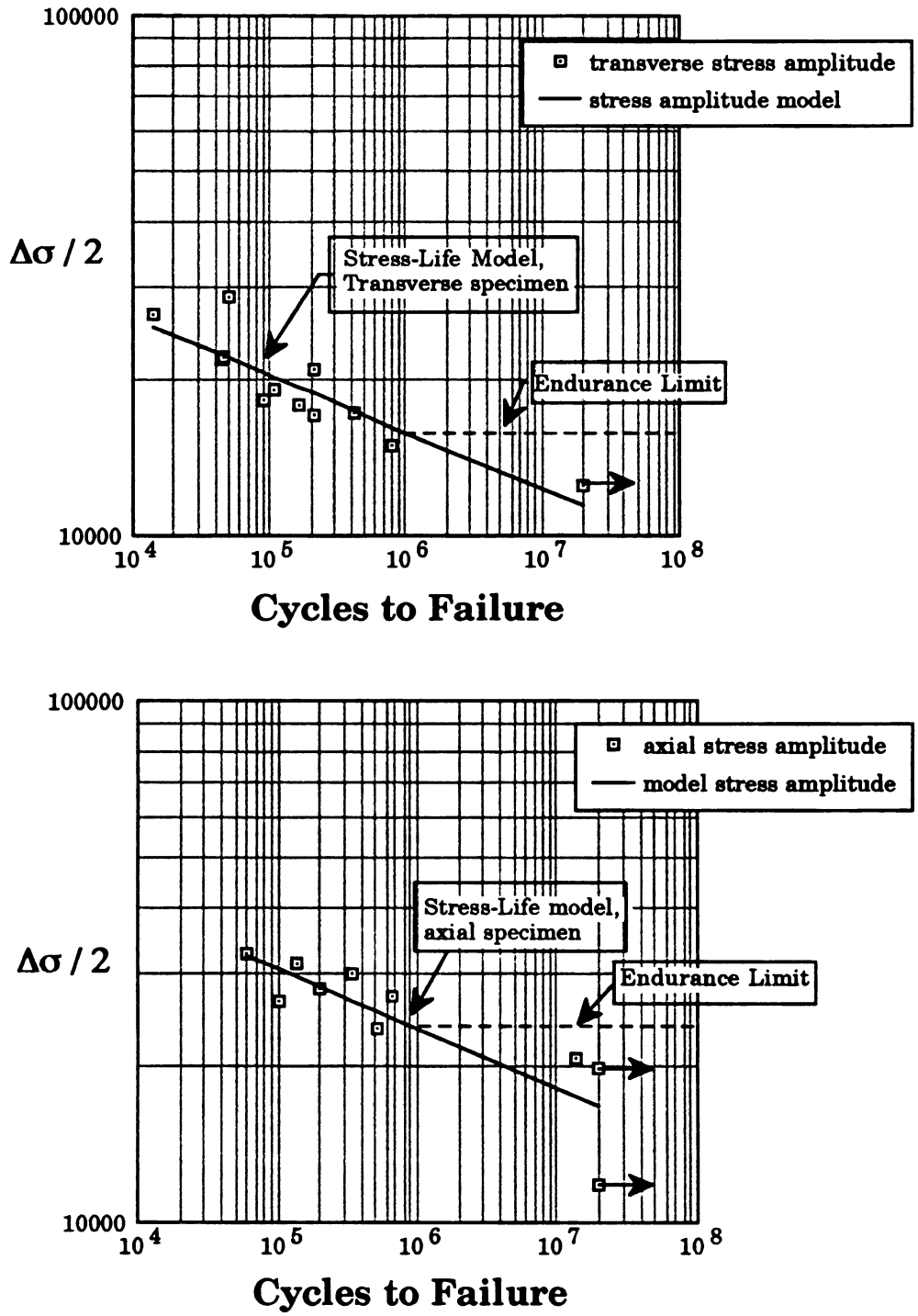

Figure 3.4 Stress-Life (S-N) plots of the cyclic-bending speciemens for the transverse (top) and axial (bottom) directions. Note the corresponding "endurance limits" and power-law models.

Table 3.1 Stress-Life (S-N) data from cyclic-bending study for the transverse specimen. The model stress was reduced from actual stress data.

Specimen Number	Nf Cycles to Failure	$\Delta\sigma/2$ Actual Stress Amplitude (PSI)	$\Delta\sigma/2$ Model Stress Amplitude (PSI)
1AB	20×10^6*	12,528	11,377
2AB	801,330	14,981	16,208
10AB	209,080	16,999	18,790
3AB	426,070	17,211	17,374
13AB	162,040	17,755	19,324
11AB	91,020	18,187	20,590
12AB	110,000	19,080	20,165
4AB	209,820	20,851	18,782
7AB	45,000	21,885	22,249
6AB	46,790	21,989	22,153
8AB	14,200	26,542	25,258
9AB	50,000	28,832	21,992

Table 3.2 Stress-Life (S-N) data from cyclic-bending study for axial specimen. The model stress data was reduced from actual stress data.

Specimen Number	Nf Cycles to Failure	$\Delta\sigma/2$ Actual Stress Amplitude	$\Delta\sigma/2$ Model Stress Amplitude
1TB	20×10^6*	11,788	16,610
2TB	20×10^6*	19,752	16,610
2ATB	13.5×10^6	20,529	17,385
17TB	522,000	23,533	25,354
8TB	100,000	26,550	30,711
12TB	650,000	27,117	24,717
10TB	200,000	28,195	28,339
5TB	340,000	29,923	26,647
3TB	135,000	31,298	29,660
7TB	60,000	33,034	32,586

then a horizontal line was drawn, and any point below this line was within the "endurance limit". The idea of the endurance limit has since been abandoned, since everything has a finite life and many of today's applications may involve several 10's, or 100's, of millions of cycles. The endurance limit plotted on the S-N curves, (Figures 3.4a & b), serve primarily as a correlation between the axial and transverse S-N graphs.

3.5.3 Strain Amplitude, $\Delta\varepsilon/2$ versus Cycles to Failure, N_f

The Strain-Life, (ε-N_f), method is based on the observation that with many components, the response of the material in critical locations (e.g. notches, cracks) is strain or deformation dependent (20). The Strain-Life technique was very important for this study since an MMC was being evaluated along both the axial, or preferred direction and transverse to the preferred axis. The elastic moduli for both the axial and transverse orientations had been measured. The axial direction was found to be approximately 42% stiffer than the transverse direction. It was also noticed that the elastic modulus varied considerably throughout the fatigue (cyclic-bending) lives of every specimen, transverse or axial, (chapter 4), even though the test was elastic in nature. This stiffness phenomenon can be seen in Tables 3.3 & 3.5, with the appropriate stress amplitude, mean stress and maximum stress for the transverse and axial specimens respectively. It is these data from which the elastic strain was reduced. Tables 3.4 & 3.6 list the cycles to failure, the actual elastic strain, model elastic strain and the model elastic strain with

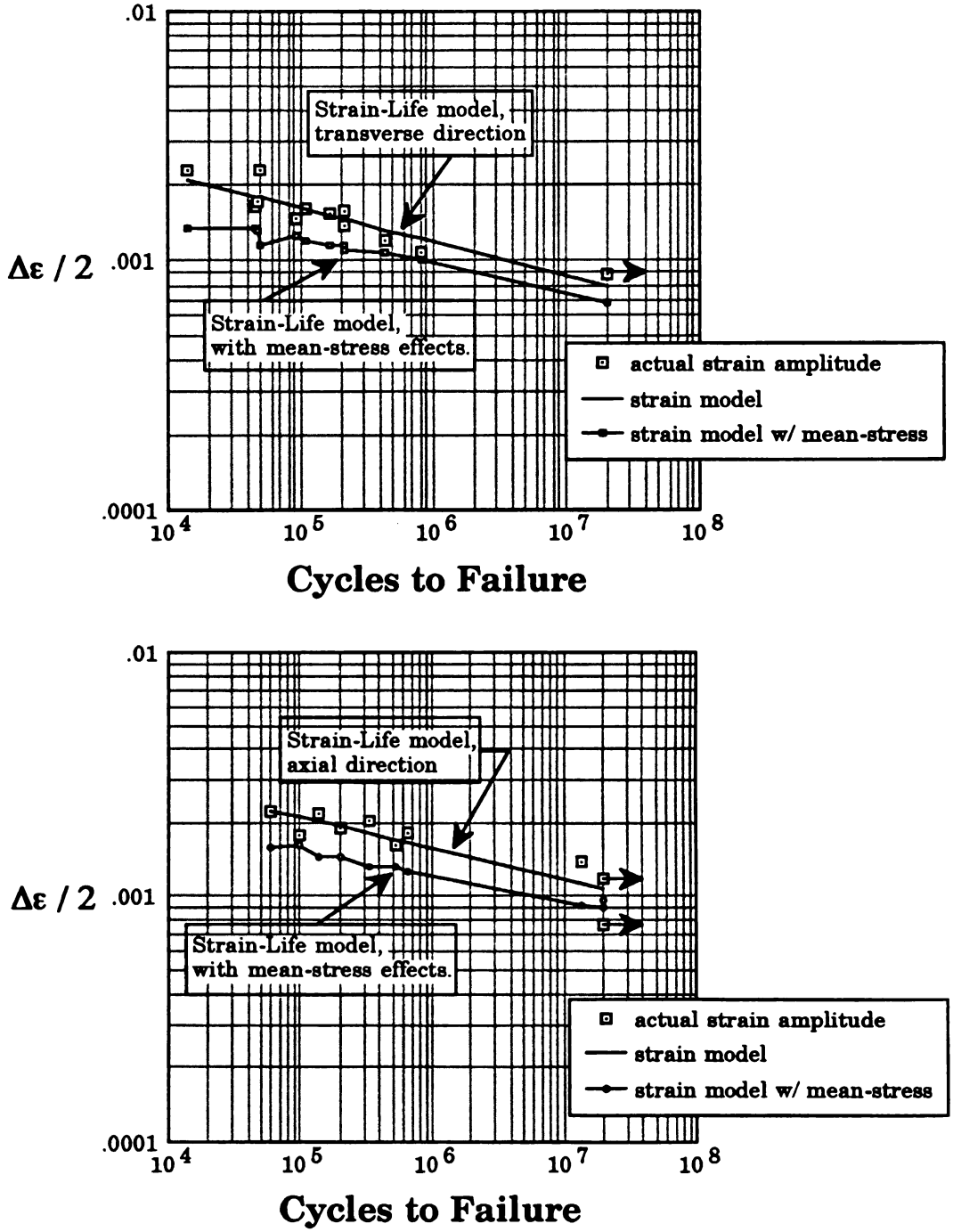

Figure 3.5 Strain-Life (ε-N_f) plots of the cyclic-bending specimens for the transverse (top) and axial (bottom) directions. Note the models with and without mean-stress effects.

Table 3.3 Elastic modulus and stress data for strain-life analysis of transverse specimen.

Specimen Number	E Elastic Modulus (Msi)	$\Delta\sigma/2$ Stress Amplitude (Psi)	σ_{mean} Mean Stress (Psi)	σ_{max} Maximum Stress (Psi)
1AB	14.29	12,528	15,312	27,840
2AB	13.72	14,981	18,311	33,293
3AB	14.31	17,211	21,035	38,246
10AB	12.18	16,999	20,777	37,776
11AB	12.38	18,187	22,229	40,416
13AB	11.49	17,755	21,701	39,456
4AB	13.31	20,851	25,485	46,336
12AB	11.79	19,080	23,320	42,400
7AB	13.39	21,885	26,749	48,634
6AB	12.73	21,989	26,875	48,864
9AB	12.57	28,832	35,240	64,073
8AB	11.50	26,542	32,440	58,982

Table 3.4 Strain-Life (ε–N_f) data from cyclic-bending study for transverse specimen. The model Strain data was reduced from the Strain-Life Models, with and without mean stress effects.

Specimen Number	N_f Cycles to Failure	Actual $\Delta\sigma/2E$ Strain Amplitude	Model $\Delta\sigma/2E$ Strain Amplitude	Model $\Delta\sigma/2E$ with Mean Stress effects, σ_o
1AB	20 x 10^{6*}	0.000877	0.000787	0.000680
2AB	801,330	.001092	.001223	.001016
3AB	426,070	.001203	.001334	.001084
10AB	209,080	.001396	.001470	.001151
11AB	91,020	.001469	.001647	.001271
13AB	162,040	.001545	.001522	.001157
4AB	209,820	.001567	.001469	.001112
12AB	110,000	.001618	.001605	.001202
7AB	45,000	.001634	.001814	.001353
6AB	46,790	.001727	.001804	.001320
9AB	50,000	.002294	.001788	.001151
8AB	14,200	.002308	.002124	.001363

Table 3.5 Elastic modulus and stress data for strain-life analysis of axial specimen.

Specimen Number	E Elastic Modulus (Msi)	$\Delta\sigma/2$ Stress Amplitude (Psi)	σ_{mean} Mean Stress (Psi)	σ_{max} Maximum Stress (Psi)
1TB	15.33	11,788	14,407	26,195
2TB	16.63	19,752	24,141	43,893
2ATB	14.76	20,529	25,090	45,619
17TB	14.38	23,533	28,763	52,296
8TB	14.97	26,550	32,450	58,999
12TB	14.78	27,117	33,143	60,260
10TB	14.72	28,195	34,461	62,656
5TB	14.61	29,923	36,573	66,496
3TB	14.45	31,298	38,254	69,552
7TB	14.79	33,034	40,374	73,408

Table 3.6 Strain-Life (ε–N_f) data from cyclic-bending study for the axial specimen. The model Strain data was reduced from the Strain-Life Models, with and without, mean stress effects.

Specimen Number	**N_f Cycles to Failure**	**Actual $\Delta\sigma/2E$ Strain Amplitude**	**Model $\Delta\sigma/2E$ Strain Amplitude**	**Model $\Delta\sigma/2E$ with Mean Stress effects, σ_o**
1TB	20×10^6*	0.000769	0.001078	0.000967
2TB	20×10^6*	.001188	.001078	.000907
2ATB	13.5×10^6	.001391	.001133	.000923
17TB	522,000	.001637	.001714	.001340
8TB	100,000	.001774	.002116	.001615
12TB	650,000	.001835	.001667	.001259
10TB	200,000	.001915	.001937	.001442
5TB	340,000	.002048	.001810	.001316
3TB	135,000	.002166	.002036	.001448
7TB	60,000	.002234	.002258	.001585

mean stress effects. The ε-N_f data points were plotted on log-log coordinates; it was these experimental values that were used to create the ε-N_f models, as shown in Figures 3.5a & b. The changing elastic modulus would be included in the Elastic Strain-Life relation Eq [3.13e], the modulus was not accounted for in the S-N models. The Elastic Strain-Life power relation used was of the form,

$$\Delta\varepsilon / 2 = \Delta\varepsilon_e / 2 = \sigma_f (2N_f)^b / E \qquad [3.13e]$$

Another reason the Strain-Life relation was used is that there is also a Strain-Life expression that accounts for mean stress, Morrow (21), and Manson and Halford (22),

$$\Delta\varepsilon_e / 2 = \Delta\sigma / 2E = (\sigma_f - \sigma_o)(2N_f)^b / E \qquad [3.14]$$

The fatigue models are as follows;

The elastic ε-N_f model for the (12) Transverse cyclic-bending specimens,

$$\Delta\varepsilon_{et} / 2 = 7.865 \times 10^{-3}(2N_f)^{-.137}$$

with a correlation coefficient = 0.91

The elastic ε-N_f model, accounting for *mean stress effects*, for the (12) Transverse cyclic-bending specimens,

$$\Delta\varepsilon_{et} / 2 = [.007865-\sigma_o/ E](2N_f)^{-.137}$$

The elastic ε-N_f model for the (10) Axial cyclic-bending specimens,

$$\Delta\varepsilon_{ea} / 2 = 9.161 \times 10^{-3}(2N_f)^{-.127}$$

with a correlation coefficient = 0.87

The elastic ε-N_f model, accounting for *mean stress effects*, for the (10) Axial cyclic-bending specimens,

$$\Delta\varepsilon_{ea} / 2 = [.009161-\sigma_o/ E](2N_f)^{-.127}$$

The coefficients for the elastic ε-N_f models, .007865 and .009161,represent the Fatigue Strength Coefficient,σ_f divided by the elastic modulus,E for the transverse and axial specimens respectively. Although, these coefficients were determined from a power-law relation, they are ,at best, approximations of the variables they represent.

The exponent(s) for the elastic ε-N_f models, -.137 and -.127, are simply the Fatigue Strength Exponent,b or Basquin's exponent. Since there is a slight discrepancy in Basquin's exponent,b between the S-N models, -.116 and -.110, and the ε-N_f models, -.137 and -.127, for the transverse and axial specimens, an explanation is in order.

To determine the power-fit from the S-N data, the variables were stress amplitude, $\Delta\sigma/2$ as a function of the number of cycles to failure,N_f ,where stress amplitude was simply a function of applied bending load. This bending load was obtained from the load-displacement data, section 3.5.1, where a maximum and minimum load were retrieved from each data interval that was analyzed per specimen. From this data, an average minimum load and average maximum load could be determined. Then, from these averages, stress amplitude and mean stress could be calculated. A power-fit was created

from the ε-N_f data; the variables were elastic strain amplitude, $\Delta\varepsilon_e/2$ as a function of the number of cycles to failure, N_f. Strain amplitude is a function of both stress amplitude and elastic modulus, i.e. $\Delta\varepsilon_e/2 = \Delta\sigma/2E$. (This elastic strain amplitude was also determined from the load-displacement data, where stress amplitude was the same as that obtained from the S-N study and the elastic modulus was reduced from a linear regression of the load-displacement data.)

A closer look in section 2.4.2 ,Eq.[2.4']&[2.5'], will demonstrate that after reducing the $\Delta\varepsilon_e/2$, it is simply a function of displacement (deflection). This may explain our discrepancy in Basquin's exponent, b. Since deflection was the controlled-variable, the exponents for the ε-N_f models might represent a more refined model than the S-N exponents since they were simply a function of load or stress.

The strain-life models have a ~ 2-3% better correlation than the respective stress-life models. For most single-phase metals, b varies between -0.05 and -0.12 and this fatigue property, as with most, is usually determined from a fully-reversed, uniaxial fatigue test, not a cyclic-bending test. Therefore these results are plausible, considering that this material is an MMC, not a single-phase alloy.

Since a mean stress was present in the cyclic-bending study, an elastic strain-life model, Eq.[3.14], that accounts for mean stress effects was created. Morrow (21) suggests that mean stress effects are significant at low values of

plastic strain, where elastic strain dominates. Figures 3.5a & b illustrate the ε-N_f models with and without mean stress effects. It is quite apparent that the strain-life model(s) that account for mean stress effects are mildly conservative for both transverse and axial models. The reason the strain-life models which account for mean stress effects are not straight-line, as with the strain-life models, is that the mean stress models are a function of cycles to failure,N_f, plus mean stress,σ_o and elastic modulus,E, thus creating greater variability. Tables 3.4 & 3.6 give the cycles to failure, actual strain amplitude, model strain amplitude and model strain amplitude w/ mean stress effects, for the transverse and axial specimens respectively.

3.5.4 Deflection Amplitude, $\Delta\delta/2$ Vs. Cycles to Failure, N_f

Since the entire cyclic-bending study was deflection-controlled, as opposed to a uniaxial, strain-controlled fatigue test, it was decided to formulate a deflection-life, δ-N_f, fatigue model. This model is of the same form as the S-N power-fit model, Eq.[3.9]. The main difference is that the dependent-variable for the deflection-life model Eq.[3.16] is elastic-deflection,$\Delta\delta/2$, not stress amplitude,$\Delta\sigma/2$,

$$\Delta\delta / 2 = D(N_f)^f \qquad [3.16]$$

The deflection models are as follows;

The elastic δ-N_f model for the (12) Transverse cyclic-bending specimens,

$$\Delta\delta_t / 2 = 0.730(N_f)^{-.170}$$

with a correlation coefficient of 0.95.

The elastic δ-N_f model for the (10) Axial cyclic-bending specimens,

$$\Delta\delta_a / 2 = 0.637(N_f)^{-.136}$$

with a correlation coefficient of 0.88.

The coefficients and exponents for these δ-N_f models are very similar to those of the S-N models. The Flexural Fatigue Coefficient(s), 0.730 & 0.637, simply represent the maximum deflection the transverse and axial cyclic-bending specimens respectively could resist for $N_f = 1$. The Flexural Fatigue Exponent, f= -0.170 & -0.136, represents the gradient of the transverse and axial $\Delta\delta/2$-N_f graphs respectively; see Figures 3.6a & b. Tables 3.7 & 3.8 list the number of cycles to failure, maximum deflection, actual deflection amplitude and model deflection amplitude for the transverse and axial cyclic-bending specimens respectively.

The correlations for the transverse and axial δ-N_f models were pleasantly acceptable, 0.95 & 0.88 respectively. The δ-N_f models fit the experimental data the best of the three models constructed. In refreshment, the δ-N_f method of modelling should have had the best fit, or correlation, since it was deflection that was the controlled-variable. Comparing the three relationships used to model the cyclic-bending study, the transverse specimens exhibited the best correlations for every model;

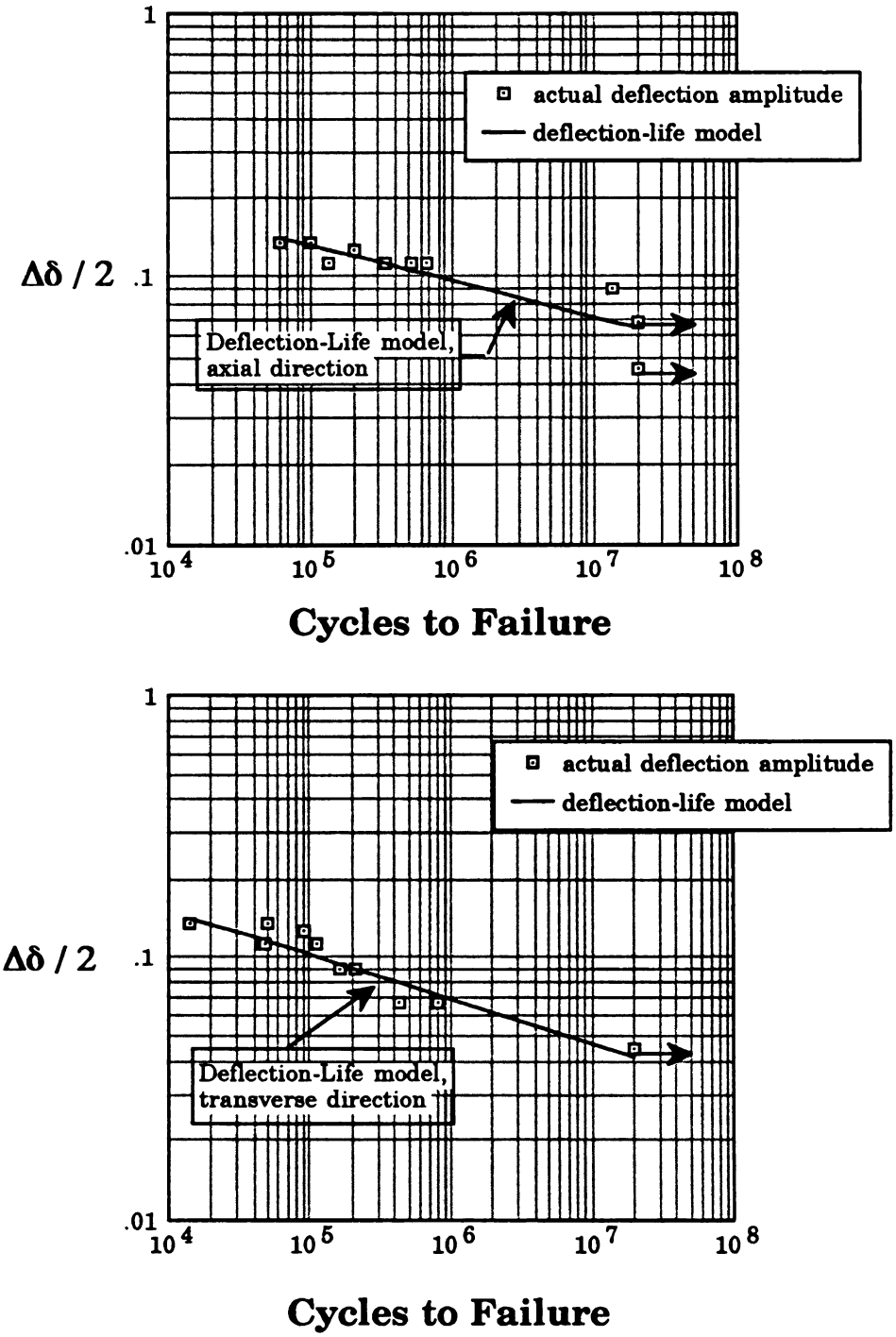

Figure 3.6 Deflection-Life (δ-N_f) plots of the cyclic-bending specimens for the transverse (top) and axial (bottom) directions. Note: deflection was the controlled variable.

Table 3.7 Deflection-life (δ-N_f) data for transverse specimen orientation. The $\Delta\delta/2$ model data was reduced from a power-law model, (δ-N_f), Eq.(3.16).

Specimen Number	N_f Cycles to Failure	δ_{max} Maximum Deflection (inch x10^{-3}) [mm]	$\Delta\delta/2$ Actual Deflection Amplitude (inch x10^{-3}) [mm]	$\Delta\delta/2$ Model Deflection Amplitude (inch x10^{-3}) [mm]
1AB	20 x 10^6*	3.973 [0.100]	1.772 [0.045]	1.654 [0.042]
2AB	801,330	5.906 [.150]	2.667 [.067]	2.835 [.072]
3AB	426,070	5.906 [.150]	2.667 [.067]	3.189 [.081]
4AB	209,820	7.874 [.200]	3.543 [.090]	3.583 [.091]
10AB	209,080	7.874 [.200]	3.543 [.090]	3.583 [.091]
13AB	162,040	7.874 [.200]	3.543 [.090]	3.740 [.095]
6AB	46,790	9.843 [.250]	4.429 [.113]	4.606 [.117]
7AB	45,000	9.843 [.250]	4.429 [.113]	4.646 [.118]
12AB	110,000	9.843 [.250]	4.429 [.113]	3.976 [.101]
11AB	91,020	11.024 [.280]	4.961 [.126]	4.134 [.105]
8AB	14,200	11.811 [.300]	5.315 [.135]	5.670 [.144]
9AB	50,000	11.811 [.300]	5.315 [.135]	4.567 [.116]

Table 3.8 Deflection-life (δ-N_f) data for Axial specimen orientation. The $\Delta\delta/2$ model data was produced from a power-law model, (δ-N_f), Eq.(3.16).

Specimen Number	N_f Cycles to Failure	δ_{max} Maximum Deflection (inch x10^{-3}) [mm]	$\Delta\delta/2$ Actual Deflection Amplitude (inch x10^{-3}) [mm]	$\Delta\delta/2$ Model Deflection Amplitude (inch x10^{-3}) [mm]
1TB	20 x 10^6*	3.937 [0.100]	1.772 [0.045]	2.539 [0.064]
2TB	20 x 10^6*	5.906 [.150]	2.667 [.068]	2.539 [.064]
2ATB	13 x 10^6	7.874 [.200]	3.543 [.090]	2.677 [.068]
3TB	135,000	9.843 [.250]	4.429 [.113]	5.016 [.127]
5TB	340,000	9.843 [.250]	4.429 [.113]	4.421 [.112]
12TB	650,000	9.843 [.250]	4.429 [.113]	4.047 [.103]
17TB	522,000	9.843 [.250]	4.429 [.113]	4.169 [.106]
10TB	200,000	11.024 [.280]	4.961 [.126]	4.752 [.121]
7TB	60,000	11.811 [.300]	5.315 [.135]	5.224 [.133]
8TB	100,000	11.811 [.300]	5.315 [.135]	5.602 [.142]

for the S-N model, 0.88 & 0.85, for the ε-N_f model, 0.91 & 0.87, and for the δ-N_f model, 0.95 & 0.88 for the transverse and axial bend specimens respectively. One explanation for the more predictable behavior of the transverse specimens is that the load transfer is primarily through the matrix only. The load transfer for the specimens in the fiber direction is through both the matrix and fiber, in this case discontinuous fibers. This composition makes for relatively difficult specimen to specimen prediction. From the material characterization, both static and cyclic-bending, it is quite clear that the fiber or reinforcement direction definitely has the preferred material integrity.

These results for the Cyclic-Bending tests were refreshing since there was initially serious speculation as to the validity of this cyclic-bending study, considering it was a different approach to an old art with the added variable that the material being investigated was also a new material, an MMC.

CHAPTER 4

DYNAMIC FLEXURAL MODULUS AS A FUNCTION OF CYCLES TO NEAR FAILURE.

The idea of evaluating the Elastic Flexural Modulus as a function of cycles was conceived midstream through the cyclic-bending study. This E-N study was deemed necessary and feasible for the following reasons: (1) It would lend insight to mechanisms such as strain hardening, (increasing E) or microcracking (decreasing E) as a function of cycles and deflection level, for the transverse and axial directions respectively. (2) It was feasible since the load-displacement, P-δ data was recorded at several designated intervals throughout each cyclic-bending test. The elastic flexural modulus was simply the gradient of the P-δ data multiplied by a constant, Eq. [2.6'], since the cyclic-bending tests were performed within the elastic limit. The number of cycles, N was simply the frequency (cycles/second) multiplied by the time interval from test initiation to when the P-δ data was captured. Since all the cyclic-bending tests were deflection-controlled, the deflection was constant for each test, so deflection-level was a given.

The E-N data is plotted on semi-log coordinates, the elastic flexural modulus is normalized with respect to the elastic modulus, E measured statically in a uniaxial state of stress, chapter 2.3, which was 13.09 msi and

18.60 msi, for the transverse and axial direction respectively. This evaluation is qualitative in nature, the prime objective was to analyze any general trends (e.g. strain hardening, microcracking, etc) and possibly to assess the feasibility and necessity of future, more quantitative analysis regarding elastic modulus in a repeated loading environment.

4.1 RESULTS FOR TRANSVERSE SPECIMENS

4.1.1 Specimens with maximum deflection of 0.10mm.

Specimen 1AB had a maximum deflection of 3.973 x 10^{-3}in. (0.10mm) and was cycled at 10hz (cycles/second) until reaching 10 million cycles, then the cyclic rate was increased to 20hz until 20 million cycles were reached, after which the was test terminated. Figure 4.1 shows what appears to be strain hardening, ~ 13%, from ~72,000 cycles to ~5,000K cycles. The elastic flexural modulus steadily decreases, ~15%, from ~5,000K cycles to ~20,000K cycles where the test was terminated. Table 4.1 gives both the absolute flexural modulus and the normalized flexural modulus for several cyclic intervals throughout the test.

4.1.2 Specimens with maximum deflection of 0.15mm.

Specimen 2AB and 3AB had a maximum deflection of 5.906 x 10^{-3}in. (0.15mm) and were both cycled at 10hz until specimen fracture, where N_f = 801,330 cycles for 2AB and 426,000 cycles for 3AB. Figure 4.2 shows both 2AB and

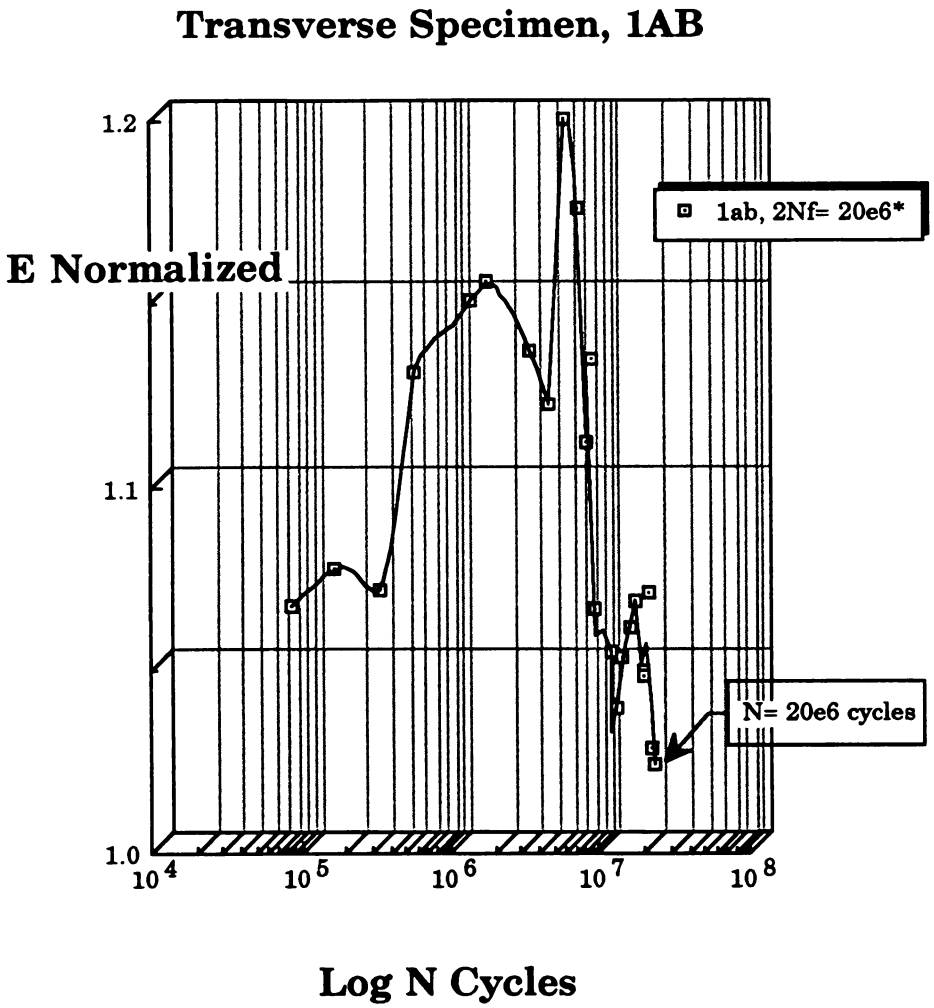

Figure 4.1 Dynamic flexural modulus as a function of cycles to near failure. Maximum deflection was 3.973 x 10^{-3} in. (0.10mm).

Table 4.1 Elastic modulus data as a function of cyclic interval for the transverse specimen (1AB) with a maximum deflection of 3.973 x 10^{-3}in. (0.10mm).

Number of Cycles	Elastic Modulus, E (Msi) [normalized]	Number of Cycles	Elastic Modulus, E (Msi) [normalized]
72,000	13.95 [1.065]	11,207K	13.58 [1.037]
144,000	14.08 [1.075]	12,001K	13.77 [1.051]
288,000	14.00 [1.069]	13,533K	13.87 [1.058]
498,000	14.78 [1.128]	15,051K	13.96 [1.066]
1,200K	15.03 [1.148]	16,522K	13.71 [1.047]
1,524K	15.10 [1.153]	17,026K	13.70 [1.046]
3,000K	14.86 [1.134]	18,160K	14.00 [1.068]
3,979K	14.66 [1.119]	19,024K	13.44 [1.026]
5,023K	15.70 [1.198]	20 x 10^6*	13.38 [1.021]
6,175K	15.36 [1.173]		
7,037K	14.53 [1.109]		
7,795K	14.83 [1.132]		
8,007K	13.93 [1.063]		
10,011K	13.78 [1.052]		

* This specimen (1AB) was cycled for 20 x 10^6 cycles, the test was then terminated, this was passing criterion for the cyclic-bending test, due to the time constraint.

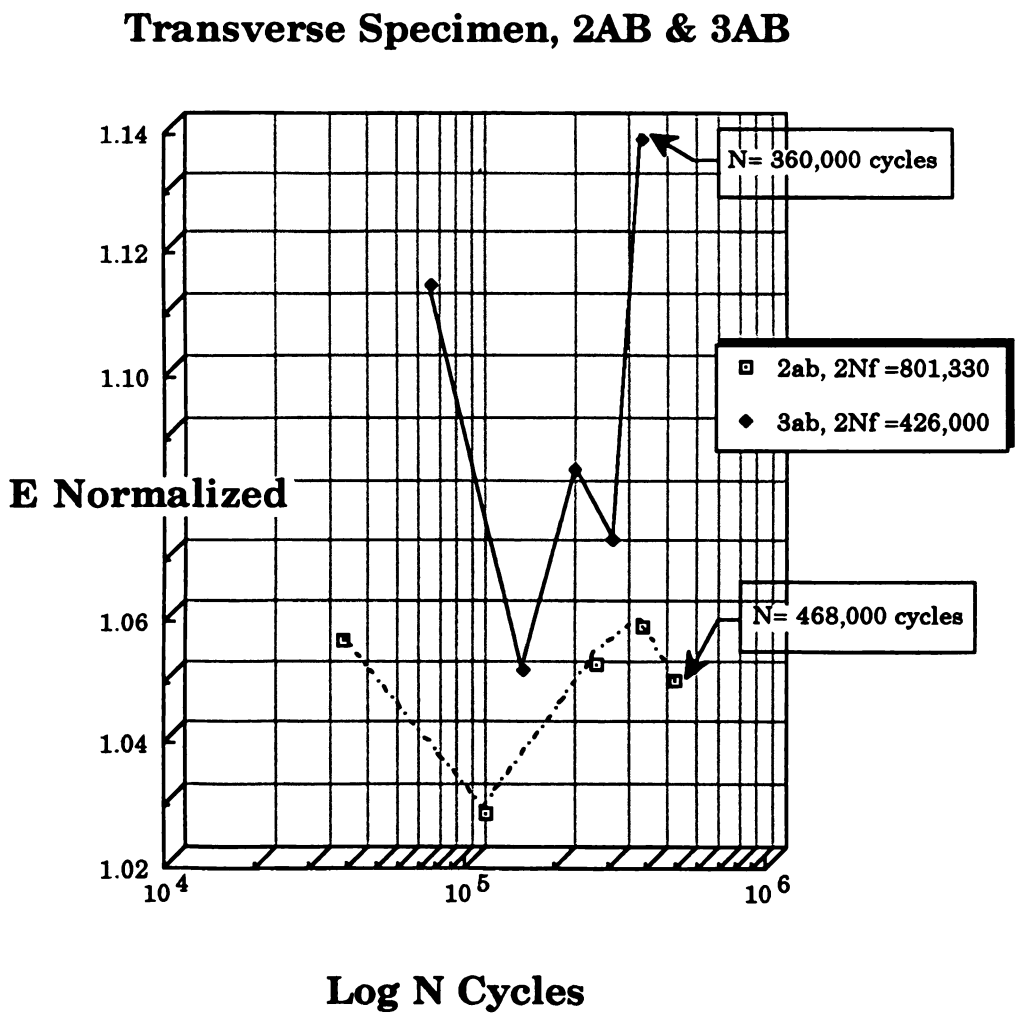

Figure 4.2 Dynamic flexural modulus as a function of cycles to near failure. Maximum deflection was 5.906 x 10^{-3} in. (0.15mm).

3AB initially cyclicly-softened, ~2% and ~5.5% respectively, both within approximately 70,000 cycles (from the first load-deflection interval). 2AB & 3AB began to both cyclic-harden at 108,000 cycles and 144,000 cycles respectively, ~2.4% and ~8.2%, until both reached 360,000 cycles. Specimen 2AB had a slight reduction in E, < 1%, until the last recorded cyclic interval of 468,000 cycles, although the specimen didn't fracture until 801,330 cycles. Specimen 3AB showed no reduction in E after reaching a maximum at 360,000 cycles until fracture (i.e. crack initiation), where N_f =426,000 cycles, although at ~ 432,000 cycles a cyclic-interval was recorded, and the flexural modulus had reduced ~ 18% in 72,000 cycles. Table 4.2 gives the absolute and normalized flexural modulus E for the respective cyclic intervals of 2AB and 3AB.

4.1.3 Specimens with maximum deflection of 0.20mm.

Specimen 4AB, 10AB and 13AB had a maximum deflection of 7.874 x 10^{-3}in. (0.20mm), and all three were cycled at 10hz throughout the entire cyclic-bending life, where N_f = 209,870, 209,080 and 162,040 cycles for 4AB, 10AB and 13AB respectively. Figure 4.3 shows specimen 4AB with a nearly negligible increase in modulus, ~1%, from 40 cycles to 1,000 cycles, although E decreased by ~ 8% from 1,000 cycles to 69,000 cycles. 4AB showed minimal strain-hardening, ~ 2.5%, from 69,000 cycles to 177,000 cycles. Specimen 10AB exhibited strain-hardening, ~ 4.8%, from 72,000 cycles to 108,000 cycles and then strain- softened nearly the same percentage from 108,000 cycles to 144,000 cycles and remained constant until near fracture, N= 209,000 cycles,

Table 4.2 Elastic modulus data as a function of cyclic interval for the transverse specimen with maximum deflection of 5.906 x 10^{-3}in. (0.15mm).

Specimen # 2AB		**Specimen # 3AB**	
Number of Cycles	**Elastic Modulus, E (Msi) [normalized]**	**Number of Cycles**	**Elastic Modulus, E (Msi) [normalized]**
36,000	13.82 [1.055]	72,000	14.58 [1.113]
108,000	13.45 [1.027]	144,000	13.76 [1.050]
252,000	13.77 [1.052]	216,000	14.19 [1.083]
360,000	13.85 [1.057]	288,000	14.04 [1.072]
468,000	13.73 [1.048]	360,000	14.90 [1.137]
N_f= 801,330	N/A	432,000	12.16* [0.929]

* Specimen 3AB failed (cracked) at approximately 426,000 cycles, this explains the reduction in the specimen's stiffness (i.e. elastic modulus).

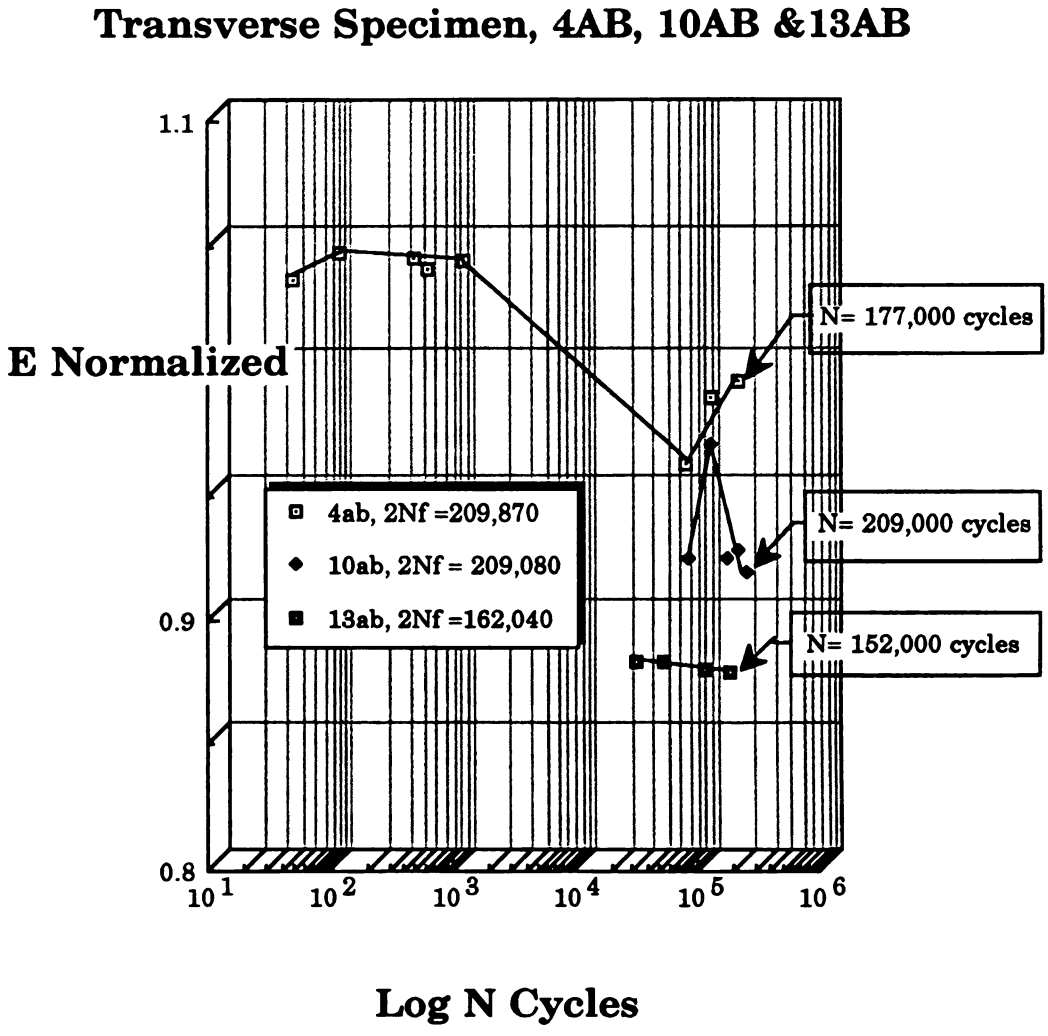

Figure 4.3 Dynamic flexural modulus as a function of cycles to near failure. Maximum deflection was 7.874 x 10^{-3} in. (0.20mm).

,and failed at 209,080 cycles. Nothing unusual happened with specimen 13AB, E remained relatively constant, < 0.5% change, for the few cyclic intervals recorded from 27,000 cycles to 152,000 cycles, and N_f = 162,000 cycles. The only unusual observation ,regarding 13AB, is that E was ~ 5% to ~15% less than E for 4AB or 10AB. Table 4.3 gives a discrete listing of the actual and normalized E for the respective cyclic intervals for 4AB, 10AB and 13AB.

4.1.4 Specimens with maximum deflection of 0.25mm.

Specimen 6AB, 7AB and 12AB had a maximum deflection of 9.843 x 10^{-3}in. (0.25mm) and all three were cycled at 5 hz. for their entire cyclic life, where N_f =46,790 cycles, 45,000 cycles and 110,000 cycles for 6AB, 7AB and 12AB respectively. Figure 4.4 illustrates a gradual, near-linear strain-hardening from specimen 6AB, ~ 6%, from 5 cycles to 45,000 cycles, this was within 2,000 cycles of specimen fracture. Specimen 7AB also illustrated strain-hardening, ~18.3%, from 2 cycles to 5,500 cycles, although this strain-hardening was significantly more than that of 6AB. The flexural modulus of 7AB decreased ~ 6.8% from 5,500 cycles to 41,500 cycles, which is within 3,500 cycles of specimen fracture. An interesting observation is that the flexural moduli of both 6AB and 7AB were nearly identical, having less than 0.1% difference at near fracture. Specimen 12AB had a mild increase in E, ~ 4.3%, from 9,000 cycles to 27,000 cycles, then an increase in E, ~ 6.1%, from 27,000 cycles to 45,000 cycles, and finally a near-linear increase in E, ~10.5%, from 45,000 cycles to 108,000 cycles, only 2,000 cycles short of the specimen's cyclic life. One notable characteristic is that the flexural modulus for 12AB is

Table 4.3 Elastic modulus data as a function of cyclic interval for the transverse specimen's 4AB, 10AB & 13AB with maximum deflection of 7.874 x 10^{-3}in. (0.20mm).

Specimen # 4AB		**Specimen # 10AB**	
Number of Cycles	**Elastic Modulus, E (Msi) [normalized]**	**Number of Cycles**	**Elastic Modulus, E (Msi) [normalized]**
40	13.52 [1.032]	72,000	12.07 [0.921]
100	13.66 [1.043]	108,000	12.65 [0.966]
400	13.63 [1.040]	144,000	12.07 [0.921]
520	13.58 [1.037]	180,000	12.11 [0.924]
1,000	13.62 [1.040]	209,000	11.99 [0.915]
69,000	12.56 [0.959]	N_f = 209,080	N/A
105,000	12.90 [0.985]		
177,000	12.99 [0.992]		
N_f = 209,820	N/A		

Specimen # 13AB

Number of Cycles	**Elastic Modulus, E (Msi) [normalized]**
27,000	11.52 [0.879]
45,000	11.52 [0.879]
98,000	11.48 [0.876]
152,000	11.46 [0.875]
N_f = 162,040	N/A

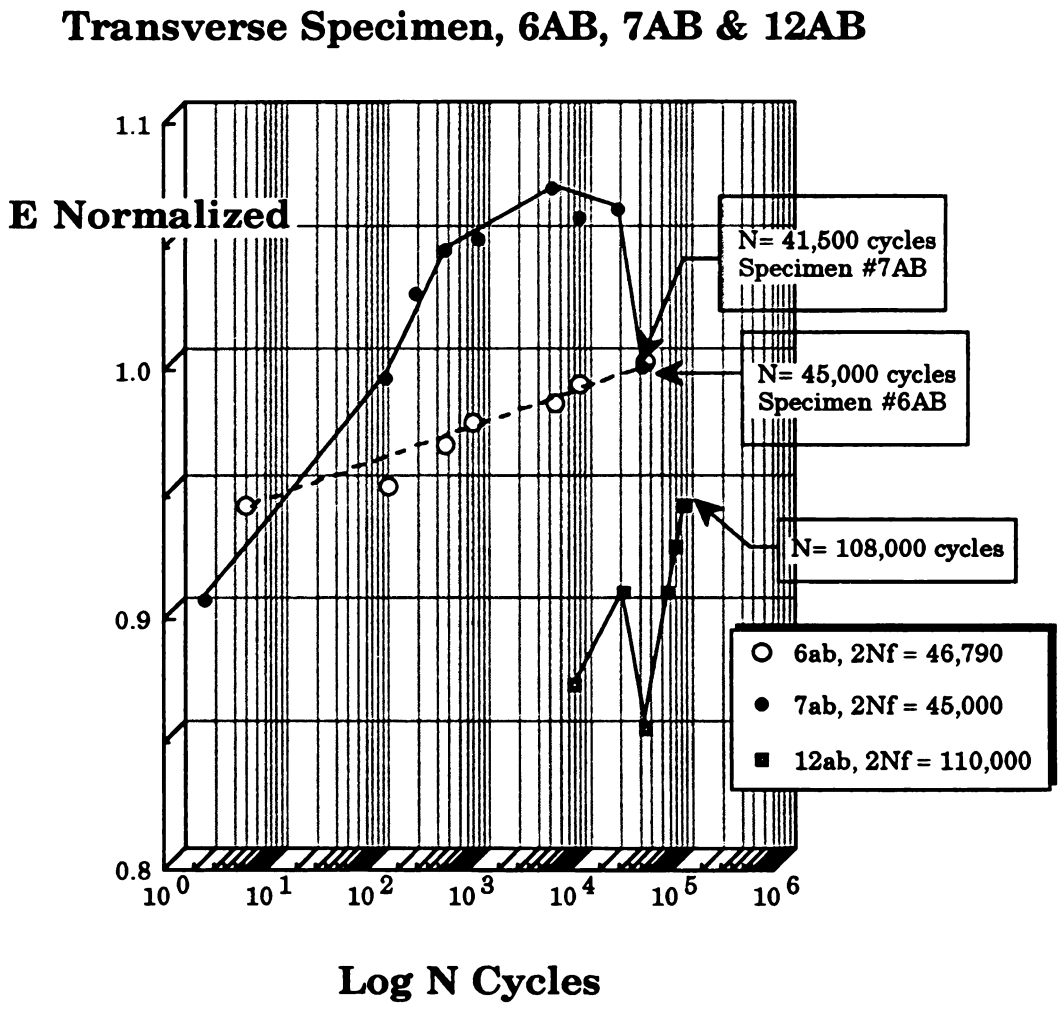

Figure 4.4 Dynamic flexural modulus as a function of cycles to near failure. Maximum deflection was 9.843 x 10^{-3} in. (0.25mm).

Table 4.4 Elastic modulus data as a function of cyclic interval for the transverse specimen's 6AB, 7AB & 12AB with maximum deflection of 9.843 x 10^{-3}in. (0.25mm).

Specimen # 6AB		**Specimen # 7AB**	
Number of Cycles	**Elastic Modulus, E (Msi) [normalized]**	**Number of Cycles**	**Elastic Modulus, E (Msi) [normalized]**
5	12.34 [0.942]	2	11.84 [0.904]
125	12.44 [0.950]	120	13.00 [0.992]
485	12.65 [0.966]	240	13.44 [1.026]
905	12.77 [0.975]	480	13.67 [1.044]
5,700	12.87 [0.982]	1,000	13.74 [1.049]
10,000	12.97 [0.990]	5,500	14.01 [1.069]
45,000	13.08 [0.998]	10,000	13.85 [1.057]
N_f = 46,790	N/A	23,500	13.89 [1.060]
		41,500	13.06 [0.997]
		N_f = 45,000	N/A

Table 4.4 (cont'd)

Specimen # 12AB

Number of Cycles	**Elastic Modulus, E (Msi) [normalized]**
9,000	11.39 [0.869]
27,000	11.88 [0.907]
45,000	11.16 [0.852]
72,000	11.88 [0.907]
90,000	12.12 [0.925]
108,000	12.33 [0.941]
N_f = 110,000	N/A

considerably less than that of 6AB and 7AB, at one point, 18% less for the same number of cycles. Table 4.4 gives a discrete listing of the actual and normalized E for the respective cyclic intervals for 6AB, 7AB and 12AB.

4.1.5 Specimens with maximum deflection of 0.28mm.

Specimen 11AB had a maximum deflection of 11.024 x 10^{-3}in. (0.28mm) and was cycled at 5 hz throughout the entire cyclic life of the specimen, where N_f = 91,020 cycles. The flexural modulus for specimen 11AB decreased , ~ 3.8%, from 8,000 cycles to 26,000 cycles and is then increased, ~ 6.2%, from 26,000 cycles to 53,000 cycles and then stabilized until reaching 80,000 cycles. At 89,000 cycles, E had decreased ~ 9%, only 2,020 cycles shy of cyclic life termination, see Fig. 4.5. Table 4.5 gives a discrete listing of the actual and normalized E for the respective cyclic intervals for 11AB.

4.1.6 Specimens with maximum deflection of 0.30mm.

Specimens 8AB and 9AB had a maximum deflection of 11.811 x 10^{-3}in. (0.30mm) and were cycled at 2 hz throughout their cyclic life, where N_f = 14,200 cycles and 49,000 cycles respectively. Figure 4.6 illustrates that specimen 8AB has virtually no increase in E from 5 cycles to 125 cycles and then gradually increases, ~2.8%, from 125 cycles to 14,000 cycles, this was only 200 cycles short of the cyclic life termination. The flexural modulus increased gradually, ~1.6%, from 5 cycles to 7,000 cycles, and then decreased minimally, less than 0.4%, from 7,000 cycles to 49,000 cycles, approximately

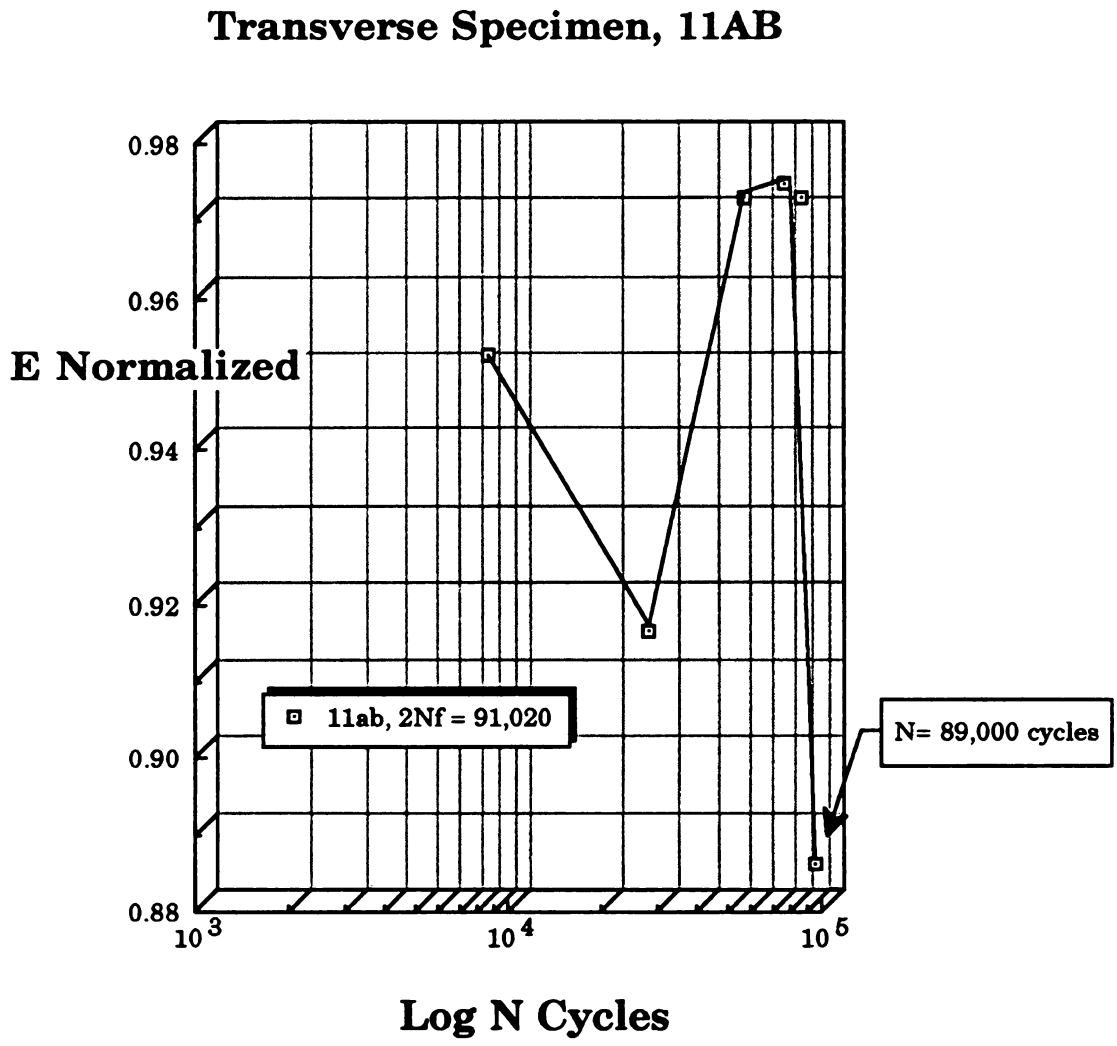

Figure 4.5 Dynamic flexural modulus as a function of cycles to near failure. Maximum deflection was 11.024 x 10^{-3} in. (0.28mm).

Table 4.5 Elastic modulus data as a function of cyclic interval for the transverse specimen 11AB, with maximum deflection of 11.024 x 10^{-3}in. (0.28mm).

Specimen # 11AB

Number of Cycles	**Elastic Modulus, E (Msi) [normalized]**
8,000	12.46 [0.951]
26,000	11.99 [0.915]
53,000	12.73 [0.972]
71,000	12.75 [0.973]
80,000	12.73 [0.972]
89,000	11.59 [0.885]
N_f = 91,020	N/A

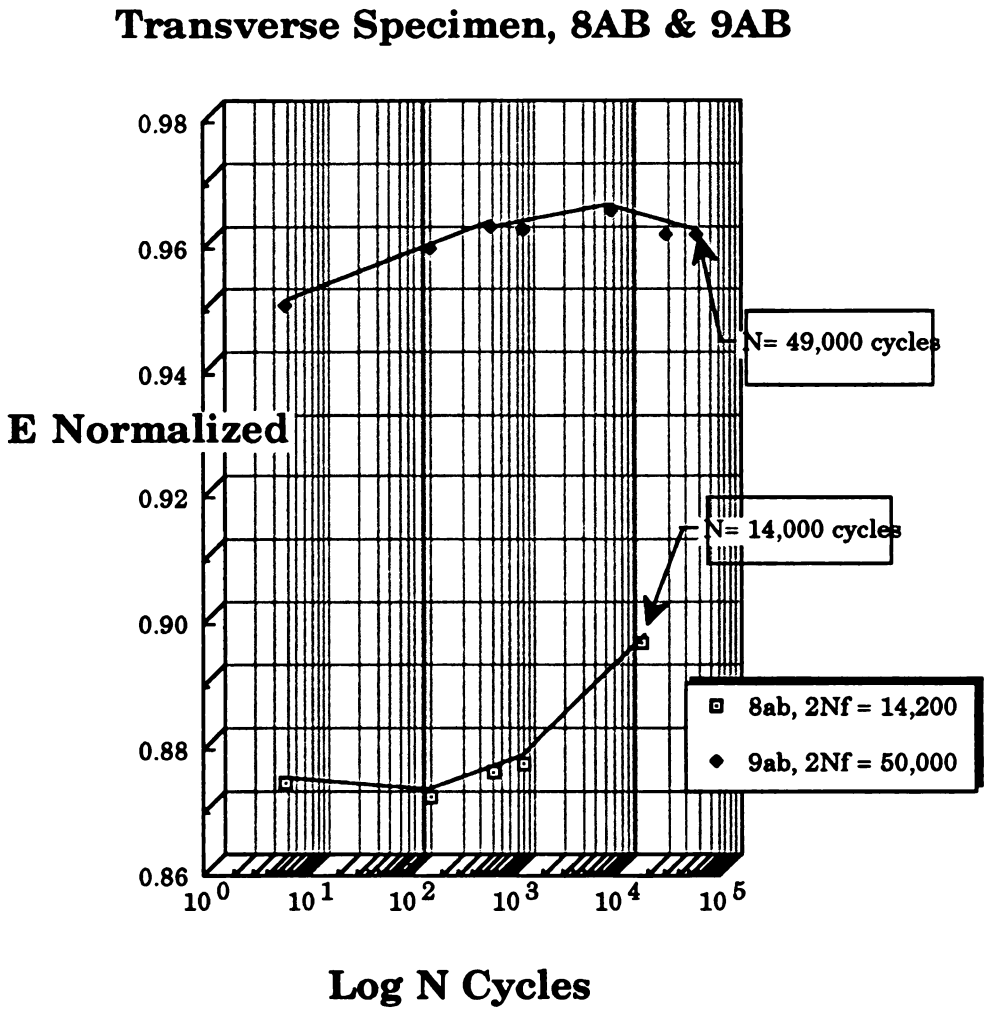

Figure 4.6 Dynamic flexural modulus as a function of cycles to near failure. Maximum deflection was 11.811 x 10^{-3} in. (0.30mm).

Table 4.6 Elastic modulus data as a function of cyclic interval for the transverse specimens 8AB & 9AB, with a maximum deflection of 11.811 x 10^{-3}in. (0.30mm).

Specimen # 8AB		**Specimen # 9AB**	
Number of Cycles	**Elastic Modulus, E (Msi) [normalized]**	**Number of Cycles**	**Elastic Modulus, E (Msi) [normalized]**
5	11.44 [0.873]	5	12.43 [0.949]
125	11.41 [0.871]	125	12.55 [0.958]
505	11.46 [0.875]	485	12.60 [0.962]
985	11.48 [0.876]	1,000	12.59 [0.961]
14,000	11.73 [0.895]	7,000	12.63 [0.964]
N_f = 14,200	N/A	25,000	12.58 [0.960]
		49,000	12.58 [0.960]
		N_f = 50,000	N/A

1,000 cycles before cyclic life termination. Table 4.6 gives a discrete listing of the actual and normalized E for the respective cyclic intervals for 8AB and 9AB.

4.2 RESULTS FOR AXIAL SPECIMENS

4.2.1 Specimens with a maximum deflection of 0.10mm.

Specimen 1TB had a maximum deflection of 3.973×10^{-3} in. (0.10) and was cycled at 10 hz until ~1.7million cycles; then the cyclic rate was increased to 20 hz until 20 million cycles were reached, and the test was terminated. Figure 4.7 shows several patterns of flexural modulus increasing and decreasing. although the modulus is gradually increasing throughout the test, ~ 11%, from 35,000 cycles to 5,048K cycles. Flexural modulus decreases slightly, ~ 3%, from 5,048K cycles to 20,000K cycles, where the test was terminated. This test is quite interesting in that there are several stages, approximately 6 stages or cycles, where the flexural modulus is increasing and decreasing. At the initiation of the third stage, where N~ 1,000K cycles, E takes an increase of nearly 8.5%, and the flexural modulus seems to somewhat stabilize at about 1,350K cycles and remain at approximately 98% of that modulus until test termination. Table 4.7 gives a discrete listing of the actual and normalized E for the respective cyclic intervals for specimen 1TB.

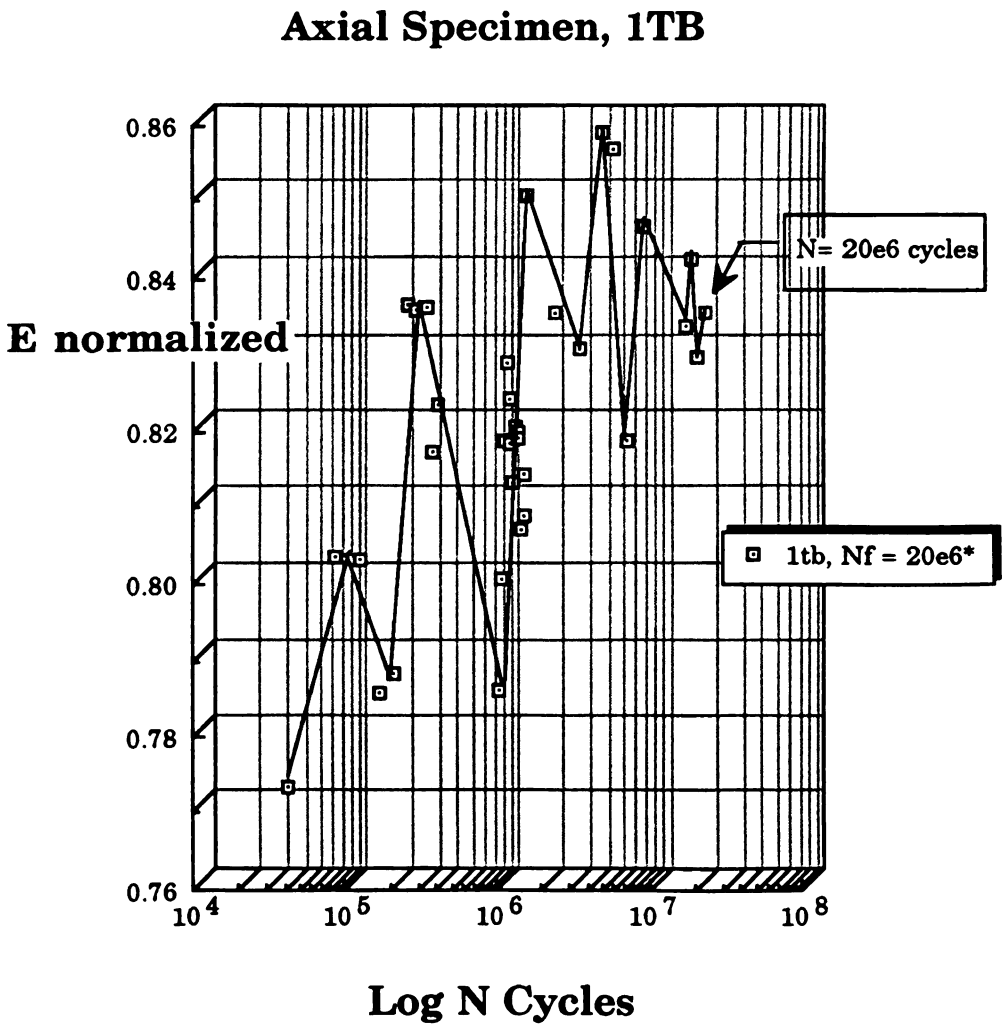

Figure 4.7 Dynamic flexural modulus as a function of cycles to near failure. Maximum deflection was 3.973 x 10^{-3} in. (0.10mm).

Table 4.7 Elastic modulus data as a function of cyclic interval for the axial specimen 1TB, with a maximum deflection of 3.973 x 10^{-3}in. (0.10mm).

Specimen # 1TB

Number of Cycles	Elastic Modulus, E (Msi) [normalized]	Number of Cycles	Elastic Modulus, E (Msi) [normalized]
35,000	14.44 [0.772]	1,134K	15.32 [0.819]
72,000	15.00 [0.802]	1,170K	15.31 [0.819]
108,000	14.99 [0.802]	1,206K	15.29 [0.818]
144,000	14.67 [0.784]	1,242K	15.07 [0.806]
180,000	14.71 [0.787]	1,278K	15.11 [0.808]
216,000	15.62 [0.835]	1,314K	15.21 [0.813]
252,000	15.61 [0.835]	1,350K	15.88 [0.849]
288,000	15.61 [0.835]	2,046K	15.60 [0.834]
324,000	15.26 [0.816]	3,054K	15.51 [0.829]
350,000	15.37 [0.822]	4,256K	16.04 [0.858]
882,000	14.67 [0.785]	5,048K	16.00 [0.856]
918,000	14.95 [0.799]	6,069K	15.28 [0.817]
954,000	15.29 [0.818]	8,038K	15.81 [0.845]
990,000	15.48 [0.828]	15,022K	15.57 [0.832]
1,026K	15.28 [0.817]	16,560K	15.73 [0.841]
1,062K	15.39 [0.823]	17,954K	15.49 [0.829]
1,098K	15.18 [0.812]	20,000K*	15.60 [0.834]

* The test was terminated at 20 x 10^6 cycles, since failure had not been induced, this was the passing criterion for the cyclic-bending study.

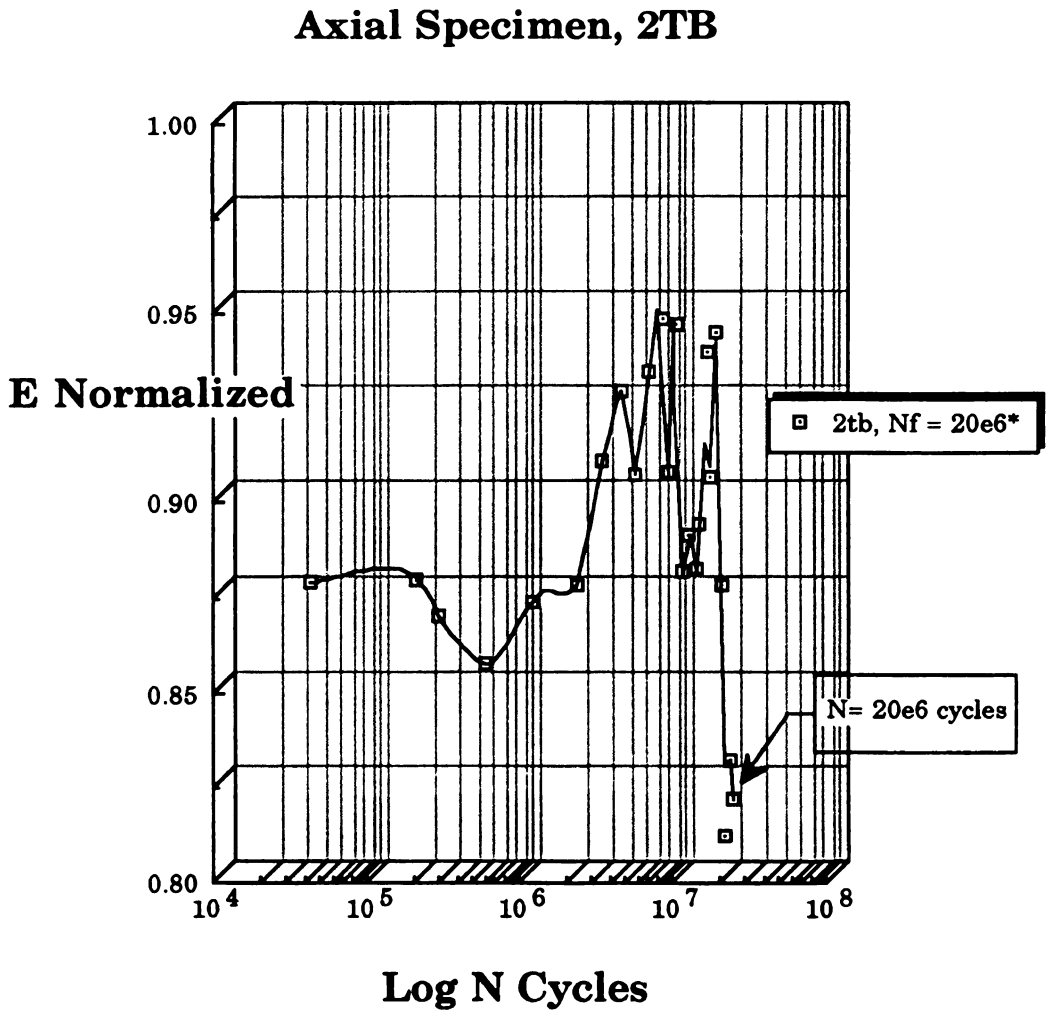

Figure 4.8 Dynamic flexural modulus as a function of cycles to near failure. Maximum deflection was 5.906 x 10^{-3} in. (0.15mm).

4.2.2 Specimens with maximum deflection of 0.15mm.

Specimen 2TB had a maximum deflection of 5.906 x 10^{-3} in. (0.15) and was cycled at 10 hz until reaching 2.9 million cycles where the cyclic frequency was increased to 20 hz until the test was terminated at 20 million cycles. Figure 4.8 illustrates a nearly constant flexural modulus from 36,000 cycles to 180,000 cycles, then E decreases, ~2.6%, from 180,000 cycles to 504,000 cycles. The flexural modulus steadily increases, ~ 10.6%, from 504,000 cycles to 7,550K cycles, (with a small drop at 4,930K cycles). Flexural modulus increases and decreases sporadically between 4,018K cycles to 16,485K cycles, and a steep, marginal drop in E, ~ 14.1%, from 16,485K cycles to 19,100K cycles and finally the test was terminated at 20 million cycles. Table 4.8 gives a discrete listing of the actual and normalized E for the respective cyclic intervals for specimen 2TB.

4.2.3 Specimens with maximum deflection of 0.20mm.

Specimen 2ATB had a maximum deflection of 7.874 x 10^{-3} in. (0.20) and was cycled at 10 hz. until 13.5 million cycles where the specimen fractured and the test was terminated. Figure 4.9 shows a nearly constant flexural modulus from 5 cycles to 4,017K cycles. The flexural modulus begins to show rapid decrement, ~ 35.6%, from 12,180K cycles to 13,089K cycles, and the specimen fractured at 13,500K cycles. Table 4.9 gives a discrete listing of the actual and normalized E for the respective cyclic intervals for specimen 2ATB.

Table 4.8 Elastic modulus data as a function of cyclic interval for the axial specimen 2TB, with a maximum deflection of 5.906 x 10^{-3}in. (0.15mm).

Specimen # 2TB

Number of Cycles	Elastic Modulus, E (Msi) [normalized]	Number of Cycles	Elastic Modulus, E (Msi) [normalized]
36,000	16.38 [0.876]	9,114K	17.65 [0.944]
180,000	16.40 [0.877]	9,870K	16.45 [0.879]
254,000	16.22 [0.867]	10,982K	16.62 [0.889]
504,000	15.98 [0.855]	12,589K	16.45 [0.880]
1,026K	16.29 [0.871]	13,021K	16.67 [0.891]
1,998K	16.38 [0.876]	14,565K	17.52 [0.937]
3,010K	16.98 [0.908]	15,069K	16.90 [0.904]
4,018K	17.33 [0.927]	16,485K	17.61 [0.942]
4,930K	16.92 [0.905]	17,981K	16.37 [0.875]
6,046K	17.65 [0.932]	19,100K	15.13 [0.809]
7,550K	17.68 [0.946]	20,036K*	15.51 [0.830]

* The test was terminated at 20 x 10^6 cycles, since failure had not been induced. This was the passing criterion for the cyclic-bending study,due to the time constraint.

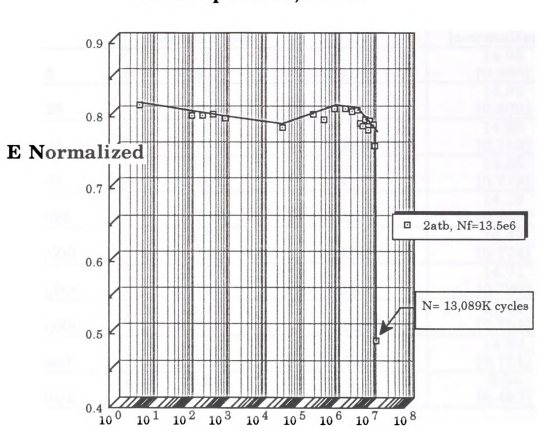

Figure 4.9 Dynamic flexural modulus as a function of cycles to near failure. Maximum deflection was 7.874 x 10^{-3} in. (0.20mm).

Table 4.9 Elastic modulus data as a function of cyclic interval for the axial specimen 2ATB, with a maximum deflection of 7.874 x 10^{-3}in. (0.20mm).

Specimen # 2ATB

Number of Cycles	Elastic Modulus, E (Msi) [normalized]	Number of Cycles	Elastic Modulus, E (Msi) [normalized]
5	15.12 [0.809]	3,018K	14.96 [0.800]
125	14.86 [0.795]	4,017K	14.99 [0.802]
245	14.84 [0.794]	5,005K	14.65 [0.783]
485	14.86 [0.795]	6,010K	14.56 [0.779]
1,025	14.77 [0.790]	6,992K	14.75 [0.789]
38,000	14.55 [0.778]	7,928K	14.47 [0.774]
254,000	14.88 [0.796]	9,030K	14.71 [0.786]
506,000	14.75 [0.789]	11,028K	14.60 [0.781]
1,020K	15.02 [0.803]	12,180K	14.04 [0.751]
2,010K	15.02 [0.803]	13,089K*	9.04 [0.483]

* The specimen 2ATB didn't noticeably fail or crack until approximately 13,500K cycles, although there was significant decrement in the elastic modulus at about 12,180K cycles.

4.2.4 Specimens with a maximum deflection of 0.25mm.

Specimens 3TB, 5TB, 12TB & 17TB had a maximum deflection of 9.843×10^{-3} in. (0.25) and were cycled at 5 hz until specimen fracture, where the test was terminated. The specimens will be discussed in ascending order of cyclic life. Specimen 3TB shows a monotonic increase in modulus, ~ 5.3%, from 5 cycles to 111,100 cycles and then a slight decrease in E, ~ 2.0%, from 111,100 cycles to 133,600 cycles, as shown in Figure 4.10. Specimen 3TB failed at 135,000 cycles. Specimen 5TB had a slight increase in modulus, ~ 1.5%, from 5 cycles to 197,000 cycles and an almost negligible decrease in E, less than 0.4%, from 197,000 cycles to 242,000 cycles, see Figure 4.10. Specimen 5TB failed at 340,000 cycles. Specimen 17TB exhibits an appreciable increase in modulus, ~ 8.1%, from 10,000 cycles to 100,000 cycles; the modulus then decreased until reaching 298,000 cycles and then E returned to the approximate modulus reached at 100,000 cycles, (just before decrease in E). The modulus dropped slightly, ~ 3.0%, from 390,000 cycles to 520,000 cycles and failed 2,000 cycles later,(i.e. N_f = 522,000 cycles). Finally, Specimen 12TB showed an increase in modulus, ~ 5.6%, from 20,000 cycles to 201,000 cycles. The modulus decreased equally as much from 201,000 cycles to 600,000 cycles and ultimately failed at 650,000 cycles. Table 4.10 gives a discrete listing of the actual and normalized values of E for specimens 3TB, 5TB, 12TB & 17TB and their respective cyclic intervals.

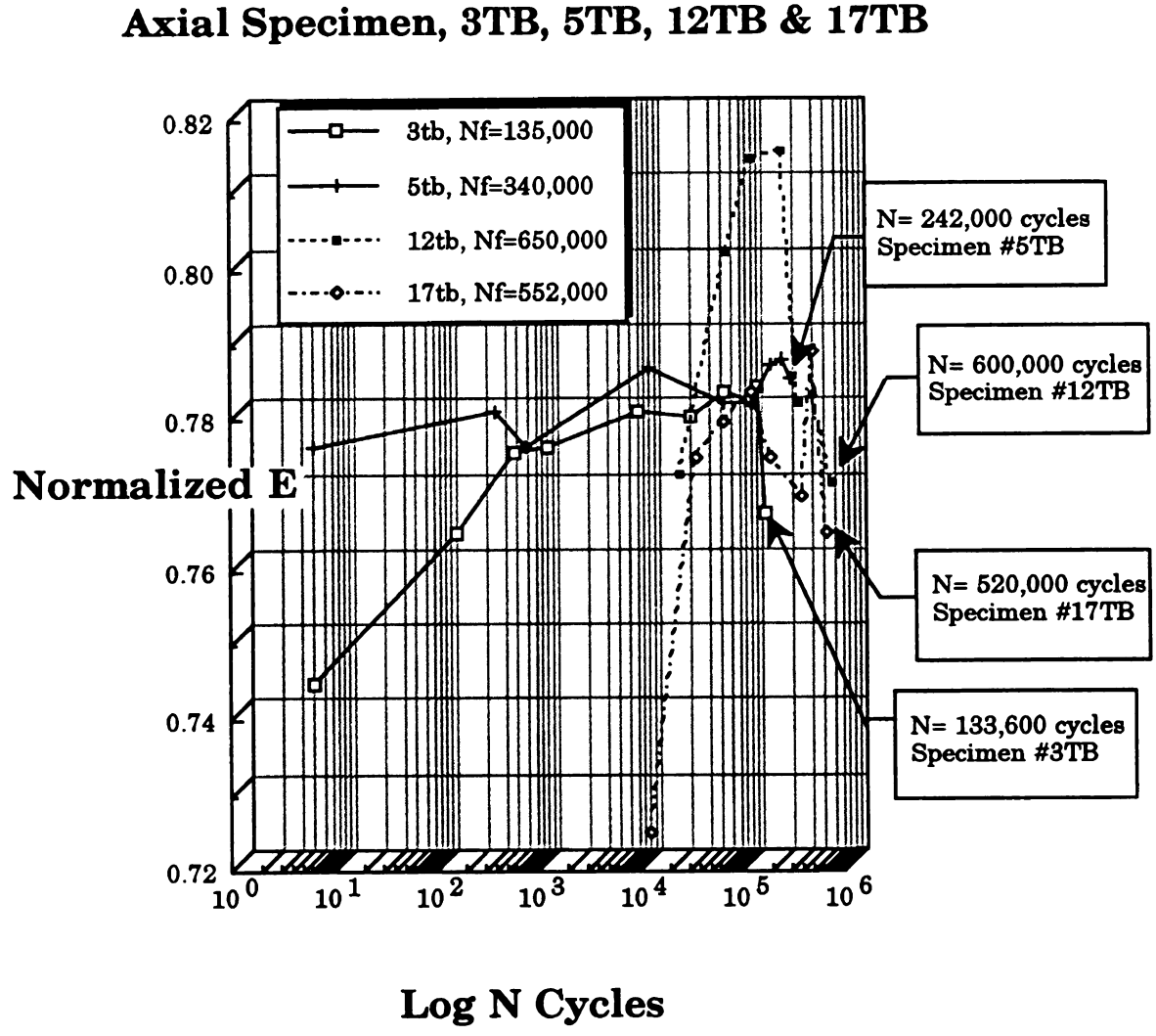

Figure 4.10 Dynamic flexural modulus as a function of cycles to near failure. Maximum deflection was 9.843 x 10^{-3} in. (0.25mm).

Table 4.10 Elastic modulus data as a function of cyclic interval for the axial specimen's 3TB, 5TB, 12TB & 17TB, with a maximum deflection of 9.843 x 10^{-3}in. (0.25mm).

Specimen # 3TB		**Specimen # 5TB**	
Number of Cycles	**Elastic Modulus, E (Msi) [normalized]**	**Number of Cycles**	**Elastic Modulus, E (Msi) [normalized]**
5	13.90 [0.743]	5	14.49 [0.775]
125	14.28 [0.764]	305	14.58 [0.780]
485	14.48 [0.774]	605	14.49 [0.775]
1,000	14.49 [0.775]	10,000	14.69 [0.786]
7,600	14.58 [0.780]	54,000	14.60 [0.781]
25,600	14.57 [0.779]	98,000	14.60 [0.781]
52,600	14.63 [0.782]	152,000	14.70 [0.786]
102,100	14.61 [0.781]	197,000	14.71 [0.787]
111,100	14.64 [0.783]	242,000	14.66 [0.784]
133,600	14.33 [0.766]	N_f = 340,000	N/A
N_f = 135,000	N/A		

Table 4.10 (cont'd)

Specimen # 12TB		**Specimen # 17TB**	
Number of Cycles	**Elastic Modulus, E (Msi) [normalized]**	**Number of Cycles**	**Elastic Modulus, E (Msi) [normalized]**
20,000	14.42 [0.771]	10,000	13.53 [0.724]
56,000	14.98 [0.801]	28,000	14.46 [0.773]
101,000	15.21 [0.813]	55,000	14.55 [0.778]
201,000	15.23 [0.814]	100,000	14.63 [0.782]
295,000	14.60 [0.781]	154,000	14.47 [0.774]
403,000	14.62 [0.782]	298,000	14.37 [0.768]
600,000	14.40 [0.770]	390,000	14.73 [0.788]
N_f = 650,000	N/A	520,000	14.28 [0.763]
		N_f =522,000	N/A

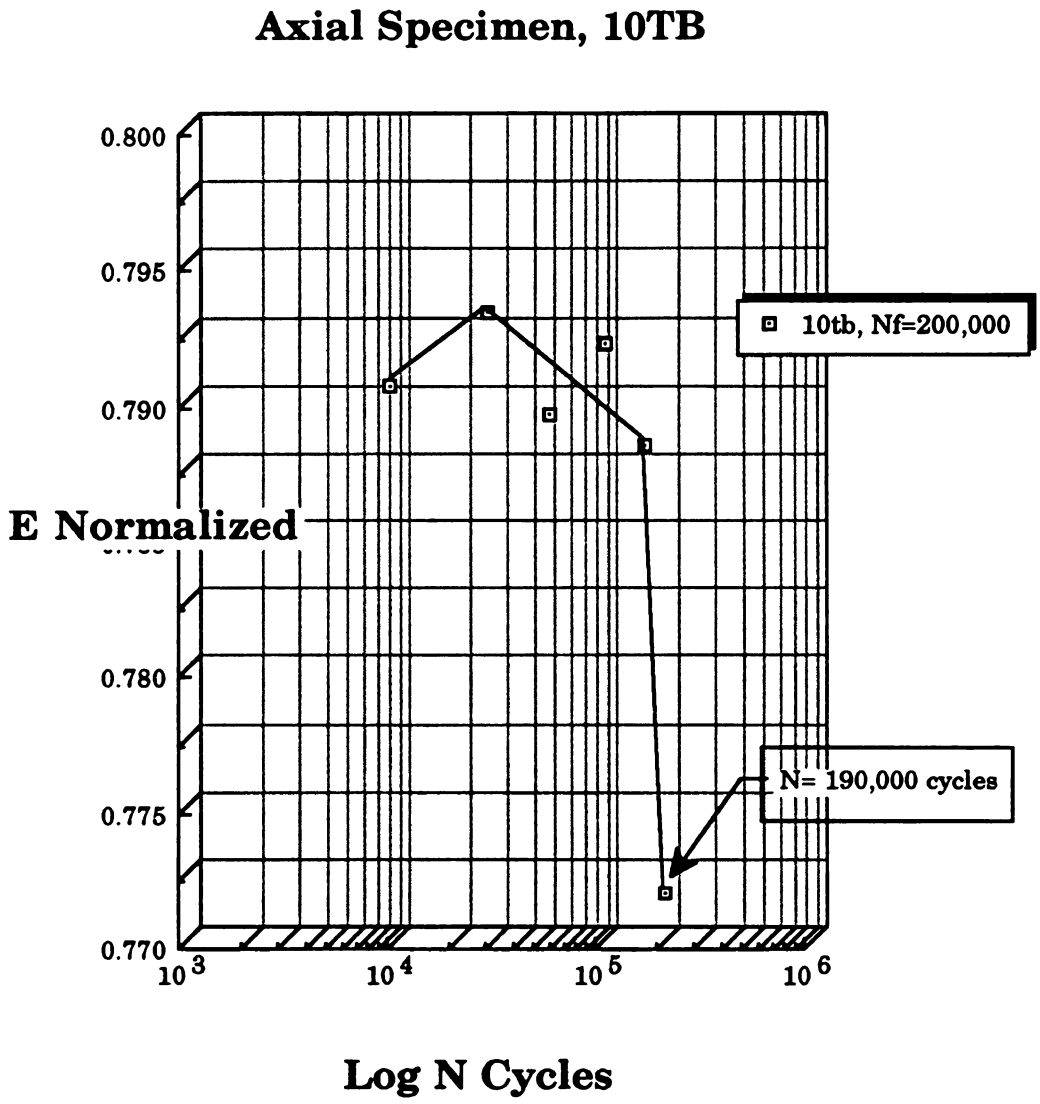

Figure 4.11 Dynamic flexural modulus as a function of cycles to near failure. Maximum deflection was 11.024 x 10^{-3} in. (0.28mm).

Table 4.11 Elastic modulus data as a function of cyclic interval for the axial specimen 10TB, with a maximum deflection of 11.024 x 10^{-3}in. (0.28mm).

Specimen # 10TB

Number of Cycles	**Elastic Modulus, E (Msi) [normalized]**
9,000	14.78 [0.790]
27,000	14.83 [0.793]
54,000	14.76 [0.789]
99,000	14.81 [0.792]
153,000	14.74 [0.788]
190,000	14.43 [0.772]
N_f = 200,000	N/A

4.2.5 Specimens with maximum deflection of 0.28mm.

Specimen 10TB had a maximum deflection of 11.024 x 10^{-3} in. (0.28) and was cycled at 5 hz until specimen fracture, at which time the test was terminated. Fig. 4.11 shows a slight increase in modulus, less than 0.5%, from 9,000 cycles to 27,000 cycles with a nearly equal decrease in modulus from 27,000 cycles to 153,000 cycles. The flexural modulus decreased ~ 2.0% from 153,000 cycles to 190,000 cycles. Specimen 10TB ultimately failed at 200,000 cycles. Table 4.11 gives a discrete listing of the actual and normalized values of E for specimen 10TB and its respective cyclic intervals to near failure.

4.2.6 Specimens with a maximum deflection of 0.30mm.

Specimens 7TB & 8TB had a maximum deflection of 11.811 x 10^{-3} in. (0.30) and were cycled at 2 hz until specimen fracture, at which time the test was terminated. For specimen 7TB, Figure 4.12 shows a constant, near-linear increase in flexural modulus, ~ 1.4%, from 10 cycles to 21,500 cycles and a slight decrease in modulus at 57,500 cycles and specimen failure occurred at 60,000 cycles. The flexural modulus was nearly constant from 5 cycles to 125 cycles and then increased, ~ 2.6%, until reaching 10,200 cycles. From 10,200 cycles to 73,200 cycles the modulus decreased approximately 2.6%, (this was approximately the same modulus as at 10 cycles), and the specimen ultimately failed at 100,000 cycles. Table 4.12 gives a discrete listing of the actual and normalized values of E for specimens 7TB & 8TB and their respective cyclic intervals to near failure.

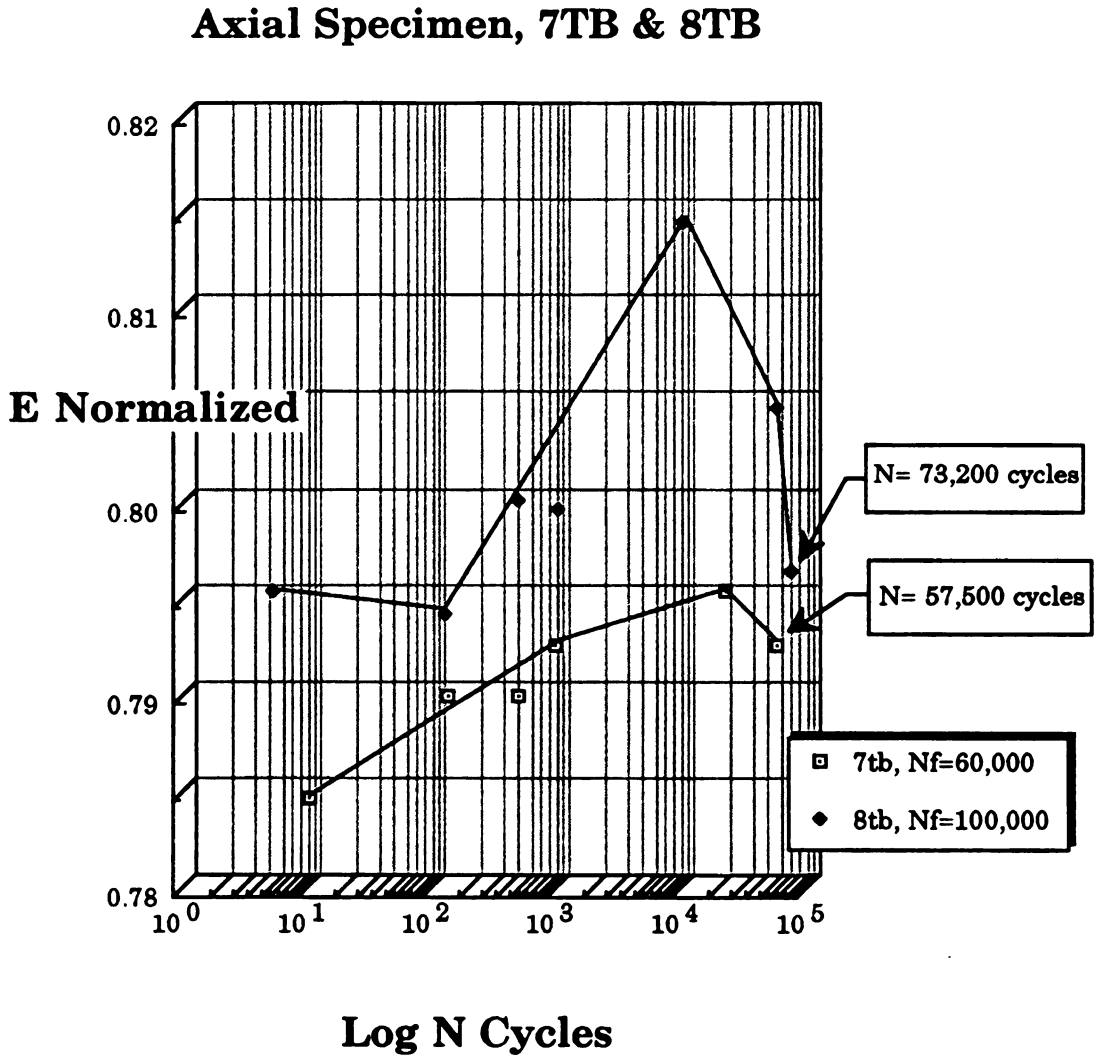

Figure 4.12 Dynamic flexural modulus as a function of cycles to near failure. Maximum deflection was 11.811 x 10^{-3} in. (0.30mm).

Table 4.12 Elastic modulus data as a function of cyclic interval for the axial specimen's 7TB & 8TB, with a maximum deflection of 11.811 x 10^{-3}in. (0.30mm).

Specimen # 7TB		**Specimen # 8TB**	
Number of Cycles	**Elastic Modulus, E (Msi) [normalized]**	**Number of Cycles**	**Elastic Modulus, E (Msi) [normalized]**
10	14.67 [0.784]	5	14.87 [0.795]
130	14.77 [0.790]	125	14.85 [0.794]
490	14.77 [0.790]	485	14.96 [0.800]
970	14.82 [0.793]	1,000	14.95 [0.799]
21,500	14.87 [0.795]	10,200	15.23 [0.814]
57,500	14.82 [0.793]	55,200	15.05 [0.805]
N_f = 60,000	N/A	73,200	14.89 [0.796]
		N_f = 100,000	N/A

4.3 DISCUSSION OF THE E-N RESULTS

Looking over the plots and results of the E-N study at first there seems to be no common trends from specimen to specimen. The only common thread for all the cyclic-bend specimens is that the elastic modulus *varies* with cycles. This variation in elastic modulus, with bending cycles, is hard to accept since the cycles are elastic, thus the elastic modulus should remain *constant*. Then the next question, is the deformation actually elastic? From our first course in mechanics we are taught that, if there is no plastic deformation, cyclic or static, the elastic constants remain constant. For this cyclic-bend study the specimens had to remain elastic, otherwise they would have failed due to impact damage.

The technique for measuring the load-displacement data for this survey was with a load-cell and an extensometer. This is at best a qualitative approach, had a similar variation in modulus with cycles not been observed by other researchers (23,24,25), it probably would have been discarded as bad data.

With the advent of exotic materials, such as ceramic-matrix composites, metal-matrix composites and polymer-matrix composites, several atypical observations have been evaluated. For example, ceramic (32), ceramic-matrix (27,28) and brittle polymer-matrix (26) materials under thermal and mechanical fatigue have encountered a elastic modulus decrement until reaching a saturation-level where they would ultimately fail. Using sonic resonance (33-36), this modulus decrement with, thermal and mechanical,

cycles has been quantified. An empirical expression (23) has been derived which models this characteristic with surprisingly good precision. The same materials under equivalent static, thermal or mechanical, conditions would see virtually no reduction in the elastic modulus. Therefore, there are clearly mechanisms under cyclic loading that are not present for static conditions (39). These fatigue conditions are addressed in more detail in Chapter 5.

The objective of this discussion was to point out that, although the results in Chapter 4 may have no quantifiable use, they have opened our eyes to the fact that the modulus fluctuated for what was assumed to be elastic mechanical cycles. Refreshingly, similar elastic modulus decrement(39) has been observed in other materials that were also assumed to be elastically cycled. Thus, this observation gives rise to the validity of a rigorous investigation, to quantify the elastic modulus variation as a function of mechanical cycles.

Currently, several researchers have purposed that for brittle materials under cyclic-loading, a plastic zone is created from such mechanisms as, crack face asperties, fracture debris from fiber or grain pullout and crack bridging.

CHAPTER 5

CONCLUSIONS AND RECOMMENDATIONS

A material characterization was conducted for a SiC_w / Aluminum metal matrix composite (MMC). The purpose of the study was two-fold: (1) to perform a static evaluation of the MMC to determine the tensile, shear and flexural monotonic properties; and (2) to perform a deflection-controlled cyclic-bending survey of the MMC. Test specimen orientations were, (1) along the preferred or axial direction, and (2) transverse to the axial direction. These two specimen orientations were used for both of the aforementioned phases of study. The two specimen directions were chosen for two reasons, (1) to verify if the MMC was isotropic, as the manufacturer claimed and (2) to serve as a comparison tool for the two specimen directions.

Initially, the microstructure of the MMC was observed under a scanning electron microscope (SEM). Three phases of the MMC were analyzed, two of which were to be evaluated. Assume the axial direction is parallel to the x-axis and the y-axis is along the transverse specimen direction, see Fig. 1.1. The planes of observation were the y-z plane, x-z plane, and x-y plane. In the y-z plane, Fig. 2.1, the whiskers resembled "dots", with relatively few whiskers lying in the y-z plane. Both,the x-z plane and x-y plane, Fig.2.2, have a majority of whiskers lying in the respective planes. This finding was the first indication that the MMC was *not* isotropic.

Static Test Conclusions:

For the tensile tests, the axial specimens averaged 30-35% greater strength (~72 ksi) than the transverse specimens (~ 54 ksi). It is interesting to note that a 2024-T4 monolithic aluminum has a tensile strength of 48 ksi (37), approaching the strength of the transverse specimens. The MMC had a T-8 heat treatment, this would account for the greater tensile strength and the reduction in ductility as seen in Fig. 2.4.

Poisson's ratio for the axial and transverse directions was $\nu = 0.235$ and $\nu = 0.323$ respectively. Poisson's ratio for most aluminum alloys (37) ranges from $\nu = 0.330$ to 0.334. Again, the transverse specimens compare closely with that of most single-phase aluminum alloys. The Poisson's ratio for the axial direction (ν=0.235) resembles that of a very brittle material, such as cast iron (ν= 0.211- 0.290).

Young's moduli, E was 18.60 msi and 13.09 msi for the corresponding axial and transverse specimens. The modulus for the axial direction is approximately 42% greater than that for the transverse direction. The elastic modulus for most aluminum alloys is between 9.9 msi and 10.3 msi (38).

An extensometer was used to measure the maximum deflection for the flexure test. The maximum deflection of the extensometer was 1mm. After reaching 1mm, the specimens for both transverse and axial directions had yielded

although didn't fracture. A second cycle was conducted, where the plastic deformation from the first cycle was just added to the deflection of the second cycle. Calculating the flexural modulus for the MMC yielded an atypical result. The modulus, for both specimen directions, was ~ 4% greater on the second cycle than the first cycle, see Fig. 2.11. The flexural moduli for the transverse direction was 11.5 msi and 12.0 msi for the first and second cycles, respectively. The bending moduli for the axial direction was 14.3 msi and 14.9 msi for the corresponding first and second cycles. This type of strain-hardening often occurs under repeated mechanical cycling, although not typically for 2 quasi-static mechanical cycles. The nominal bending strength for the respective axial and transverse directions was 89,072 psi and 116,300 psi. These strengths are anomalous as stated in 2.5.4, since the assumption of linearly-elastic behavior is violated. It was initially assumed that the bending behavior would be similar to the tensile test, in which the linear-elastic expressions for bending stress, Eq. [2.5], would have been valid.

The shear properties for the composite were determined using the Iosipescu Shear Test Method. This method is becoming the technique of choice for polymer-matrix and metal-matrix composites (22) due to the small coupon size, Fig. 2.15. The shear strengths were similar for both specimen directions. The corresponding transverse and axial shear strengths were 24,400 psi and 28,278 psi. A 2014-T4 aluminum has a shear strength of $\approx$ 38,000 psi. The experimental (Iosipescu) shear moduli for the transverse and axial directions was 5.43 msi and 8.04 msi, respectively. Since Poisson's ratio, ν and Young's moduli, E had been determined for both specimen directions, it was decided to

use the relationship for isotropic material , Eq. (2.11), to determine the shear moduli, G for both directions. It was suprising to note that the "isotropic" relationship yielded a shear modulus only ~ 5% less than the experimental (Iosipescu) shear modulus. This was true for both specimen directions. The shear moduli for most aluminum alloys is between 3.7msi and 3.9 msi.

Cyclic-Bending Conclusions;

The cyclic-bending phase of investigation yielded some very interesting findings. This study was simply applying an old science to a new material. The cyclic-bending testing was deflection-controlled, thus invariant of specimen stiffness or direction. This condition made for a fair comparison between the axial test specimens and transverse test specimens. The test was compression-compression, with R=0.1, to reduce the chance for impacting the specimen and resulting in premature specimen fracture. The test criterion also assumed elastic strain (deflection). Several load-displacement data sets were captured and stored on computer for each cyclic-bend test. Each data set was analyzed to verify if the load-displacement was linearly, elastic. The second method to verify if the cyclic-bend test was elastic was nearly infallible. If the specimen did plasticity deform, and didn't follow the machine actuator, it would be destroyed within only a few cycles due to impact. The cyclic-bend test was conducted at six deflection levels for both specimen directions. From the reliability results three fatigue models were constructed per transverse and axial direction. The fatigue models all consist of power-law equations linearized on log-log plots.

The first model used was Stress-Life (S-N), Eq.[3.9], where the endurance-limits for the axial direction was approximately 50% greater than that for the transverse direction, see Fig. 3.4. The endurance limit for the axial direction was, $\Delta\sigma/2$ = 23,000 psi and for the transverse direction, $\Delta\sigma/2$ = 15,000 psi. The endurance limit for 20xx-T4 aluminum is ~ $\Delta\sigma/2$ = 18,000 psi (38). The S-N fatigue test is acceptable when the deformation is primarily elastic, since the S-N model doesn't account for plastic deformation. The S-N test method was devised over 100 years ago and was the first approach (20) used in an attempt to understand and quantify metal fatigue.

The Strain-Life (ε-N_f) method was the second technique used to evaluate the cyclic-bend data. The strain-life model is based on the idea that, with several components, e.g. cracks and notches, the response of the material is strain dependent. In this study, two strain models were used; the first model, Eq.[3.13^e], did not account for mean stress and the second model, Eq.[3.14], did account for mean stress effects. The cyclic-bend test had a mean stress, thus it was hoped that Eq.[3.14] would closely parallel the test results.

The strain-life model w/o mean stress effects resembled that of the S-N models, the correlations for the strain-life models were slightly better than the S-N models for both directions. The strain-life model with mean stress effects are not only a function of strain, but also elastic modulus and mean stress. The nominal elastic modulus and nominal mean stress was measured for each

specimen. The elastic modulus varied from specimen to specimen, even from data interval to data interval, this helps explain why the strain-life models which account for mean stress effects are not straight, see Fig. 3.5. The strain-life models with mean stress effects were slightly conservative for both specimen directions.

The deflection-life (δ-N_f) model was created specifically for this study, since the controlled-variable was *deflection*, not stress or strain. Not surprising, the correlations for this model were the best of the three fatigue models, for both directions. The correlation coefficients for the corresponding axial and transverse deflection-life models were 0.88 and 0.95 respectively.

It was decided midstream in the cyclic-bend study to analyze Young's modulus as a function of cycles to near failure. Since the load-displacement data was already captured at several intervals throughout each test, I had all the information needed to perform the E-N perusal. The dynamic flexural modulus was normalized against the static flexural modulus.

A first glance, Figs. 4.1-4.12, it may appear as though no obvious trends are apparent, although one trait that is very distinct is that the moduli are not *constant* throughout the cyclic-bend tests. This behavior doesn't make sense at the macroscopic-level, the elastic moduli should remain unchanged if no plastic deformation is present. one explanation might be, at the microscopic-level a plastic-strain zone is induced due to such mechanisms as asperities, crack face rubbing, etc. Regardless of the reason for the variation in E with

elastic bending cycles, this situation is not one to be overlooked. Since this mechanical phenomenon has been observed, a rigorous investigation is in order, using more quantitative methods.

This cyclic-bending study has prompted several avenues of additional research. These areas of recommended additional study are stated below with appropriate justification.

Recommended Additional Research:

Using the SiC_w / Al MMC extrudate evaluated in this thesis, perform a study of strain-controlled, uniaxial fatigue loadings. The specimens to be analyzed will be along the extrudate axis and several off-axis angles until reaching the transverse axis. This survey would allow for the creation of Strain-Life (ε-N_f) models that would include both the elastic and plastic strain components, Eq.[3.13]. The elastic component of the uniaxial Strain-Life (ε-N_f) models, along the axial direction and transverse direction, can be compared with the cyclic-bending Strain-Life (ε-N_f) models.

Continue the deflection-controlled cyclic-bending of the SiC_w / Al MMC, with a few amendments from the technique used in Chapter 4. The purpose of this study would be to *quantify* the elastic modulus decrement with mechanical cycles. The test specimens would be cut along the axial or extrudate axis, and several off-axis angles until reaching the transverse axis. The elastic modulus

would be measured using sonic resonance at the pre-determined cycles of interest.

Similar thermal fatigue work has been executed for brittle polymer composites (24,25) and ceramics and ceramic composites (23,31). Recently, Case et al. (23) has observed and evaluated this thermal fatigue via sonic resonance. Case has derived an empirical relation to describe the thermal fatigue damage of the elastic modulus with thermal cycles to near failure. This equation basically states that as the number of thermal shocks (cycles) increases, the elastic modulus decreases linearly until the thermal shock damage reaches a steady-state, or saturation level. Case et al. (33-36) has compared damage saturation behavior on a number of brittle materials, including his own ceramics and ceramic-matrix composites (23,31), along with that of other researchers' work on brittle polymer-matrix composites (24,25). Using the aforementioned empirical expression (23), the modulus decrement and saturation-levels with thermal cycles were modeled with surprisingly acceptable precision.

An interesting finding was that a damage saturation similar to that observed for the thermal fatigue has also been observed for cyclic *mechanical* loading for brittle materials such as, ceramics (32), ceramic composites (27,25) and fiber-reinforced epoxies (26). These cyclic mechanical loading studies in brittle materials show damage saturation for a variety of loading modes (29,30). Some of the proposed mechanisms for this saturation of fatigue damage include friction processes such as, crack deflection, asperity rubbing and crack

face bridging.

On a slightly different note, Reece et al. (39) discovered that for an alumina COD specimen subjected to repeated mechanical loading resulted in crack propagation. For an equivalent static load applied for the same amount of time, or static fatigue, there was no additional crack propagation. some of the proposed mechanisms for this crack propagation are, asperities on the crack faces and/or fracture debris produced by grain crushing. Although the mechanisms in brittle materials are not well understood, it is just apparent that there is crack growth for cyclic loading. Cyclic fatigue of brittle materials has be largely overlooked in the past. The reason is probably due to the perception that since brittle materials have limited crack tip plasticity, they will not degrade significantly when cyclically loaded.

The previous two paragraphs help give credibility to the variation in the elastic modulus with "elastic" mechanical cycles. The literature review in no way describes the mechanical phenomenon, it just acknowledges that this condition exists. The MMC evaluated behaves similar to a brittle material under uniaxial tension to failure, see Fig. 2.4. The MMC is more ductile for 3-point bending, although it exhibits the elastic modulus decrement with "elastic" cyclic-bending cycles. Thus, it is thought justifiable to re-evaluate the MMC similar to that of the brittle materials mentioned above to see if they exhibit trends similar to that of the corresponding rigid materials. This type of survey has never been conducted for MMC's, only for ceramics, ceramic-matrix composites and rigid polymer-matrix composites.

REFERENCES

-REFERENCES-

1. Goddard, N.D.R., "Test Techniques for Metal Matrix Composites," in *Proceedings of the meeting organized by The Institute of Physics, Materials and Testing Group*, Baden Powell House, London, No. 28, 28 Nov. 1990.

2. Daimaru, A., Hata, T. and Taya M., pp. 505-521 in reference 3.

3. Vinson, J.R. and Taya M., (Eds.) STP 864, ASTM ,(1985), "Recent Advances in Composites in USA and Japan".

4. Hosking, F.M., Portillo, F.F., Wunderlin, R. and Mehrabian, R., *J. Mat. Sci.*, (1982), 17, pp. 447-498.

5. Dermaker, S., *Met. and Matls.*, March (1986), pp. 144-146.

6. Girot, F.A., Albingre, L., Queisset, J.M. and Naslain, R., *J. of Metals*, Nov. (1987), pp. 18-21.

7. Milliere, C. and Surey, M., *Mat. Sci. and Tech.*, (1988), 4, 41.

8. Dumant, X., Beaugnon, E. and Regazzoni, G., *J. of Metals,* Nov. (1988), pp. 46-51.

9. Klipfel, Y.L., He, M.Y., McMeeking, R.M., Evans A.G. and Mehrabian, R., *Acta. Met.*, (1990), 38, pp. 1063-1074.

10. "Standard Test Method for Plain-Strain Fracture Toughness of Metallic Materials," ASTM E 399-83, pp. 480-487.

11. "Standard Test Method for Tensile Properties of Fiber-Reinforced Metal-Matrix Composites," ASTM D 3552-77 (Reapproved 1989)$^{\varepsilon 1}$,Ed., pp. 164-168.

12. Timoshenko, S.P. and Goodier, J.N., "Theory of Elasticity", McGraw-Hill Publishing Co., New York, 1987.

13. Riley, W.F. and Zachary, L., "Introduction to Mechanics of Materials", John Wiley and Sons, Inc., New York, 1989.

14. Walrath, D.E. and Adams, D.F., "Analysis of the Stress State of an Iosipescu Shear Test Specimen," Report UWME-DR-301-102-1, Dept. of Mechanical Engineering, Univ. of Wyoming, Laramie WY, (June 1983).

15. Iosipescu, N., "New Accurate Procedure for Single Shear Testing of Metals," *J. of Materials*, Vol. 2, (3), Sept. 1967, pp. 537-566.

16. Adams, D.F., "The Iosipescu Shear Test Method as used for Testing Polymers and Composite Materials," *Polymer Composites*, Vol. 11, No. 5, (October 1990), pp. 286-290.

17. Basquin, O.H., "The Exponential Law of Endurance Tests," *Am. Soc. Test Mat. Proceedings*, Vol. 10, (1910), pp. 625-630.

18. Coffin, L.F., "A Study of the Effects of Cyclic Thermal Stresses on a Ductile Metal," *Trans. ASME*, Vol. 76, (1954), pp. 931-950.

19. Manson, S.S., "Behavior of Metals Under Conditions of Thermal Stresses," *Heat Transfer Symposium*, Univ. of Michigan, Engineering Research Institute, 1953, pp. 9-75, (also published as NACA TN 2933, 1953).

20. Bannantine, J.A., Comer, J.J. and Handrock, J.L., "Fundamentals of Metal Fatigue Analysis," Prentice-Hall Inc., Englewood Cliffs, New Jersey 07632, 1990.

21. Morrow, J., "Fatigue Design Handbook," *Advances in Engineering*, Vol. 4, Society of Automotive Engineers, Warrendale PA, (1968), Sec. 3.2, pp. 21-29.

22. Manson, S.S. and Halford, G.F.,"Practical Implementation of the Double Linear Damage Rule and Damage Curve Approach for Treating Cumulative Fatigue Damage," *Int. J. Fract.*, Vol. 17, No. 2, (1981), pp. 169-172, R35-R42.

23. Lee, W.J. and Case, E.D., "Comparison of Saturation Behavior of Thermal Shock in a Variety of Brittle Materials," *Mat. Sci. and Engr.*, Michigan State Univ., E. Lansing MI, (1992), pp. 1-9.

24. Herakovich, C.T. and Hyer, M.W., "Damage Induced Property Changes in Composites Due to Cyclic Thermal Loading," *Engr. Frac. Mech.*, 25, (5-6), (1986), pp. 779-791.

25. Liu, S. and Nairn, J.A., "Fracture Mechanics Analysis of Composite Microcracking: Experimental Results in Fatigue," in *Proceedings of the American Society for Composites*, 5th Technical Conference, 1990, pp.287-295.

26. Ogin, S.L., Smith, P.A. and Beaumont, P.W.R., "Matrix Cracking and Stiffness Reduction of $(0/90)_s$ GFRP Laminate," *Com. Sci. and Tech.*, 22, (1985), pp. 23-31.

27. Suresh, S. and Han, L.X., "Fracture of Si_3N_4-SiC Whisker Composites Under Cyclic Loading," *J. Amer. Ceram. Soc.*, 71, (1988), (C-158-C-161).

28. Morrone, A.A., Nutt, S.R. and Suresh, S., "Fracture Toughness and

Fatigue Crack Growth Behavior of an Al_2O_3-SiC Composite," *J. Mat. Sci.*, 23, (1988), pp. 3206-3213.

29. Lu, M.E. and Evans, A.G., "Influence of Cyclic Tangential Loads on Indentation Fracture," *J. Am. Ceram. Soc.*, 68, (9), (1985), pp. 505-515.

30. Swanson, P.L., Fairbanks, C.J., Lawn, B.R., Mai, Y-M and Hockey, B.J., "Crack-Interface Bridging as a Fracture Resistance Mechanism in Ceramics," *J. Am. Ceram. Soc.*, 70, (4), (1987), pp. 279-289.

31. Case, E.D., Smyth, Jay R. and Hunter, O. Jr.,"Microcrack Healing During the Temperature Cycling of Single-Phase Ceramics," in *Frac. Mech. of Ceram.*, 5, (1983), pp. 507-530.

32. Case, E.D., "The Effect of Microcracking Upon the Poisson's Ratio for Brittle Materials," *J. of Mat. Sci.*, 19, (1984), pp. 3702-3712.

33. W.J. Lee and E.D. Case, "Cyclic thermal shock in SiC whisker/alumina composites", *Mater. Sci. Engr.*, A119 (1989), pp. 113-126.

34. W.J. Lee and E.D. Case, "Thermal fatigue in polycrystalline alumina", *J. Mater. Sci.*, 25 (1990), pp. 5043-5054.

35. Y. Kim, W.J. Lee and E.D. Case, "Thermal fatigue in SiC fiber reinforced aluminosilicate glass ceramic composite", *Metal and Ceramic Matrix Composites: Processing, Modeling and Mechanical Behavior*, The Minerals, Metals and Minerals Society, 1990, pp. 479-486.

36. Y. Kim, W.J. Lee and E.D. Case, "Thermal fatigue behavior of ceramic matrix composites: a comparison among fiber reinforced, whisker reinforced and monolithic ceramics", *Proceedings of the American Society for Composites*, 5th technical conference, 1990, pp. 871-881.

37. Avalone, E.A. and Baumeister, Theo. III, Marks' STANDARD HANDBOOK for MECHANICAL ENGINEERS, McGraw-Hill Publishing, New York, 9th ed., 1986, pp. 5.2-5.5.

38. Riley,W.F. and Zachary,L.W., Introduction to Mechanics of Materials, John Wiley & Sons Inc., New York, first ed., 1989.

39. Reece,M.J., Guiu,F. and Sammur,M.F.R., "Cyclic Fatigue Crack Propagation in Alumina under Direct Tesion-Compression Loading", *J. Am. Ceram. Soc.*, 72, [2], pp. 348-352 (1989).

-additional references not directly cited in the thesis-

-Feest, E.A. and Cook, J., "Test Methods for Small Quantities of MMC Material," AEA Industrial Technology, Harwell Laboratory, Didcot OX 11 ORA, (1991).

-McCartney, L.N., "Testing of Metal Matrix Composites - An Overview," Division of Materials Metrology, National Physical Laboratory, Teddington, Middx. UK TW11 OLW, (1991), pp. 129-143.

-Lee, S. and Munro, M., "Evalution of Testing Techniques for the Iosipescu Shear Test for Advanced Composite Materials," *J. Comp. Mat.*, Vol. 24, (April 1990), pp. 419-440.

APPENDIX A

QUICKBASIC CODE TO CAPTURE THE LOAD-DISPLACEMENT DATA, FOR THE CYCLIC-BENDING SURVEY, AT DESIGNATED TIME INTERVALS.

```
DECLARE SUB Readadint (Ch0%, Ch1%)
'                                   DECLARE SUB Readadint (Ch0%,
Ch1%)
        DEFINT A-Z
        DEFLNG N, S
        DIM Adl(10), Adh(10)

        ScanNumber = 0
        Format$ = "|  ###    |\       \| \            \| \
                                    \|"
        DIM Xdata(252), Ydata(252)
'        GOSUB ClockSet
'
-------------------------------------------------------------
---------
'       Get initial information

        CLS
        LOCATE 5, 10: PRINT "Enter the number of minutes
between scans...: ";
        INPUT "", Interval$
        Interval = VAL(Interval$)
        IF Interval < 1 THEN Interval = 1
        IF Interval > 181 THEN Interval = 181
        SecInterval = Interval * 60

        LOCATE 7, 10: PRINT "Using an interval of";
Interval; "minute(s)"
        LOCATE 8, 10: PRINT "                    or";
SecInterval; "seconds"

        LOCATE 11, 10: PRINT "Enter a 4 letter prefix for
data files...: ";
        INPUT "", Prefix$
        IF Prefix$ = "" THEN Prefix$ = "NONE"
        Prefix$ = UCASE$(LEFT$(Prefix$, 4))
        LOCATE 13, 10: PRINT "Data files will be saved as ";
Prefix$; "####.DAT"

        LOCATE 20, 10: PRINT "Press X to exit or any other
key to start"

50      A$ = INKEY$: IF A$ = "" THEN GOTO 50
        IF UCASE$(A$) = "X" THEN GOTO Done

'
-------------------------------------------------------------
---------
'       Set up screen to display incoming scan information


        CLS
        PRINT TAB(10); "Test started on "; DATE$; " at ";
```

```
TIME$
        PRINT TAB(10); "Using a time interval of"; Interval;
"minute(s)"
        COLOR 18: LOCATE 2, 65: PRINT "< Waiting > ": COLOR
7
        PRINT
        PRINT "╒═══════════╤═══════════╤═══════════════════╕" +
STRING$(45, "=") + "╕"
        PRINT "|  Scan   |  Time   |                   |
" + SPACE$(34) + "|"
        PRINT "| Number | Taken |    Saved as    |  Comments
" + SPACE$(34) + "|"
        PRINT "├─────────┼─────────┼─────────────────┤" +
STRING$(45, "-") + "┤"

'
-------------------------------------------------------------
---------
'       The main testing loop

100     StartTime = TIMER
        NextTime = TIMER + SecInterval

150     IF TIMER > NextTime THEN
           GOSUB ItsTimeToScan
           GOTO 100
        END IF
        IF INKEY$ <> "" THEN GOTO Done
        GOTO 150


'
-------------------------------------------------------------
---------
ItsTimeToScan:

        VIEW PRINT: COLOR 19
        LOCATE 2, 65: PRINT "< Scanning >": COLOR 7

        ScanNumber = ScanNumber + 1
        Filename$ = Prefix$ + LTRIM$(STR$(ScanNumber)) +
".DAT"

        OPEN Filename$ FOR OUTPUT AS #2
        ScanTime$ = TIME$

        FOR NumOfPoints = 1 TO 100
            CALL Readadint(Ch0%, Ch1%)
            Xdata(NumOfPoints) = Ch0%
            Ydata(NumOfPoints) = Ch1%
        NEXT NumOfPoints

        FOR N = 1 TO 100
```

```
            PRINT #2, Xdata(N), CHR$(44), Ydata(N)
        NEXT N
        CLOSE #2
        VIEW PRINT 8 TO 25

        IF ScanNumber > 16 THEN
           LOCATE 24, 1
           PRINT USING Format$; ScanNumber; ScanTime$;
Filename$; " "
           PRINT
        ELSE
           LOCATE (ScanNumber + 7), 1
           PRINT USING Format$; ScanNumber; ScanTime$;
Filename$; " "
        END IF

        VIEW PRINT
        COLOR 18: LOCATE 2, 65: PRINT "< Waiting > ": COLOR
7

RETURN

'
---------------------------------------------------------
---------
Done:
        VIEW PRINT: CLS : CLOSE : END


'
---------------------------------------------------------
---------
'       List of important variables

'       ScanNumber      :  Keeps track of the number of
scans completed
'       SecInterval     :  The time between scans, in
seconds
'       Interval        :  The time between scans, in
minutes
'       Prefix          :  The four letter prefix for saved
data files
'       Format$         :  Format for the printed line of
scan information
'       FileName$       :  The current name of the saved
data file
'       Ch0%, Ch1%      :  Returned values of AD conversion
for channels 1 & 2
'       StartTime$      :  The time that the current scan
was started
'       NumOfPoints     :  Dummy loop variable to read in a
number of points
'       PauseLoop       :  Dummy loop variable for a pause
between reads
```

```
ClockSet:
        WAIT (&H2EC + 1), &H2, &H2
        WAIT (&H2EC + 1), &H4
        OUT (&H2EC + 1), &H3

        WAIT (&H2EC + 1), &H2, &H2
        OUT (&H2EC), 208
        WAIT (&H2EC + 1), &H2, &H2
        OUT (&H2EC), 7

RETURN

DEFSNG A-Z
SUB Readadint (Ch0%, Ch1%)

        DIM Adl(10), Adh(10)

'       Stop and clear the dt2818

        OUT (&H2EC + 1), &HF
        Temp = INP(&H2EC)
        WAIT (&H2EC + 1), &H2, &H2
        WAIT (&H2EC + 1), &H4
        OUT (&H2EC + 1), &H1

'       set up a/d.

        WAIT (&H2EC + 1), &H2, &H2
        WAIT (&H2EC + 1), &H4
        OUT (&H2EC + 1), &HD

'       Write A/D gain byte. (gain is always zero)

        WAIT (&H2EC + 1), &H2, &H2
        OUT (&H2EC), 0

'       Write A/D start channel byte.

        WAIT (&H2EC + 1), &H2, &H2
        OUT (&H2EC), 0

'       Write A/D end channel byte.

        WAIT (&H2EC + 1), &H2, &H2
        OUT (&H2EC), 1

'       Write high and low bytes of NCONVERSIONS#.

        WAIT (&H2EC + 1), &H2, &H2
        OUT (&H2EC), 3
        WAIT (&H2EC + 1), &H2, &H2
        OUT (&H2EC), 0
```

```
'       Write READ A/D command.

        WAIT (&H2EC + 1), &H2, &H2
        WAIT (&H2EC + 1), &H4
        OUT (&H2EC + 1), &HE

        FOR LP = 0 TO 3: WAIT (&H2EC + 1), &H5
           Adl(LP) = INP((&H2EC))
           WAIT (&H2EC + 1), &H5
           Adh(LP) = INP((&H2EC))
        NEXT LP

        Ch000# = Adh(0) * 256! + Adl(0)
        IF Ch000# > 32767 THEN Ch000# = Ch000# - 65536!
        Ch0% = Ch000#

        Ch111# = Adh(1) * 256! + Adl(1)
        IF Ch111# > 32767 THEN Ch111# = Ch111# - 65536!
        Ch1% = Ch111#

'       Check for ERROR.

        WAIT (&H2EC + 1), &H2, &H2
        WAIT (&H2EC + 1), &H4:
        Status = INP((&H2EC + 1))
        IF (Status AND &H80) THEN
           PRINT "error on A/D operation"
           STOP
        END IF

END SUB
```